EXPERIMENTAL INVESTIGATION OF THE EFFECT OF SPIN ON TRACTION IN ELASTOHYDRODYNAMICALLY LUBRICATED CONTACTS

by

Arsavir T. Andonian

Thesis submitted to the Graduate Faculty of the
Virginia Polytechnic Institute and State University
in partial fulfillment of the requirements for the degree of

MASTER OF SCIENCE

in

Mechanical Engineering

APPROVED

N. S. Eiss, Jr., Chairman

H. H. Mabie

M. J. Furey

May, 1975

Blacksburg, Virginia

ACKNOWLEDGEMENTS

The author wishes to express his appreciation to his major professor, Dr. Norman S. Eiss, Jr., for his many hours of assistance and guidance on this research. Special thanks must be extended to Dr. Hamilton H. Mabie and Dr. Michael J. Furey for their advice and technical assistance.

A special note of thanks is extended to Mr. R. M. Jones for his friendly help in preparing the program for the CALCOMP computer plots.

Appreciation is extended to Miss Willie Mae Hylton for her unfailing good humor and her expert typing of the manuscript.

TABLE OF CONTENTS

TABLE OF CONTENTS - continued

LIST OF FIGURES

LIST OF FIGURES - continued

*Zero to 100% Slip

LIST OF FIGURES - continued

*Zero to 100% Slip

LIST OF FIGURES - continued

*Zero to 100% Slip

LIST · continued

LIST OF TABLES

LIST OF SYMBOLS

a	Radius of Hertzian contact
A	Area
f_c	Centrifugal force due to spin
E	Young's modulus of elasticity
F	Friction (or tractive) force
F_b	Force measured by the platform balance
F_c	Compressive force on each driving unit
h	Film thickness
h_o	Mid-point film thickness
h_{min}	Minimum film thickness
ℓ	Equivalent length of driving unit
L	Length of lever arm of eddy-current brake
m	Mass
M	Moment
p	Pressure to which the lubricant is subjected
p_{max}	Maximum Hertzian pressure
P	Platform load
R_1	Radius of ball 1 (driving ball)
R_2	Radius of ball 2 (driven ball)
R	Reduced radius = $(R_1^{-1} + R_2^{-1})^{-1}$
T	Lubricant temperature at contact zone
T_o	Room temperature
u	Surface velocity
u_c	Surface velocity at the center of contact area

LIST OF SYMBOLS (continued)

u_p	Surface velocity at any point of contact area
Δu	Sliding velocity
ω_1	Angular velocity of ball 1
ω_2	Angular velocity of ball 2
ω_{spin}	Angular spin velocity
W	Normal load
W_h	Horizontal force on each driven ball
T.C.	Coefficient of traction
α	Pressure viscosity coefficient
η	Viscosity
η_o	Viscosity at atmospheric pressure
ρ	Distance from center to any point in the contact area
θ	Angular coordinate of contact area
ζ	Viscous shear stress
ψ	Angle of Contact

I. INTRODUCTION

In recent years, the discovery of elastohydrodynamic (EHD) lubrication has been instrumental in explaining the mechanism of lubrication for highly stressed machine elements, such as cam-follower mechanisms and gear teeth. This new regime of lubrication lies between hydrodynamic and boundary lubrication, and considers the increase of viscosity of oils and the elastic deformation of the surfaces in contact which occurs at extremely high contact pressures. The pressure distribution and the area of contact during EHD lubrication can be approximated using the Hertz equations (1)*. In Figure 1 the pressure profile predicted by the EHD theory is compared with the one predicted by the Hertz equations.

Recent trends in machine design towards higher speeds and higher load carrying capacity require supplementary knowledge about rolling contact phenomena. Of particular interest are high speed rolling bearings, gears and traction drives. The traction drives operate with considerable traction forces superimposed over the normal load.

Traction drives tend to slip† even under the required high contact pressures. Until recently, they have been limited to low power applications and have been generally regarded as light-duty specialized items. Now the picture is changing. New steels and new lubricants permit significantly higher rolling-contact pressures with little wear. Taking advantage of the higher allowable pressures, new drives can transmit

*Number in parentheses refers to a similarly numbered reference in the List of References.

†Slip is defined as the relative tangential motion of the lubricated elements in contact.

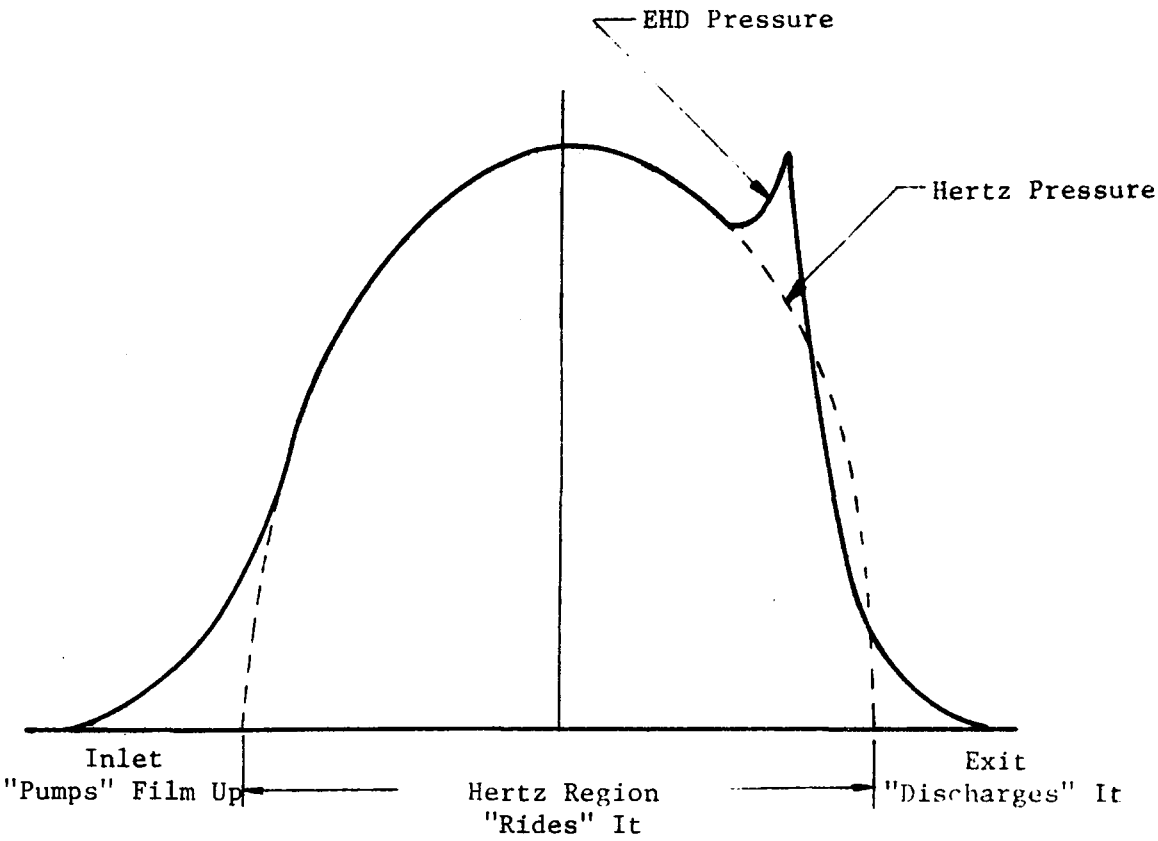

Figure 1. Comparison of EHD Pressure with Hetz Pressure

considerably more torque with a smaller transmission package and greatly increased service life. Traction drives can be generally characterized by the absence of backlash, low noise, high damping, high efficiency, simplicity and extremely high speed capability. For fixed speed ratio, cylinders are often used as the loaded EHD lubricated elements. Hewko (2) describes a roller traction drive developed for quiet power transmission.

Variable speed ratio transmission units are continuously variable over a certain speed range. One advantage they have over most conventional variable speed transmissions is the ability to change speed over full load without power interruption. As a result, traction drives are cropping up on machine tools, conveyors, textile machines, printing presses, recreational vehicles and even some experimental automobiles. Wide range variable speed traction drives can cut fuel consumption 30 percent and help meet emission requirements by keeping the engine at maximum efficiency (3).

Deformation and fatigue limits on the rolling elements have been extended by cleaner steels having high fatigue strengths and the ability to take high Hertzian stresses. These steels are double vacuum remelted (vacuum induction melt, vacuum arc melt) to eliminate impurities that cause surface flaking under repeated high local stresses.

Also some newly improved traction lubricants are available. Green (4) states that, "Traction coefficient seems to depend on the molecular structure of the lubricant. Until recently, the highest coefficient was found in a naphtenic petroleum oil, but synthetic cycloaliphatic

hydrocarbons have a much higher coefficient . It is worthwhile to mention that the upper limit of pressure was 250 KSI in most of the EHD traction studies.

In order to transmit a shear force across a fluid there must be relative motion between the two surfaces. This motion or slip is generally very small for fixed speed ratio traction drives. However, when dealing with variable speed ratio traction drives other velocity components are generally produced. For example, there may exist a velocity component perpendicular to the radius from the center of the contact which varies linearly with the distance from the center of contact. The latter component is called "spin." The spin component may cause losses in transmission efficiency and thus be an important parameter in the design of variable ratio traction drives.

An example of a variable drive configuration is one in which two spheres are rotated on axes which are perpendicular. Spin will exist under these conditions when the contact angle*, ψ, takes on any value other than 45°. Figure 2 shows a sketch of the balls in contact and indicates the contact angle ψ. The kinematic analysis of this system is given in Appendix A.

This thesis reports an investigation of the effect of spin on traction during EHD lubrication. Included in the thesis are descriptions of modification of the test rig utilizing balls which have perpendicular axes of rotation designed by J. F. Hann (5), of the experimentation and evaluation of experimental results by theoretical analysis. The

*Contact angle is the angle between the axis of the driven ball and the normal to the contact area.

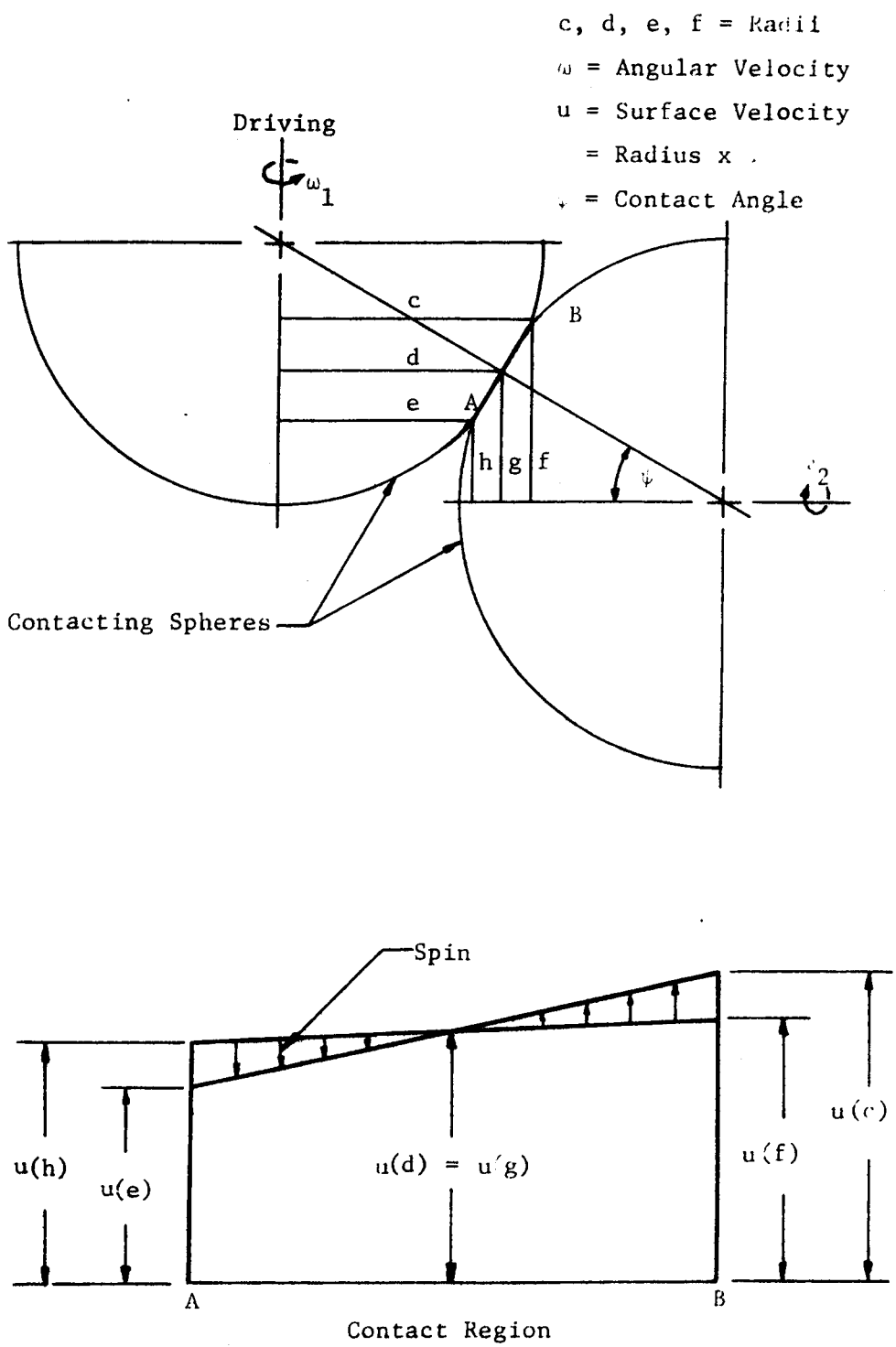

Figure 2. Ball Contact Geometry & Velocity Distribution

experimentation and the theoretical analysis of the experimental results represent the major portion of this work.

II. REVIEW OF LITERATURE

The effects of various parameters upon the film thickness in the EHD region is perhaps one of the most interesting areas in the field of EHD lubrication. Cameron (1) has investigated this and Figure 3 shows a plot of film thickness from his work.

Crook (6) states that the minimum film thickness depends upon sliding velocity, speed, thermal properties and inlet conditions but is not dependent upon load.

One of the most convincing experimental procedures used to measure film thickness is one using optical interference techniques. Cameron (1) describes the technique and its operational characteristics.

The transition from hydrodynamic to EHD lubrication is not set at any fixed point. The parameter most sensitive to the transition zone is the traction force. In the EHD region the traction force is orders of magnitude greater than that in the hydrodynamic region where the traction is relatively small.

Tallian (7) has investigated the factors affecting the traction coefficient; Figure 4 illustrates his results. The straight line portion to the left of the peak is that region in which traction drives operate. To the right of the knee the drop in the traction coefficient causes this area to be undesirable since an increase in slip would produce a drop in output.

The dropping off of the traction coefficient with increasing slip may be due to several factors. This may be due to the heating in the film as the sliding speed is increased, which would decrease the viscosity. One theory (7) states that due to the very high viscosity gradient present

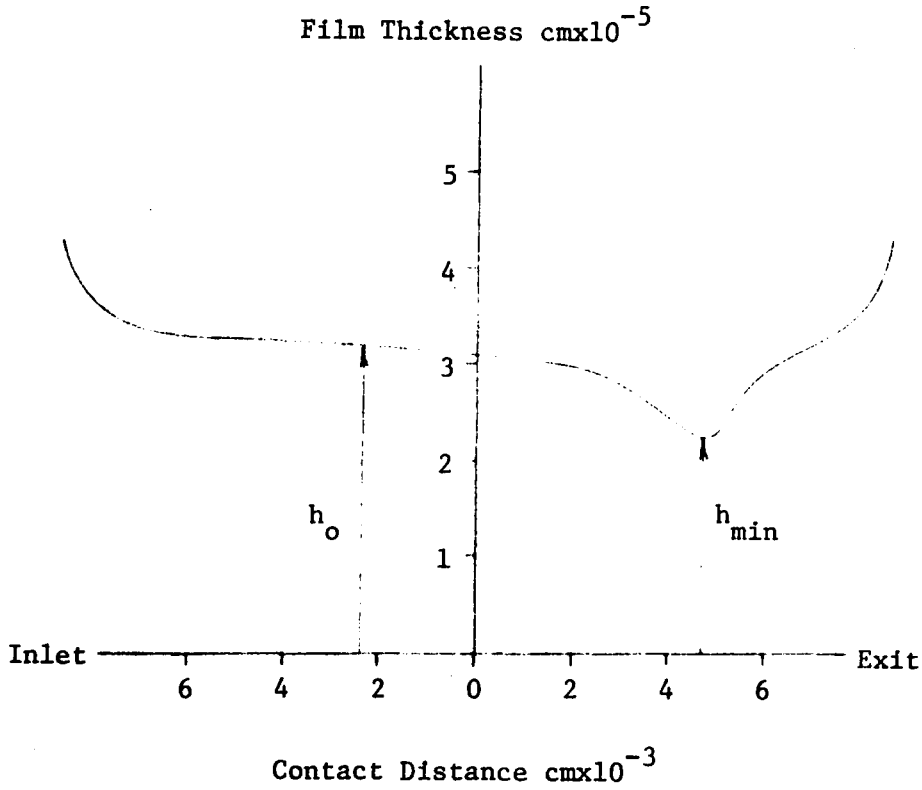

Figure 3. EHD Film Thickness for Point Contact [from Cameron (1)]

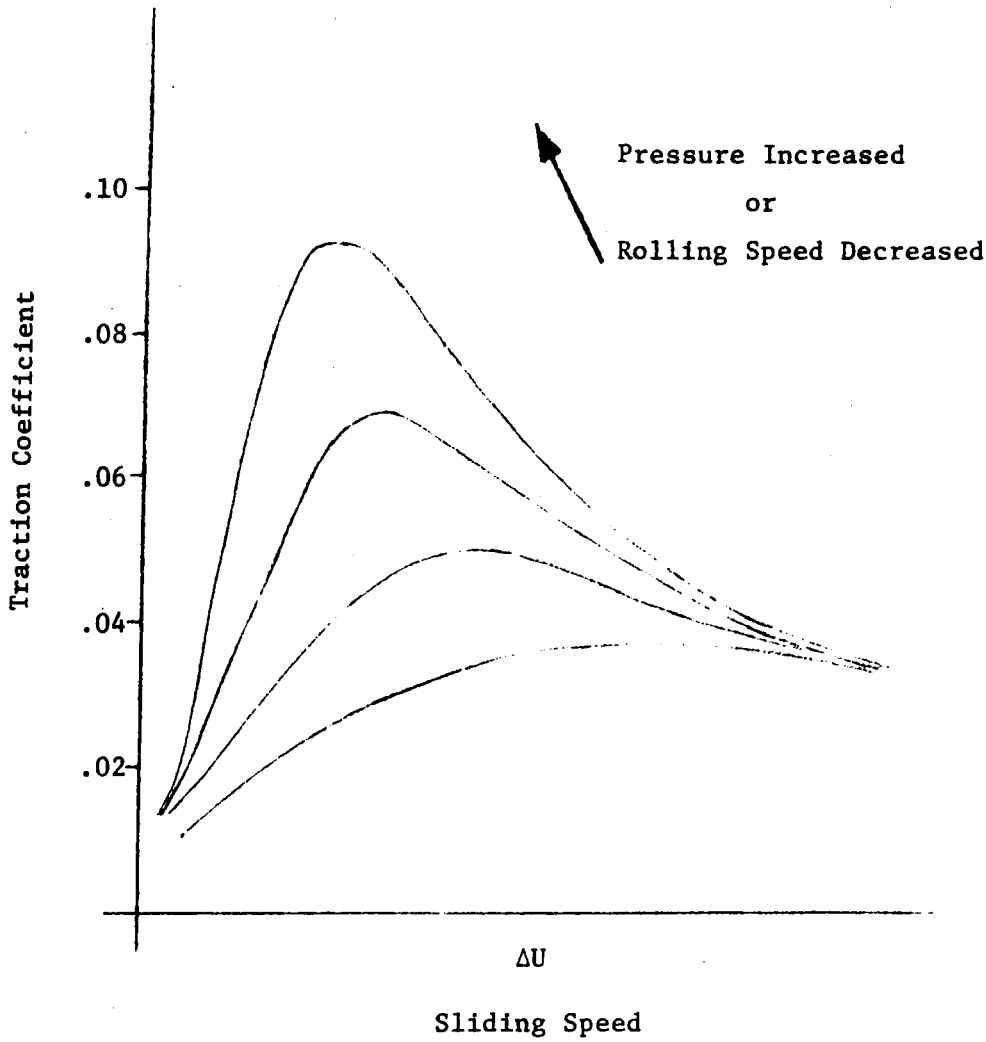

Figure 4. Traction Coefficient During EHD Lubricated Contact

across the film, the lubricant behaves as a non-Newtonian fluid. A viscoelastic behavior of the lubricant can be assumed as well.

The fact that a liquid lubricant might not behave as a liquid but as a solid was first presented by Smith (8) in 1960 to explain the tractive behavior of an ester-based and silicone lubricant. Smith's traction measurements were made at a constant normal stress, and, therefore, he saw no load dependence of the "limiting shear stress." Gentle and Cameron (9) in 1972 suggested the behavior of the lubricant in EHD contact was similar to the shear behavior of granular materials, such as sandstone, in which the limiting shear stress is a linear function of the normal stress. Towsend et al. (10), in 1973 presented a rheological model by assuming that the limiting shear stress at high normal loads is proportional to normal stress. Finally, Miller (11) quantitatively illustrated that the solid-like mechanical properties of liquids can control the low slip tractive behaviors of highly loaded EHD contacts and illustrated that the low slip tractive behavior of lubricants is functionally similar to the shear stress transmission capability of grossly deformed solids.

The tractive response of a liquid synthetic hydrocarbon lubricant in high speed,highly loaded EHD line contacts has been obtained by Trachman and Cheng (12), as a function of load, rolling speed, sliding speed, and temperature, and it is similar to the response of other liquids obtained by other investigators (8,13,14). The low shear rate data can be summarized as follows:

a) At constant rolling speed, load, and inlet temperature, the traction coefficient is a linear function of the sliding speed.

b) At constant rolling speed, sliding speed and inlet temperature, the traction coefficient increases to a maximum and then decreases as the load is increased.

c) At constant load, rolling velocity, and slip velocity the traction coefficient decreases as the temperature increases.

Qualitative predictions based on any rheological model should be consistent with these observations.

Miller (11) states that the shear moduli and yield stress behavior of lubricants in highly loaded, high speed EHD contacts are similar to the behaviors of solids. He shows that the average shear modulus of the lubricant is a linear function of average normal stress for a constant average rolling velocity.

The relation generally used to describe the variation of viscosity with pressure is as follows [from Cameron (1)]:

$$\eta = \eta_o e^{\alpha p}$$

This simple form is acceptable for most work involving naphthenic based oils. Crook (6) states that the increase in viscosity with pressure becomes less as the time it takes for the oil to pass through the contact region is decreased. Therefore, even if shear rate data on lubricants were available, much would still be lacking when considering its properties under transient conditions.

A point contact disc machine was used by Johnson and Roberts (14) to investigate the viscoelastic behavior of EHD lubricant films. Utilizing this machine a surface spin was produced in the contact region as

described in the Introduction. They state that the coefficient of traction increases as the spin is increased.

The spin of balls in ball bearing races has been studied by Rounds (15) and Zaretsky (16). But the effect of spin upon the traction coefficient has not been extensively studied.

III. EXPERIMENTAL INVESTIGATION

A. Object

The object of this research was to study the effect of spin on the traction coefficient at various loads and rolling and sliding speeds during EHD lubrication of point contacts and to determine if the results can be predicted by EHD lubrication theory.

B. Experimental Apparatus

The test machine has the capability for rotating the balls, loading the balls, applying a retarding torque to the balls, and checking the metal-to-metal contact. Figures 5 and 6 show two different views of the machine. In spite of the fact that the machine was designed for operation at speeds up to 5000 rpm, the experiments to be reported were run at speeds below 1500 rpm because of resonant vibration frequencies that existed above this speed. These resonant vibrations would break the lubricant film causing metal-to-metal contact. The maximum Hertzian pressure was set at 500 KSI which was the threshold for metallic contact. The angle of contact was varied by changing the position of the driving balls relative to the axis of the driven balls. The retarding torque was applied using an eddy current brake. By measuring the magnitude of this torque the coefficient of traction was calculated at various loads, speeds and contact angles. See Appendix J for the procedure of calculating the coefficient of traction.

In the following paragraphs details are presented on the four major capabilities of the machine.

Figure 5. Side View of Test Apparatus

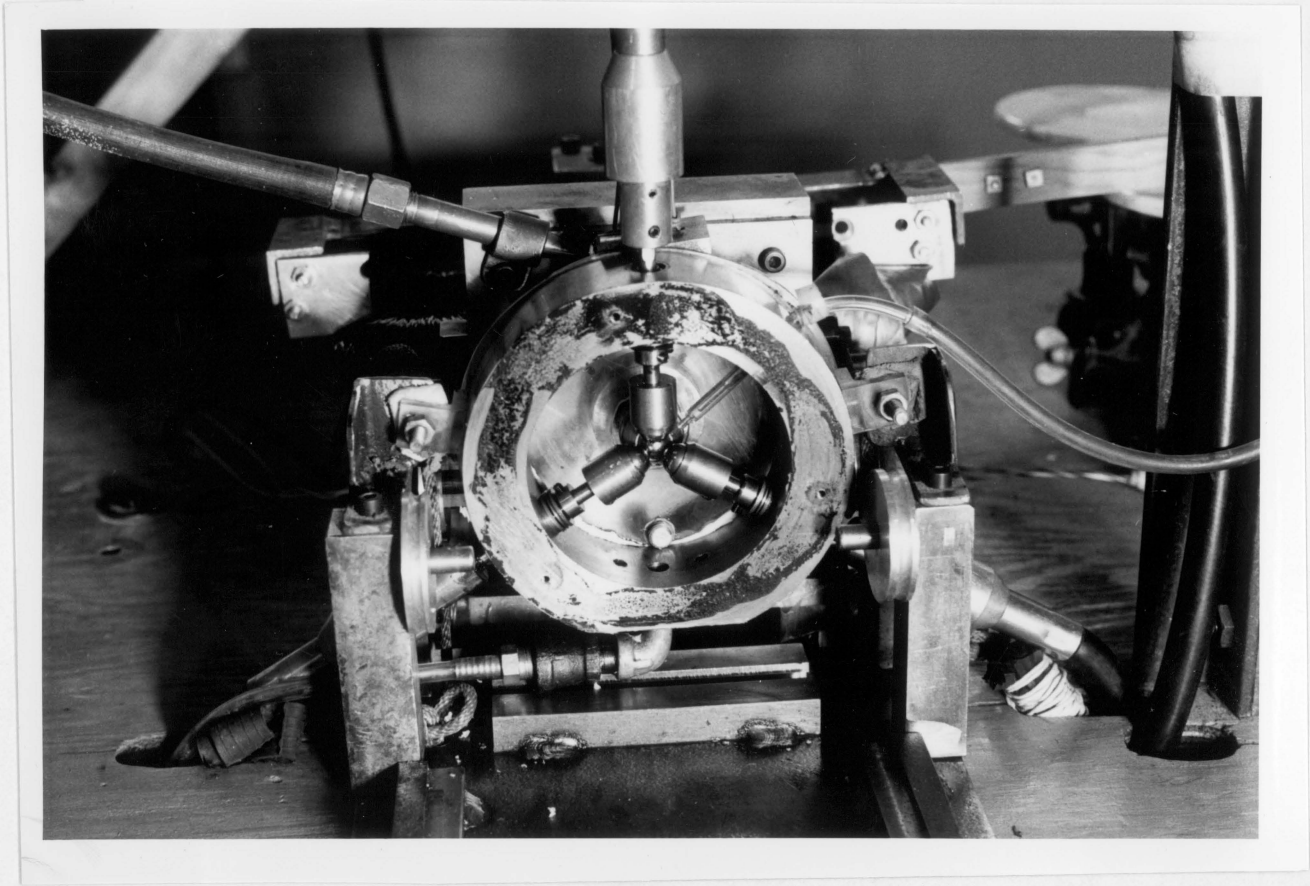

Figure 6. Driving and Driven Balls in Contact

1. Ball Rotation

The driving elements were mounted in a 4-inch diameter ball housing assembly at 120° to each other (see Figure 7). The three driving balls were pressed into the driving collets which were driven by flexible shafts. Each ball was 0.5 inch in diameter. The driving collets were locked in position by the use of an adjusting collar which was tightened by set screws. Positioning of the balls was accomplished with the aid of a centering rig (see Figure 8). The balls were each placed against the dowel of the centering rig. This was accomplished by moving the shaft and tightening the collar next to the thrust bearing. The diameter of the centering dowel corresponded to a specific angle of contact. Table I gives a number of dowel sizes and the corresponding contact angles. The driving element deflection due to yield is estimated to be 2.5×10^{-3} inches (see Appendix H). The decrease of the length of each driving element increases the space bounded by three balls. To compensate for this increase the dowel diameters were decreased 5×10^{-3} inches. The centering device was itself positioned by mating its outer edge with the inner diameter of the ball housing. This arrangement insured concentricity and symmetric placement of contact points.

The lubricant was applied by gravity feed to a point where the axis is rotation intersected the surface of the driven ball. Lubricant was carried to the contact zone by centrifugal forces.

The driving shafts were driven by flexible shafting. The flexible shafts were all rotated at the same speed and in the same direction. This was accomplished by a single gear driving three other identical gears.

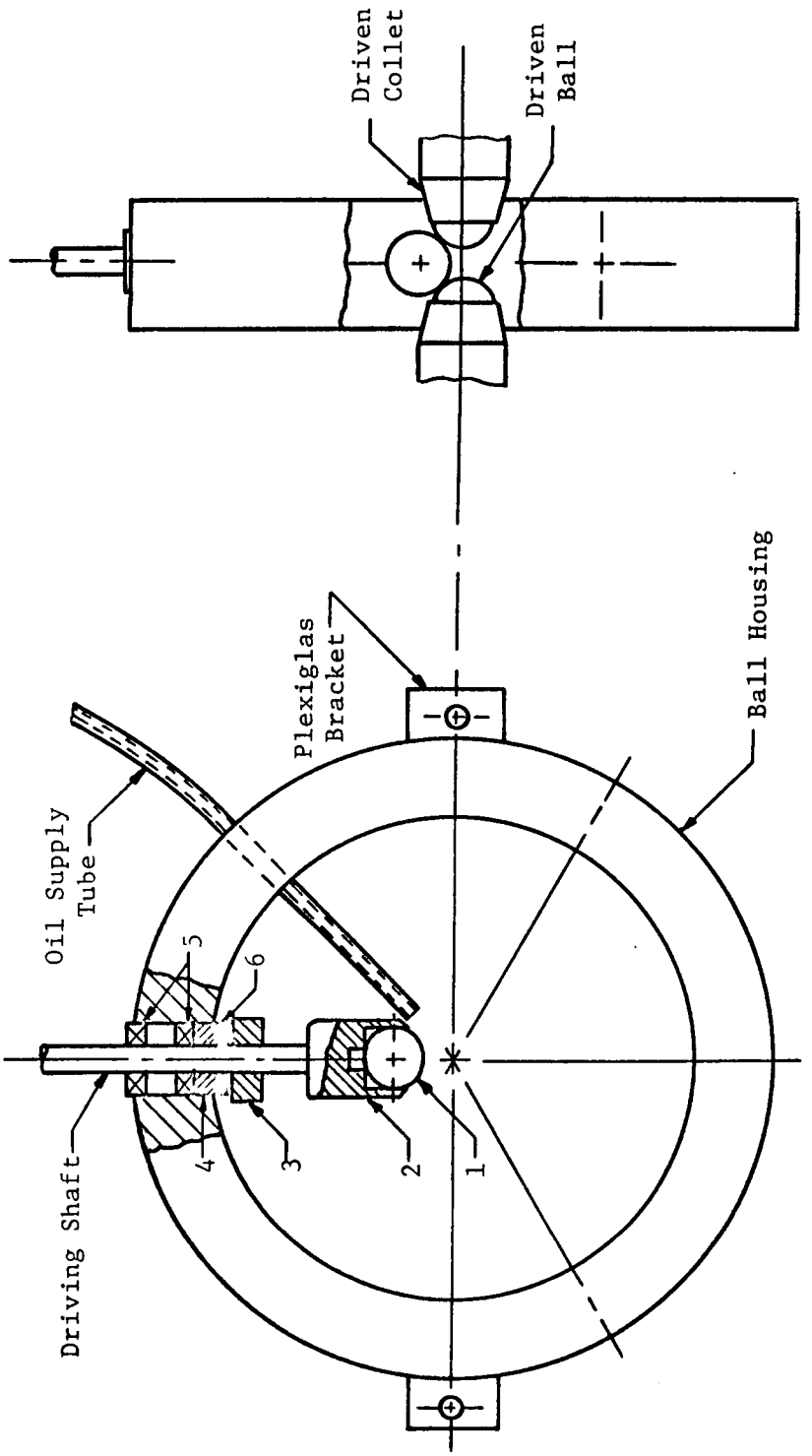

1 - Driving Ball
2 - Driving Collet
3 - Collar
4 - Bushing
5 - Radial Ball Bearings
6 - Thrust Bearing

Figure 7. Ball Housing Assembly

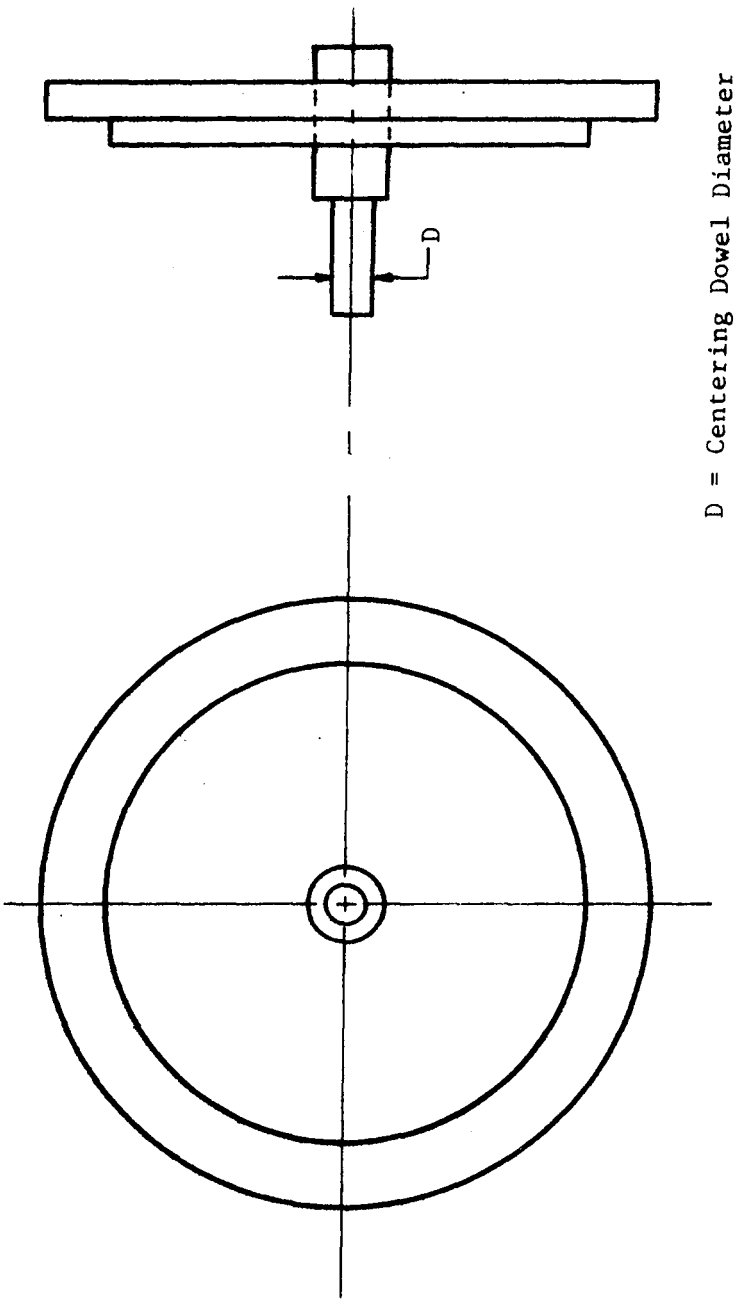

Figure 8. Ball Centering Rig

TABLE I

Ball Positioning Information

Contact Angle ψ	Dowel Diameter (inch)
40°	0.138
45°	0.202
50°	0.260
55°	0.310
60°	0.360

Dowel Diameter = 2 (Ball Diameter) (sin ψ - .500) - 2 $\Delta \ell$

For this case, Ball Diameter = .500 inch $\Delta\ell = 2.5 \times 10^{-3}$ inch (see Appendix H)

Therefore,

Dowel Diameter = (sin ψ - .505) inch

The drive system is represented in Figure 9. The pulley (5.5 inch diameter) was driven by a 12 inch pulley through the drive belt. The 12 inch pulley was keyed to the output shaft of a one horsepower variable speed motor.

To promote better seating of the driven balls, one driven shaft assembly was modified so that it applied only an axial load. The modified driven shaft is illustrated in Figure 10. The reason for this modification was to correct the misalignment which caused three different surface velocities at each contact. This arrangement resulted in balanced axial forces. The remaining driven ball could be seated with the three driving balls without interference from the modified driven shaft, since the modified shaft exerted no misaligning forces on the driving assembly.

The driven shaft (Figure 11) was rotated about its axis by the action of the rotating driving balls acting on the driven ball across the EHD film. The driven collet, the air turbine and the brake plate were all fastened to the shaft by set screws. The driven shaft was supported by a single row radial ball bearing (see Figure 12). The thrust load was carried by a needle thrust bearing.

An air turbine was mounted on the driven shaft to compensate for the bearing friction losses in the output shaft (Figure 13). Turbine pressure was supplied from a regulated air supply (0 to 80 psi). The air pressure was adjusted so that the surface velocities of the driving and driven balls were equal. It was found that equal surface velocities could be maintained for only small changes in pressure over a velocity range of 7 to 30 inches per second. The turbine pressures versus maximum Hertzian pressures were plotted in Figure 14 for 45° contact angle.

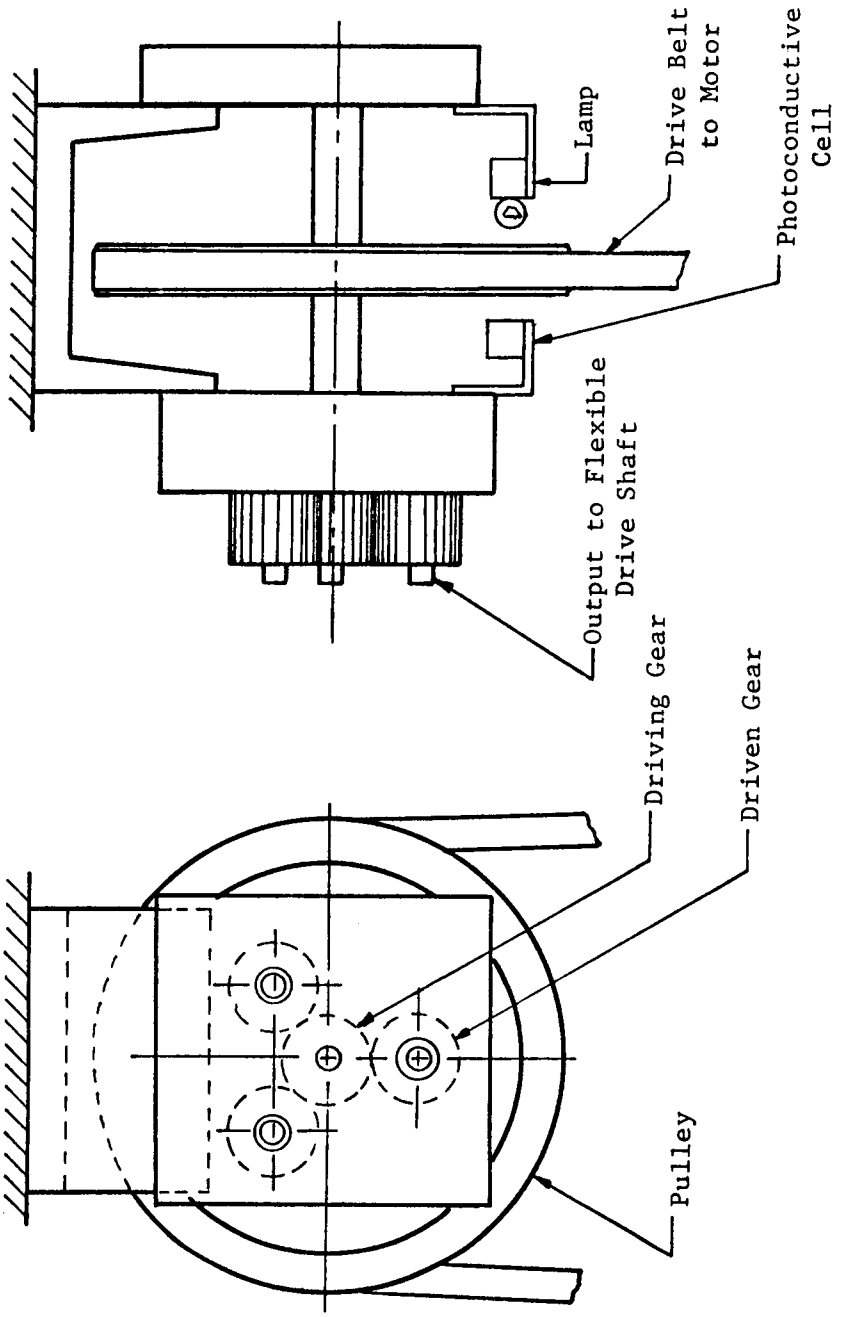

Figure 9. Gear Drive System

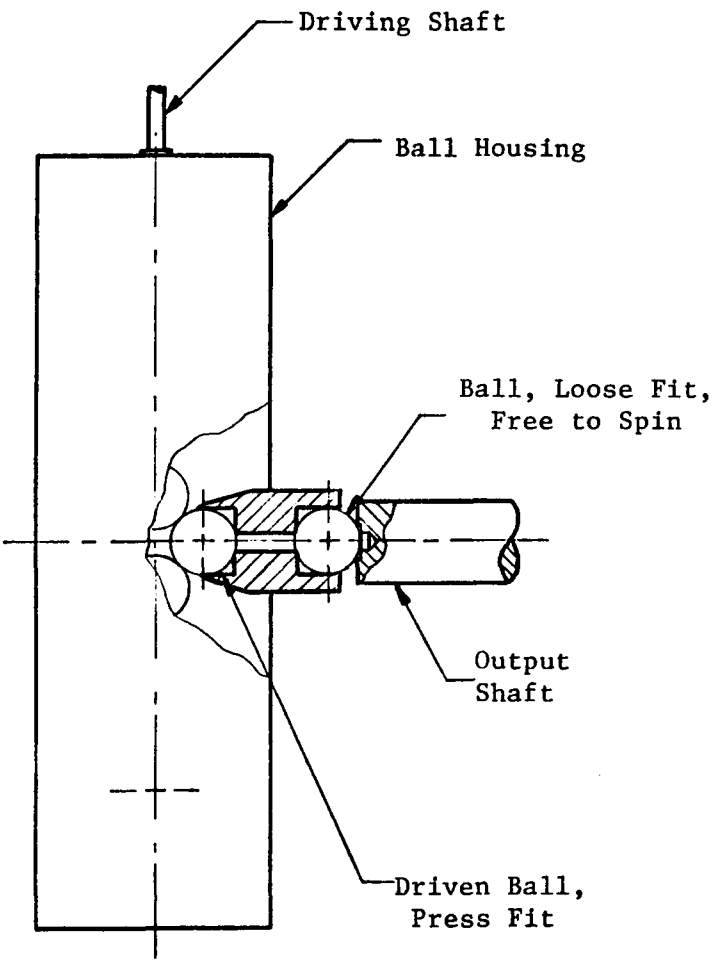

Figure 10. Modified Output Assembly

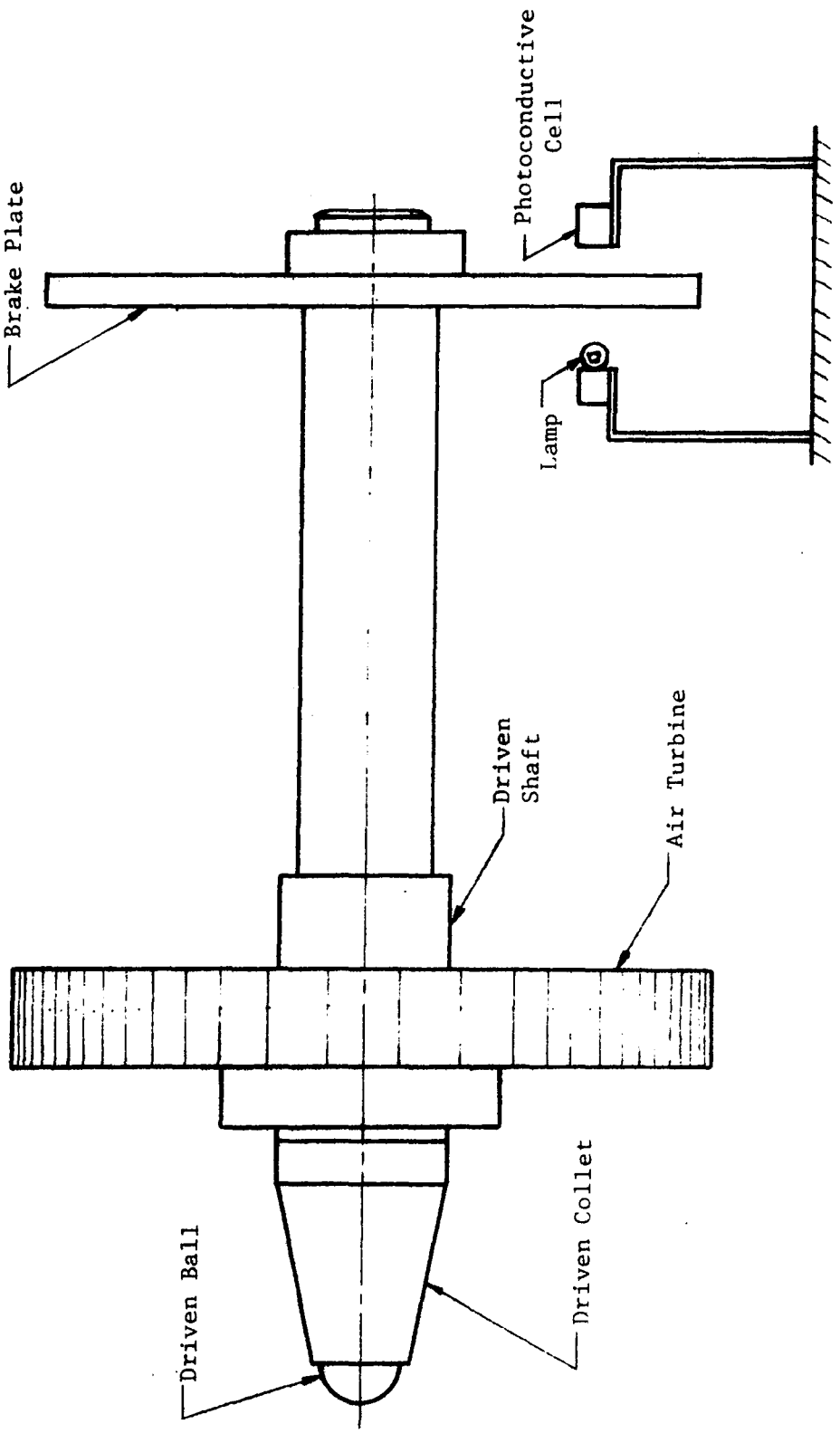

Figure 11. Driven Shaft Assembly

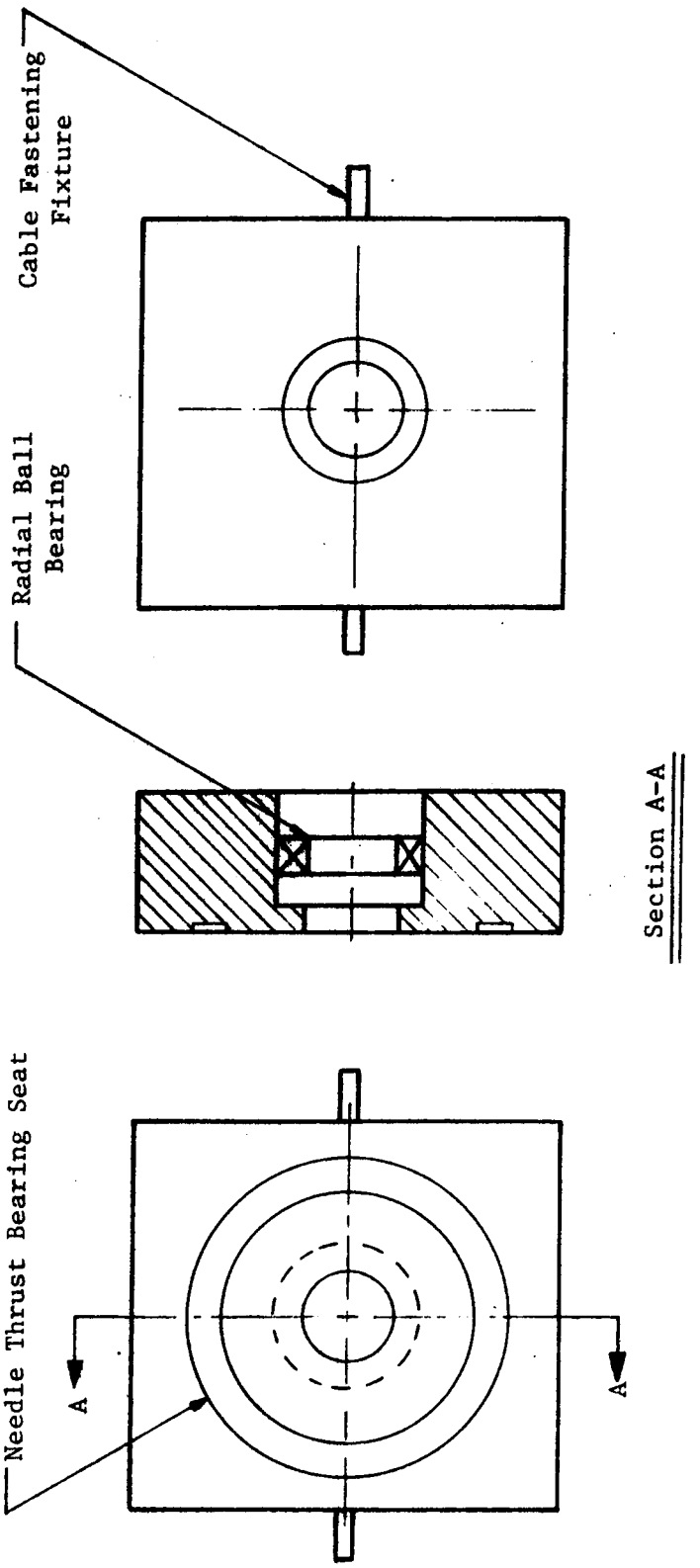

Figure 12. Bearing Block Assembly

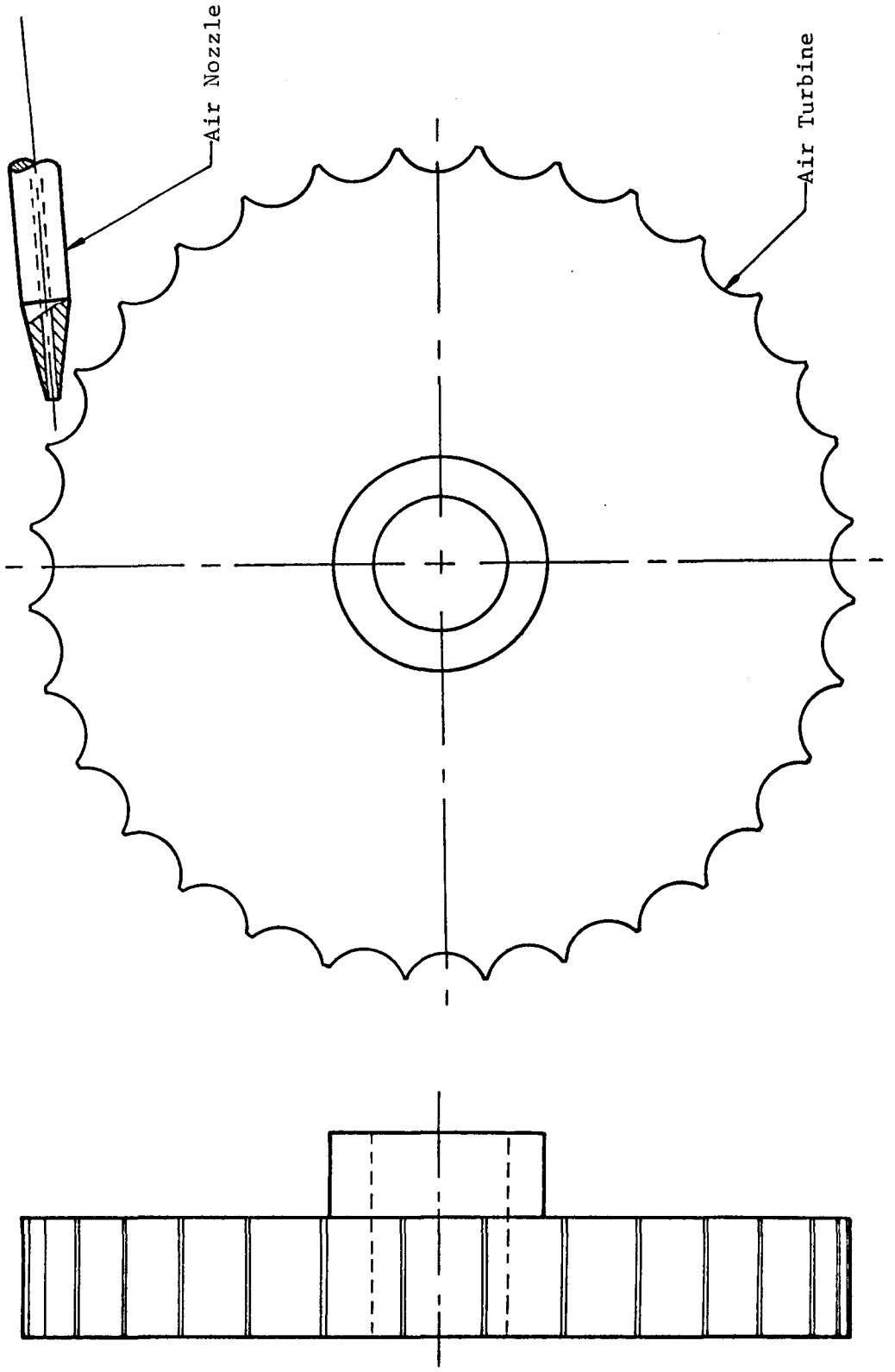

Figure 13. Air Turbine Assembly

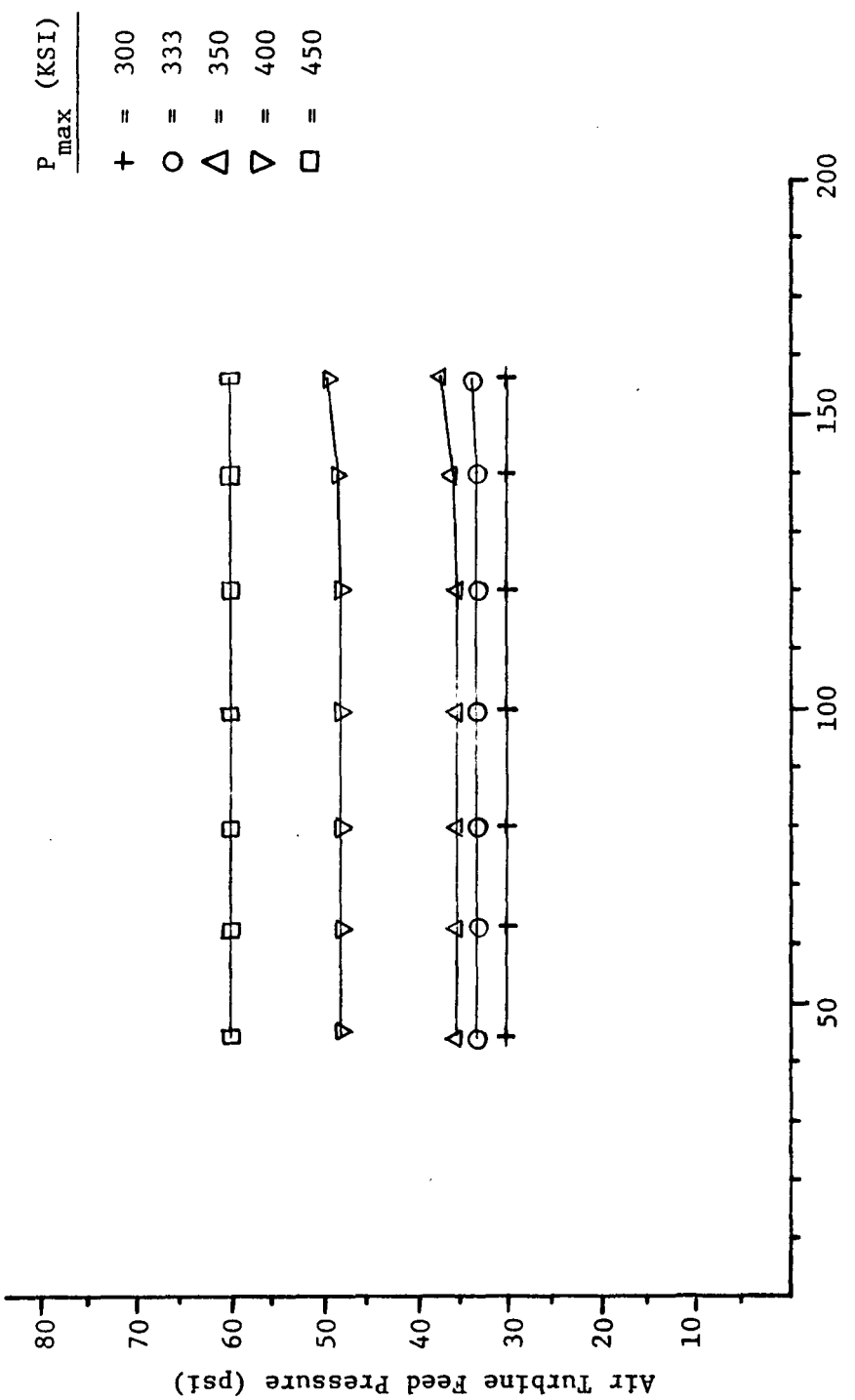

Figure 14. Air Turbine Calibration (for $\psi = 45°$)

Speed was monitored at two points. The driving speed measurement was made at the pulley connected to the main drive gear (see Figure 9). The driven speed was monitored separately at the brake plate. Both speeds were measured using photoconductive cells. Two holes were drilled in the brake plate. The photoconductive cell was mounted on one side of the plate. A small light source was also mounted directly opposite it on the other side of the plate (see Figure 11). Neither was allowed to touch the plate. They were positioned such that the holes would pass directly between the two components. The pulley was covered with a piece of sheet metal and two holes were drilled in the metal so that the same arrangement was used in both speed measurements.

The circuit schematic is given in Figure 15. As light passed over the cell, the resistance dropped, thus producing a voltage change across the output resistor. This change triggered the counter. The output voltage was controlled by changing the value of the variable resistor.

With the counter gate open for a sampling period of ten seconds, at a speed of 300 rpm, a maximum speed measurement uncertainty of 1 percent was achieved. Faster running speeds resulted in proportionately lower measurement uncertainty values; for example, at 1500 rpm the uncertainty was 0.1 percent. Appendix B outlines the procedure used to calculate the uncertainty.

2. Ball Loading

The platform load was transmitted to the balls by use of cables, pulleys, and a lever arm. The loading cables were fastened such that the axial load was on the same horizontal plane as the driven shaft as well

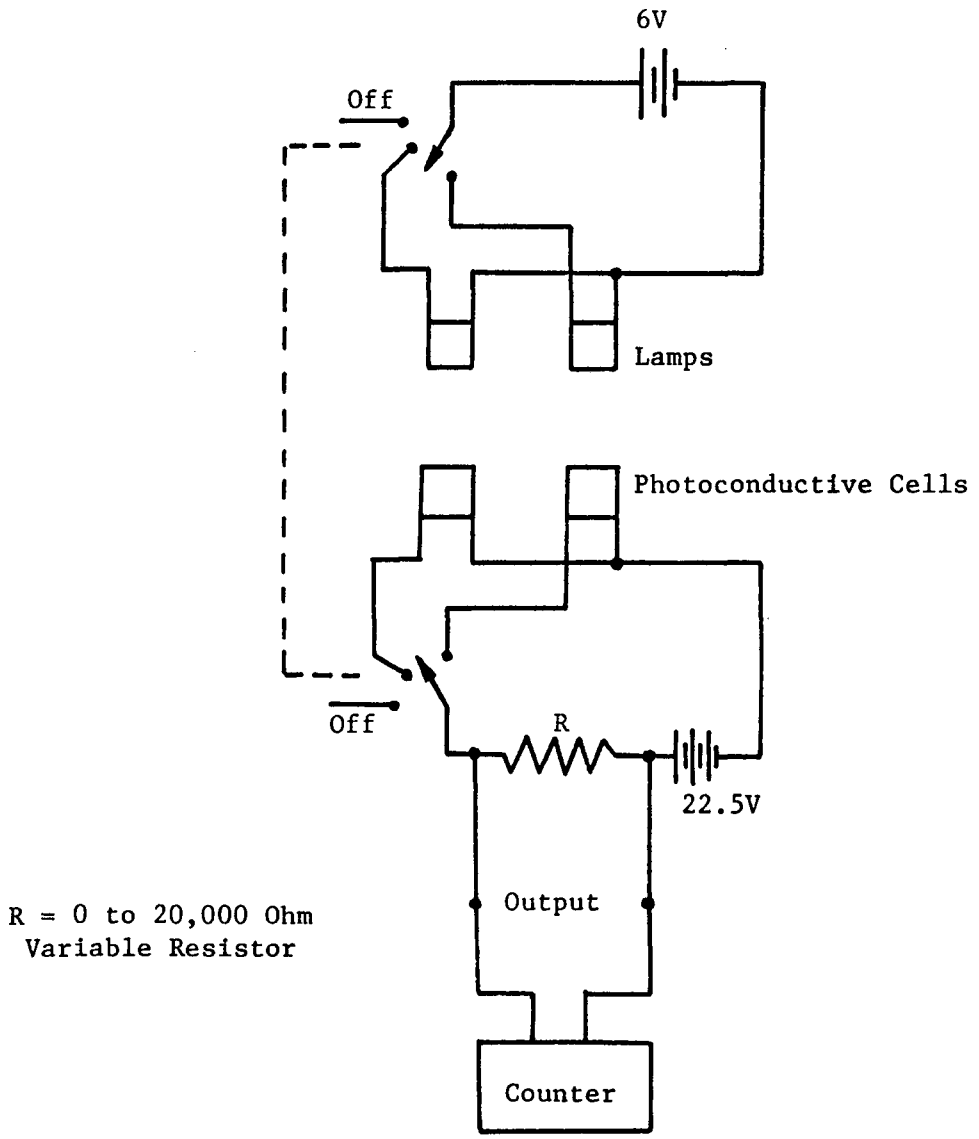

Figure 15. Speed Measurement Schematic

as being parallel to the axis of the driven shaft. The loading mechanism is diagrammed in Figure 16.

The loading mechanism was designed so that each of the four loading cables would carry an equal load. The ratio of the arms of the lever was 3.84 which produced a mechanical advantage while loading the system. For each maximum pressure and contact angle the corresponding platform loads are given in Table II.

The housing of the output shaft was fastened on the base plate which was allowed to move in a track on the base. This arrangement is shown in Figure 17.

Friction in the loading mechanism (pulleys, pivots, etc.) limited the ability of the test machine for Hertzian pressures below 300 KSI. Although friction in the loading mechanism was present for Hertzian pressures over 300 KSI, the possible uncertainties in the calculated pressured were found, by using a probe ring, to be less than 3 percent (see Appendix I).

3. Ball Retardation

The driven shaft was retarded through the use of an eddy current brake which is shown in Figure 18.

As suggested by Tallian (7), the traction curves were expected to behave like those in Figure 4. The brake to be used should not lock up for decreasing values of torque with slip. The torque developed by an eddy current brake is dependent on the speed of the disc. Therefore, it does not lock up for decreasing values of torque with slip. With this

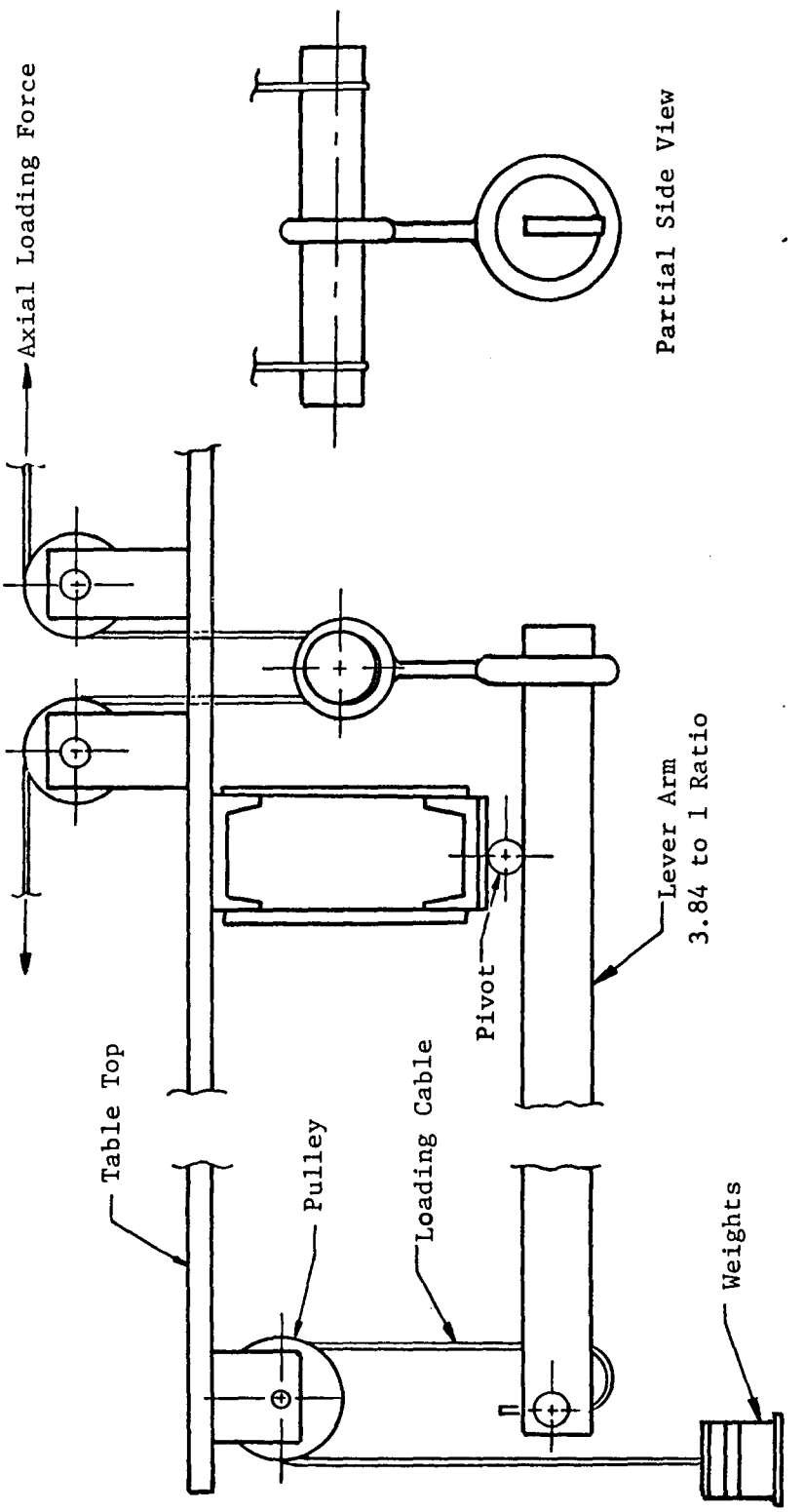

Figure 16. Loading Mechanism

TABLE II

Axial Loading Information

Platform Load (Pounds)

P_{max} (KSI)	Contact Angle ψ			
	40°	45°	50°	55°
200	1.2	1.0	0.8	0.5
250	3.9	3.4	3.0	2.6
300	7.9	7.2	6.4	5.6
333	11.4	10.0	9.3	8.2
350	13.5	12.4	11.1	9.8
400	21.0	19.3	17.4	15.5
450	30.6	28.1	25.5	22.7
500	42.5	39.2	35.6	31.8
550	57.2	52.7	47.9	42.8
600	74.7	68.9	62.6	56.1
650	95.5	88.0	80.0	71.8
700	114.5	110.3	100.4	90.0

Platform Load = (1.56) [(Normal Load) (cos ψ) - 1.05]

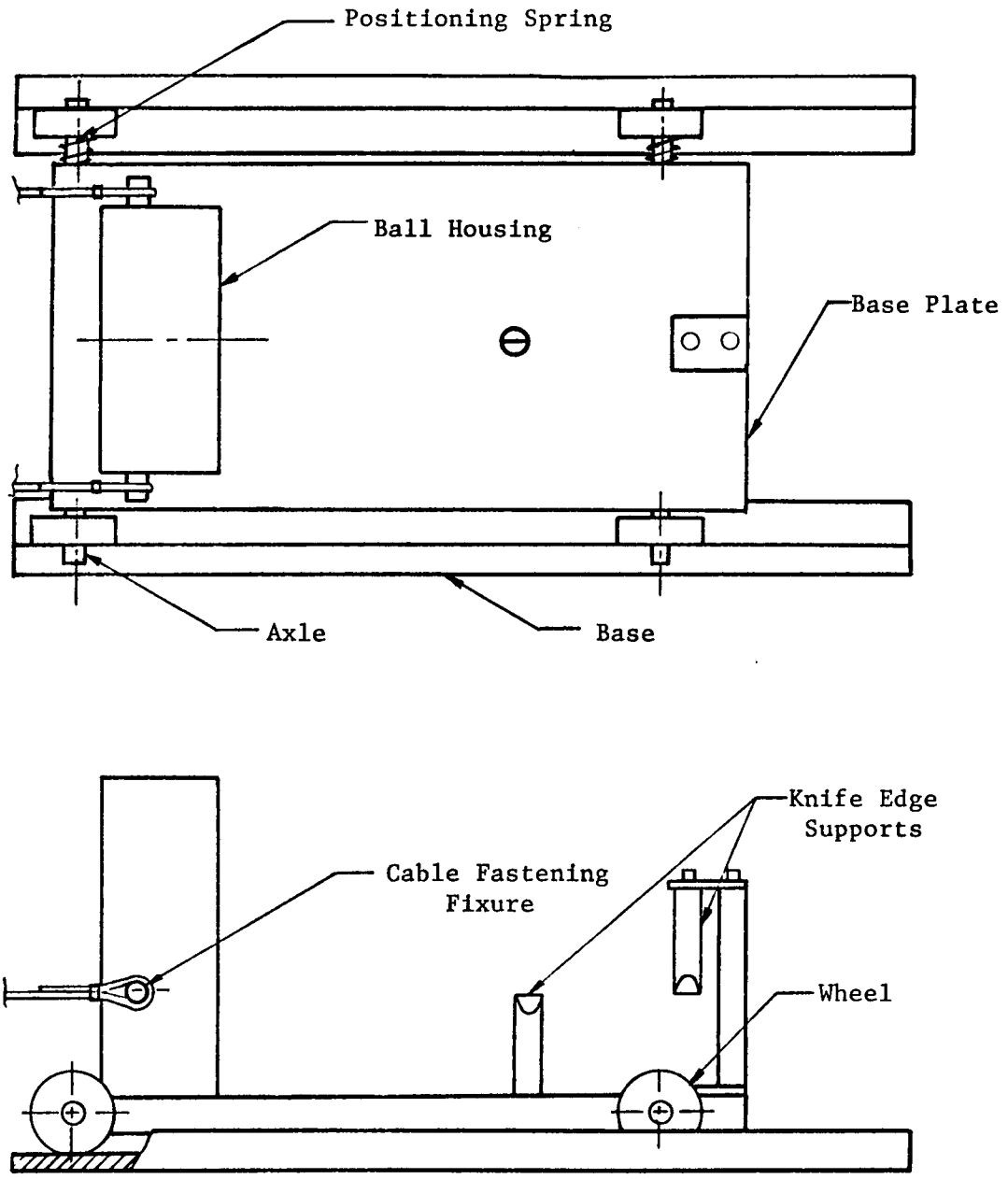

Figure 17. Base Assembly

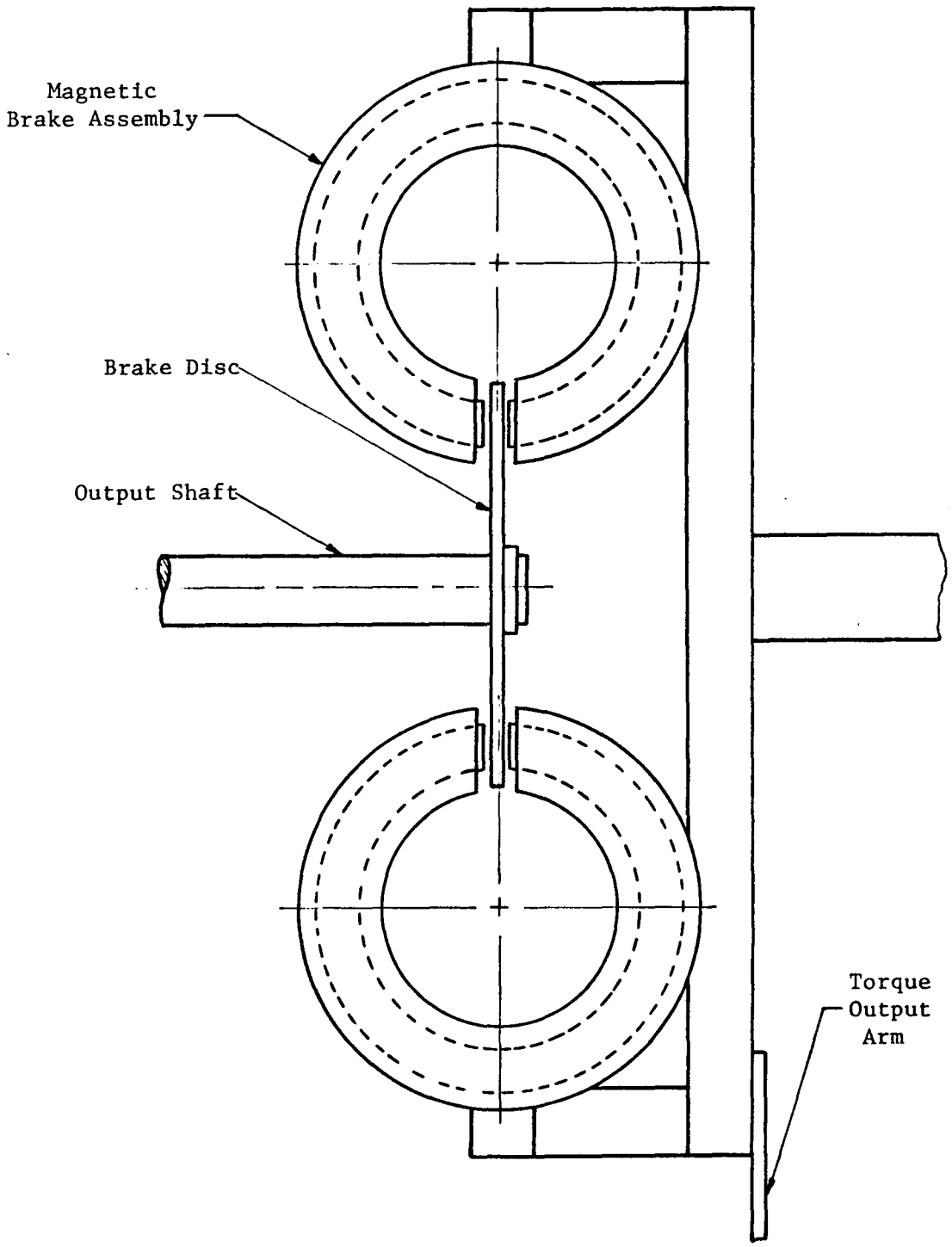

Figure 18. Eddy-Current Brake Assembly

braking the system the traction can be measured up to 85 percent of slip*. The maximum voltage that can be applied to the eddy current brake is 100 Volts, which sets the higher limit for percent sliding.

The eddy-current brake was designed by Mr. P. V. Blarigan, according to the methods given in Reference 17. The magnets had very little leakage, being round with no open ends (see Figure 19). Also, the windings were placed close to the gap where they would do the most good.

Both magnets were designed to produce a maximum retarding torque of 10 in-lb at 1200 rpm according to the method outlined by Drysdale and Jolley (18). The procedure is in Appendix F.

Two knife-edge supports, like those used in a balance, were used to hold the brake assembly in position and to minimize friction in the pivots (see Figure 20). The traction force was measured by the torque exerted on the pivoted magnet assembly. A lever arm which was attached to the magnets rested on a platform balance. The distance from the axis of the output shaft to the tip of the lever arm was one foot. A 0 to 200 gram platform balance was used for measurements.

4. Checking the Metallic Contact

The basic function of a lubricant is to prevent contact between sliding surfaces. Therefore, it has to be checked if there is a lubricant film or not. If metallic contact occurs the traction forces

---

*Percent sliding $= \frac{u_1 - u_2}{u_1} \times 100 = \frac{\Delta u}{u_1} \times 100$

where Δu = relative surface velocity of the driving ball to that of the driven ball at the center of contact area

u_1 = surface velocity of the driving ball at the center of the contact area.

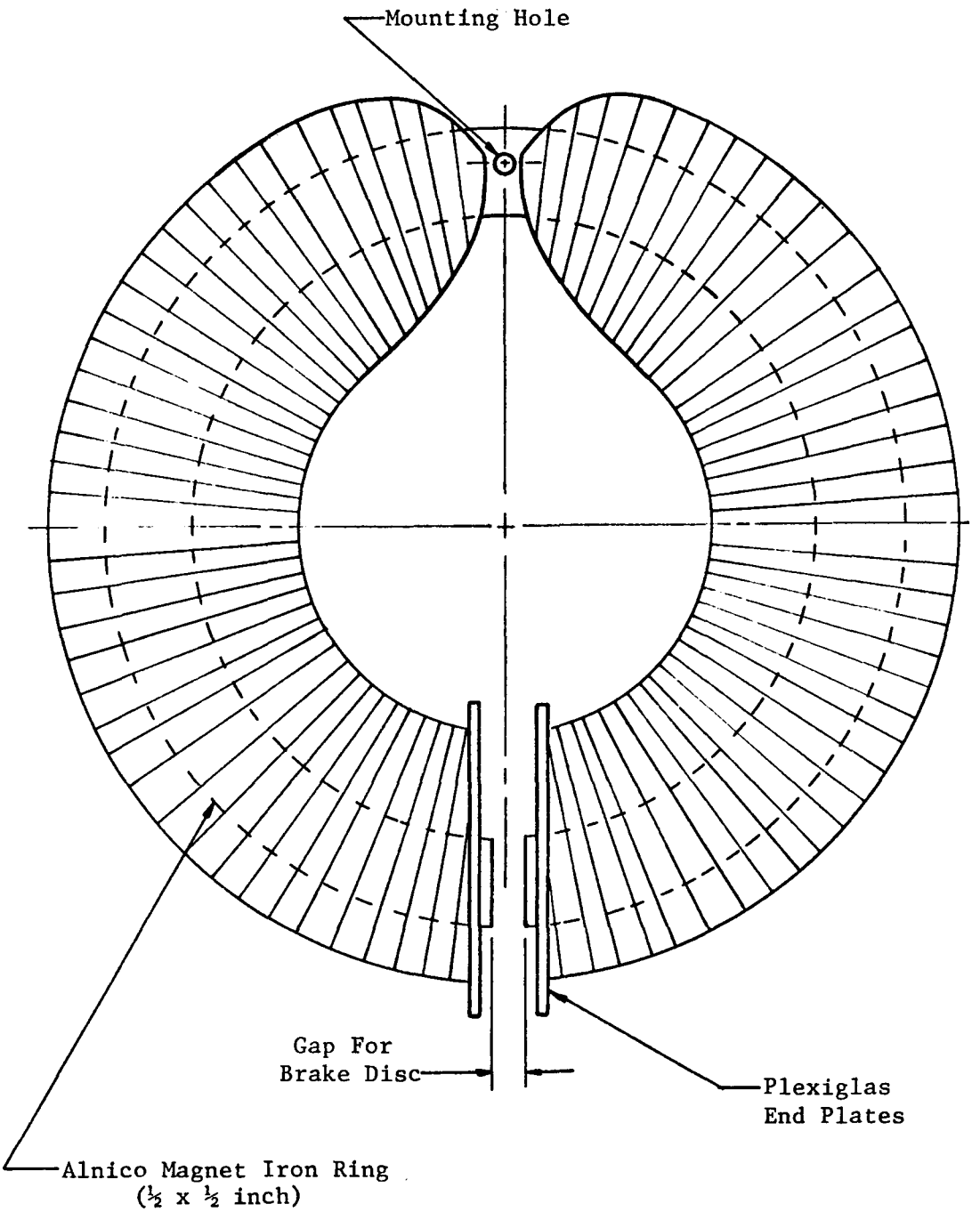

Figure 19. Magnetic Brake

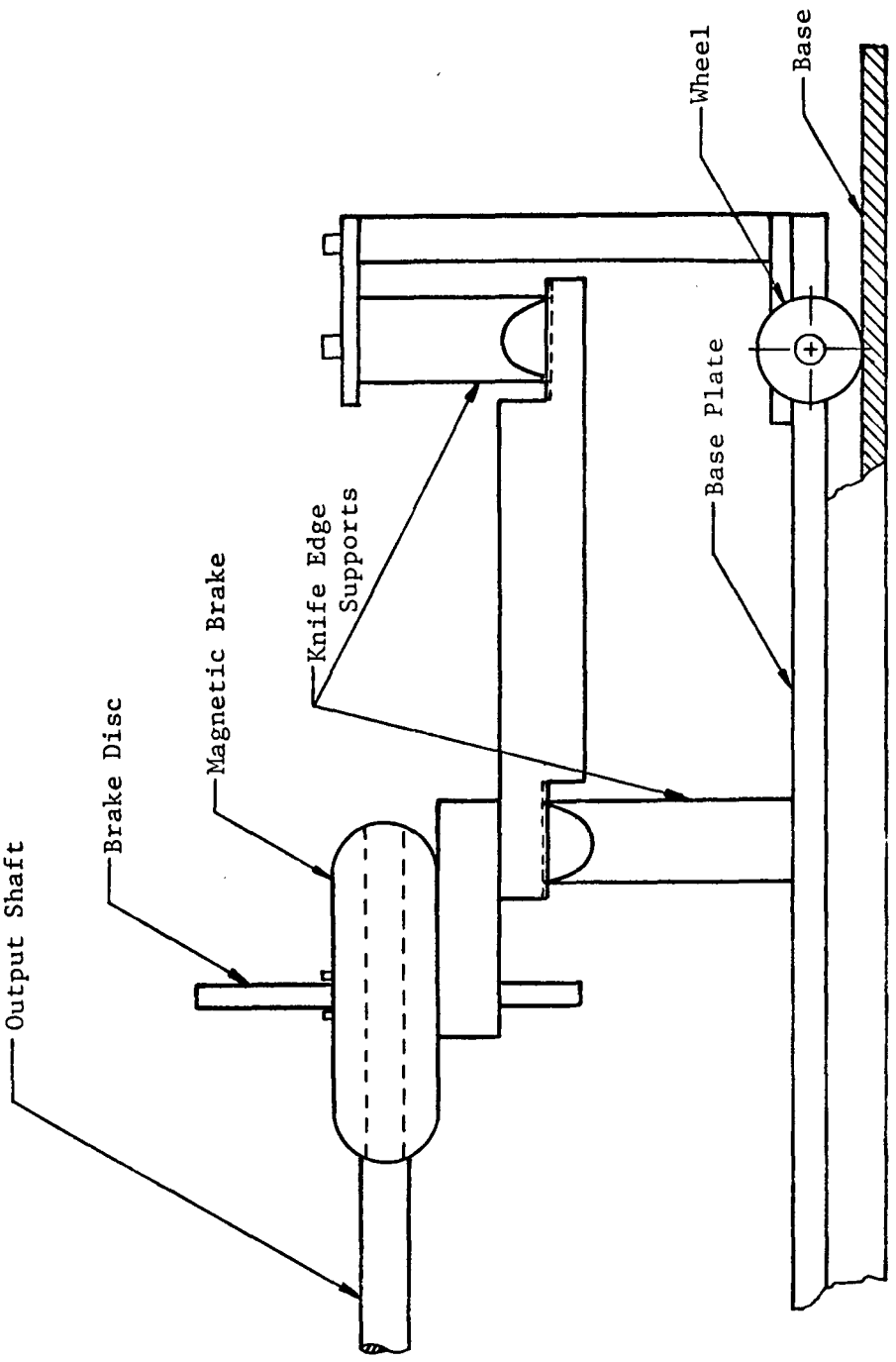

Figure 20. Brake Pivot Assembly

measured will be the sum of the lubricant shear forces, and the deformation and adhesion forces between contacting asperities.

In order to insure that only lubricant shear forces were measured during the tests, a method developed by Furey (18) was used to detect metal-to-metal contact. The circuit used for this purpose is shown in Figure 21 schematically, where point A represents the output ball and point B represents any one of the three input balls. The ball housing and the output shaft support were insulated very carefully such that when there was a lubricant film between the driving and the driven balls the voltage recorder would draw a constant 15 mVolt line. If the lubricant film was broken, because of the metallic contact, the circuit would be shorted and 0 Volts would be recorded. In general, at the beginning of metallic contact the voltage was found to oscillate rapidly suggesting that metallic contact was discontinuous.

The average resistance of an oil film in such a dynamic system is, therefore, a time average, that is, a measure of the percent of the time that metallic contact occurs. Based on this fact, one can show that the recorded voltage data would give an idea about the frequency of metallic contact for high values of slip. Metallic contact was also monitored by an oscilloscope for slip ranges between 0 to 20 percent.

C. Experimental Procedure

The traction coefficient was investigated as a function of four variables; the contact angle, maximum Hertzian pressure, rolling speed,

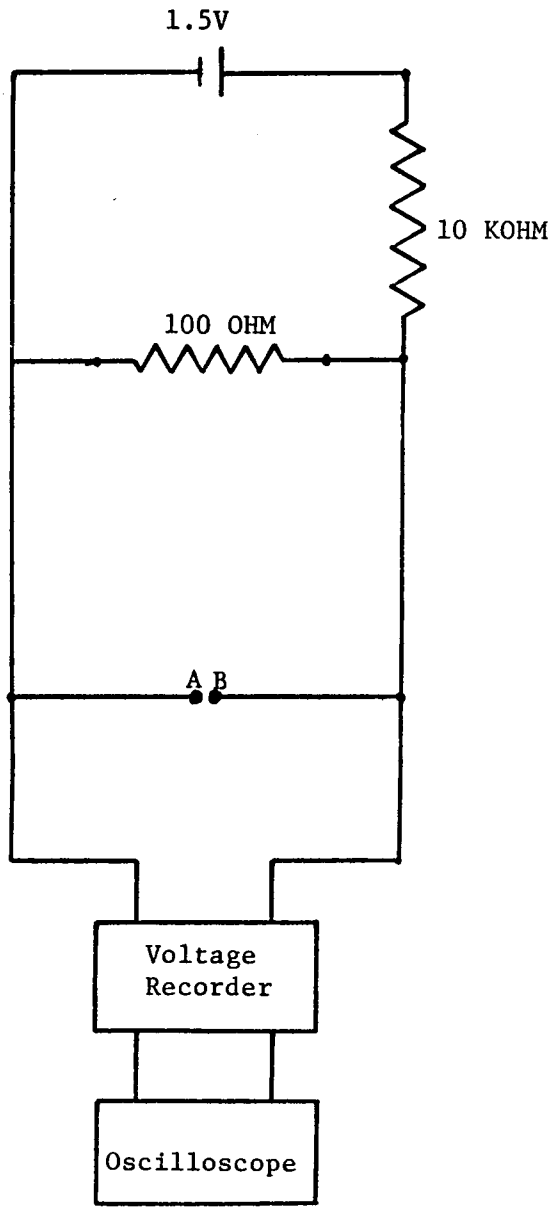

Figure 21. Determination of Metallic Contact Schematic

and sliding speed. All tests were run with a synthetic hydrocarbon base lubricant with additives to give extremely low-foaming characteristics. The properties of the lubricant are listed in Table III.

The procedure followed was relatively simple. The position of the driving balls were set at the desired angle using the ball centering rig (Figure 8). A plastic cover plate was mounted on each side of the ball housing to prevent oil from being thrown all over the test equipment. The ball housing was then suspended by elastic cables and the flexible shafts were mated to the driving shafts. The housing was centered between the driven balls, and the driven shafts were guided in to nest with the three driving balls. After aligning the ball housing in position it was fastened to the base by Plexiglas brackets. The vibration of the ball housing was partially damped by the use of foam washers which were placed between the housing brackets and the brackets of the base. Next, weights were added to the loading platform to get the desired maximum Hertzian pressure. Lubricant was then provided from a container which was placed above the ball housing and the level was kept constant as much as possible so that the flow rate could be assumed to be steady. The lubricant entered the ball housing assembly through a hole drilled at an angle about 30° from the vertical driving shaft. Next, the variable speed drive motor was started. Finally, the desired driving speeds were set.

The input and output speeds were measured by an electronic counter at each braking load starting with zero load. Only one reading was

TABLE III

Properties of the Lubricant

(Synthetic Cycloaliphatic Hydrocarbon)

Property	Typical Value
Pressure viscosity coefficient (psi^{-1}) at 50 KSI	2.19×10^{-4}
Kinematic Viscosity (cs)	
at -20°F	31,600
100°F	22.7
210°F	3.68
Pour Point (°F)	-45
Density (g/cc)	
at 100°F	0.886
200°F	0.850
300°F	0.814
Coefficient of expansion (1/°F)	4.42×10^{-4}
Vapor Pressure (mm Hg abs)	
at 350°F	12
Specific Heat (BTU/lbm °F)	
at 100°F	0.460
200°F	0.514
300°F	0.569
Thermal Conductivity (Btu/hr. ft. °F)	
at 100°F	24.4
200°F	21.4
300°F	18.4
Flash Pt., (°F)	300
Fire Pt., (°F)	325
AIT, (°F)	600

recorded for the input speed since there was not a significant variation in it during any test run. Output speeds were monitored three successive times at each load and an average taken. For each contact angle the test was randomized considering the two variables, namely, the maximum Hertzian pressure and the rolling speed so that the results would not be grossly affected by the atmospheric pressure changes, inlet temperature of the lubricant, humidity changes and some other unknown factors that could be present during the test. At each brake load, the load was measured using the platform balance. The weights were progressively shifted until the balance needle was at rest on zero. After the normal load and speed were set, the angular velocity of the output shaft would oscillate, the oscillations gradually dying out. Balance readings were taken after the oscillations. It is found that this procedure resulted in an overall load measurement accuracy to within $\pm$ 2 percent. After the braking force was recorded, a greater braking load was applied by increasing the current flowing through the eddy-current brake. This procedure was repeated until one of the following conditions occurred:

a) The maximum allowable current in the eddy-current brake was reached.

b) Metal-to-metal contact was recorded.

After tests at pressures of 300 KSI, 333 KSI, 350 KSI, 400 KSI and 450 KSI were run, the driving balls were set for a new contact angle and and entire randomized procedure was repeated for different pressures and rolling velocities. This testing scheme was duplicated for each of the three different contact angles (40°, 45°, and 50°).

After the whole procedure was completed, similar tests were run to get more detailed data for slip values between 0 to 20 percent. This is the portion of the traction curves which is important in applications involving traction drives.

For each test run at constant contact angle, load, rolling velocity, and percent slip, the required amount of time for making the measurements averaged 10 minutes per run. The coefficient of traction and percent slip were then calculated and plotted (see Appendix G).

The same set of balls were used in all experiments. The ball surfaces were examined by a microscope (1 X 1000 magnification) and no visible damage was observed.

IV. RESULTS

The test results are plotted in two sets of figures. Each graph depicts the coefficient of traction versus the percent slip. Figures 22 through 36 present traction curves for slip ranging from 0 to 100 percent. Figures 37 through 51 present traction curves for slip ranging from 0 to 22 percent. The first five figures in each of these sets are for 40° contact angle. The next five are for 45° contact angle. The final five figures are for 50° contact angle.

For each contact angle, five different maximum Hertzian pressures were used, those being, 300 KSI, 333 KSI, 350 KSI, 400 KSI, and 450 KSI.

For each contact angle and maximum Hertzian pressure, the driving balls were rotated with the angular velocities 44.3, 62.8, 94.25, 125.7, and 157.1 rad/sec. The resulting surface rolling velocities of the driving balls are listed in Table IV.

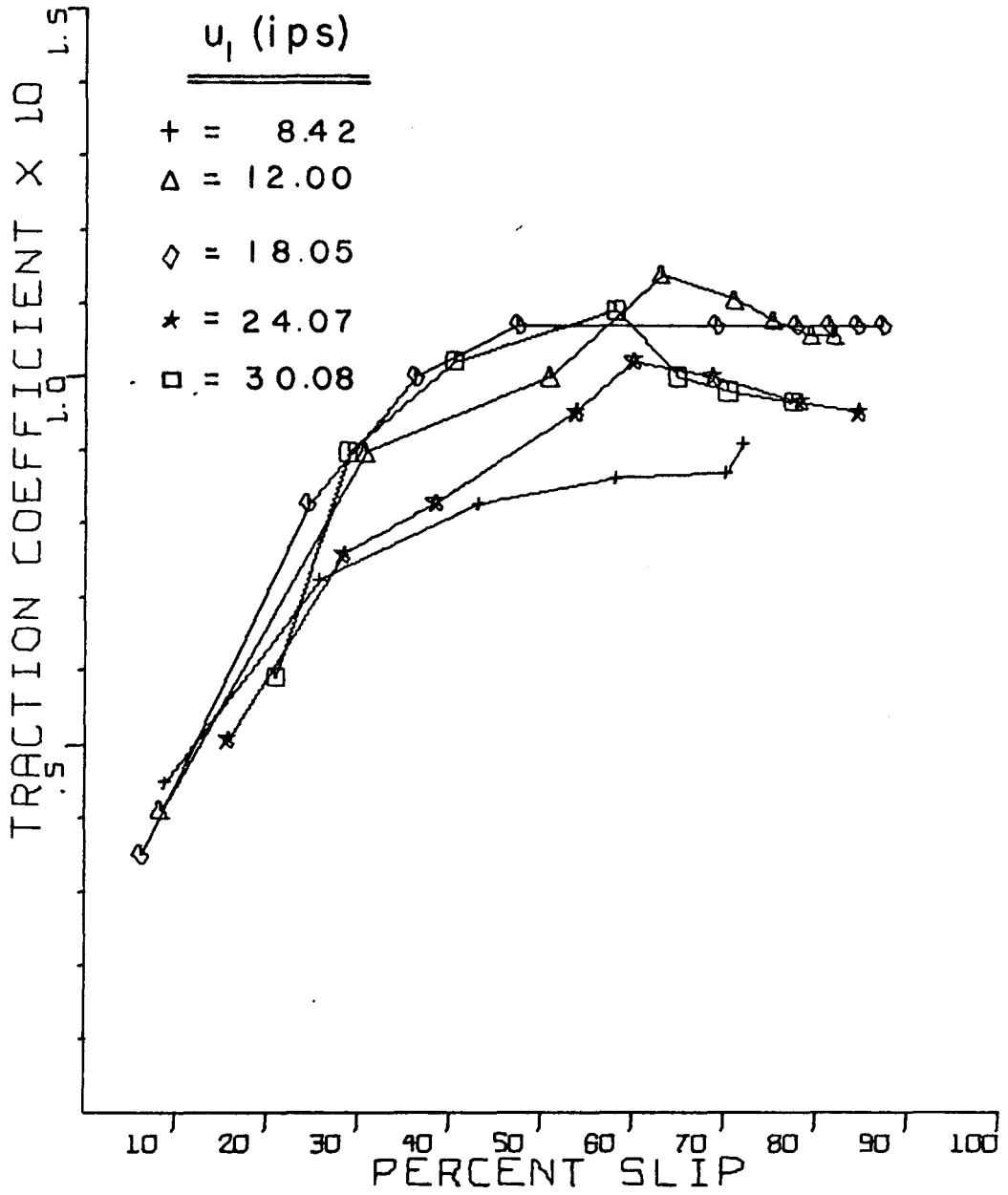

Figure 22. 40° Contact Angle and 300 KSI Maximum Contact Pressure Test Results

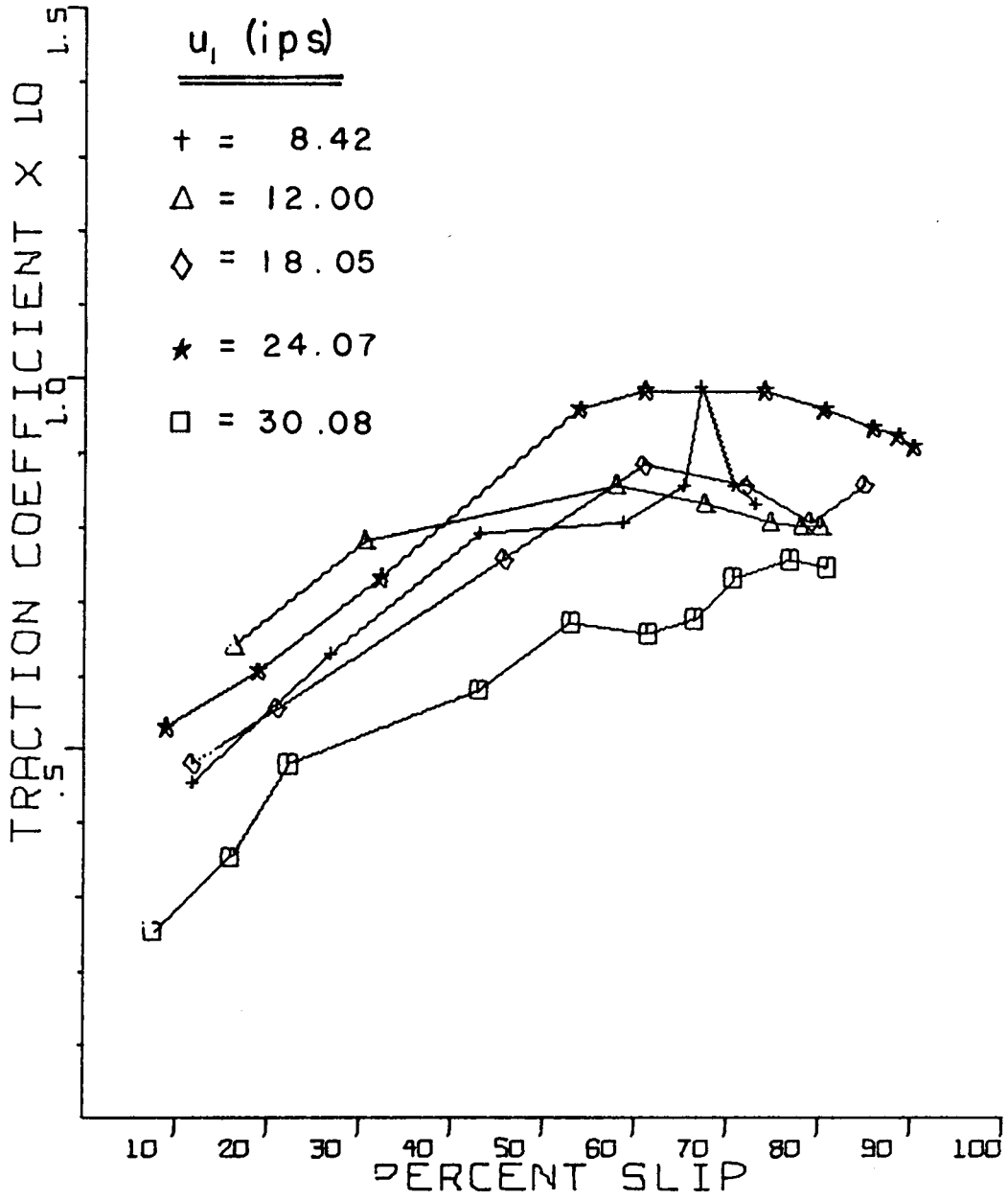

Figure 23. 40° Contact Angle and 333 KSI Maximum Contact Pressure Test Results

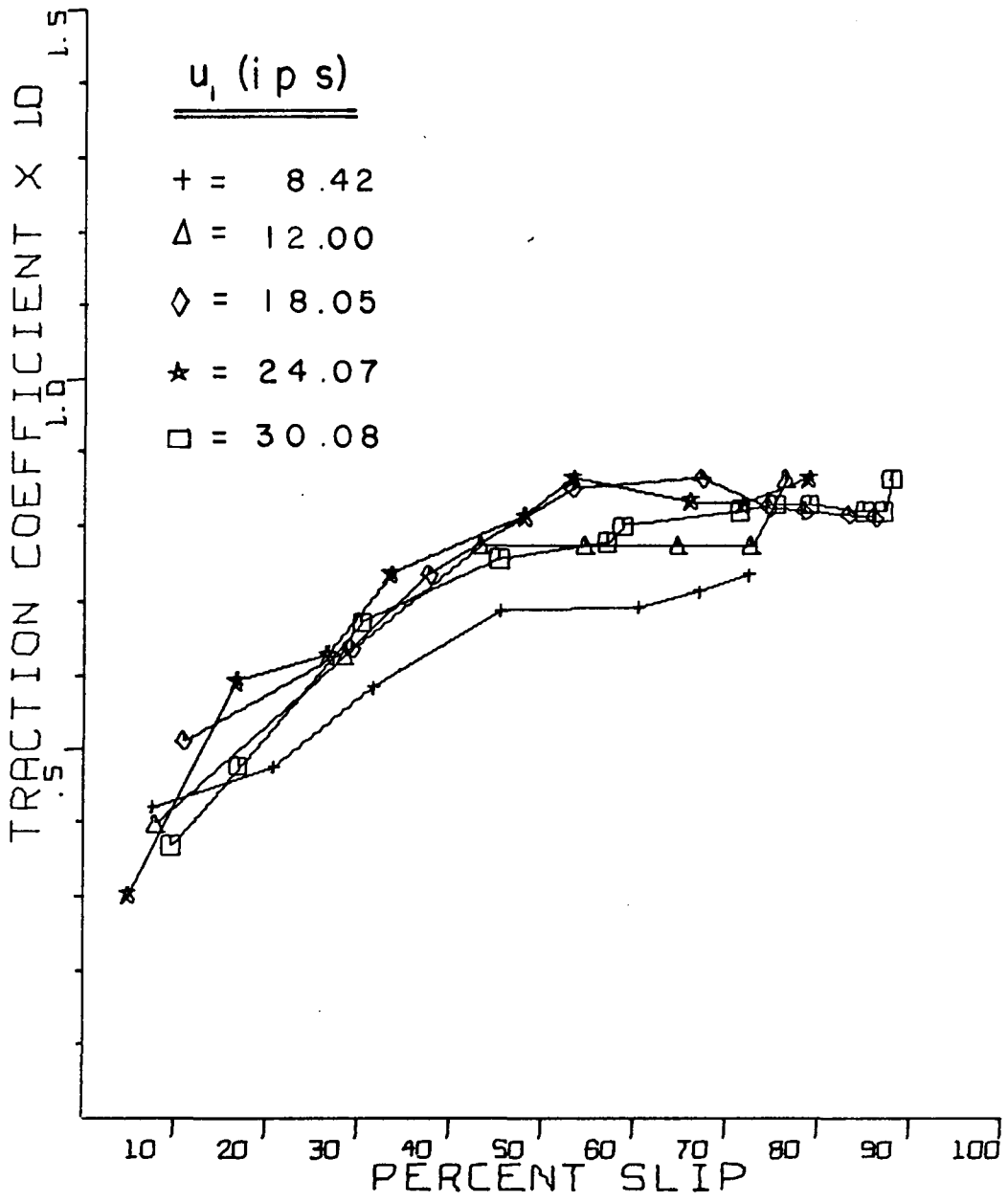

Figure 24. 40° Contact Angle and 350 KSI Maximum Contact Pressure Test Results

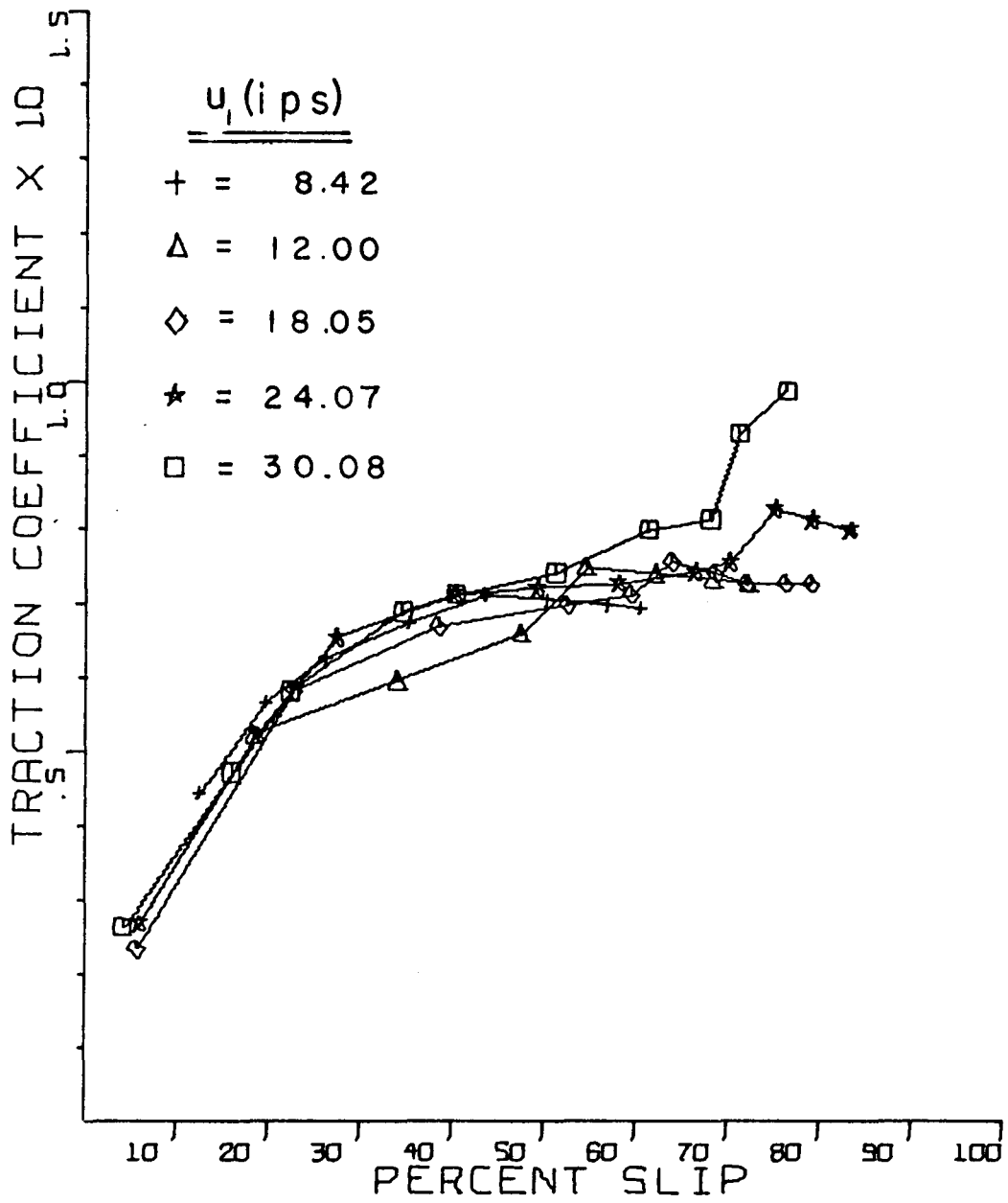

Figure 25. 40° Contact Angle and 400° KSI Maximum Contact Pressure Test Results

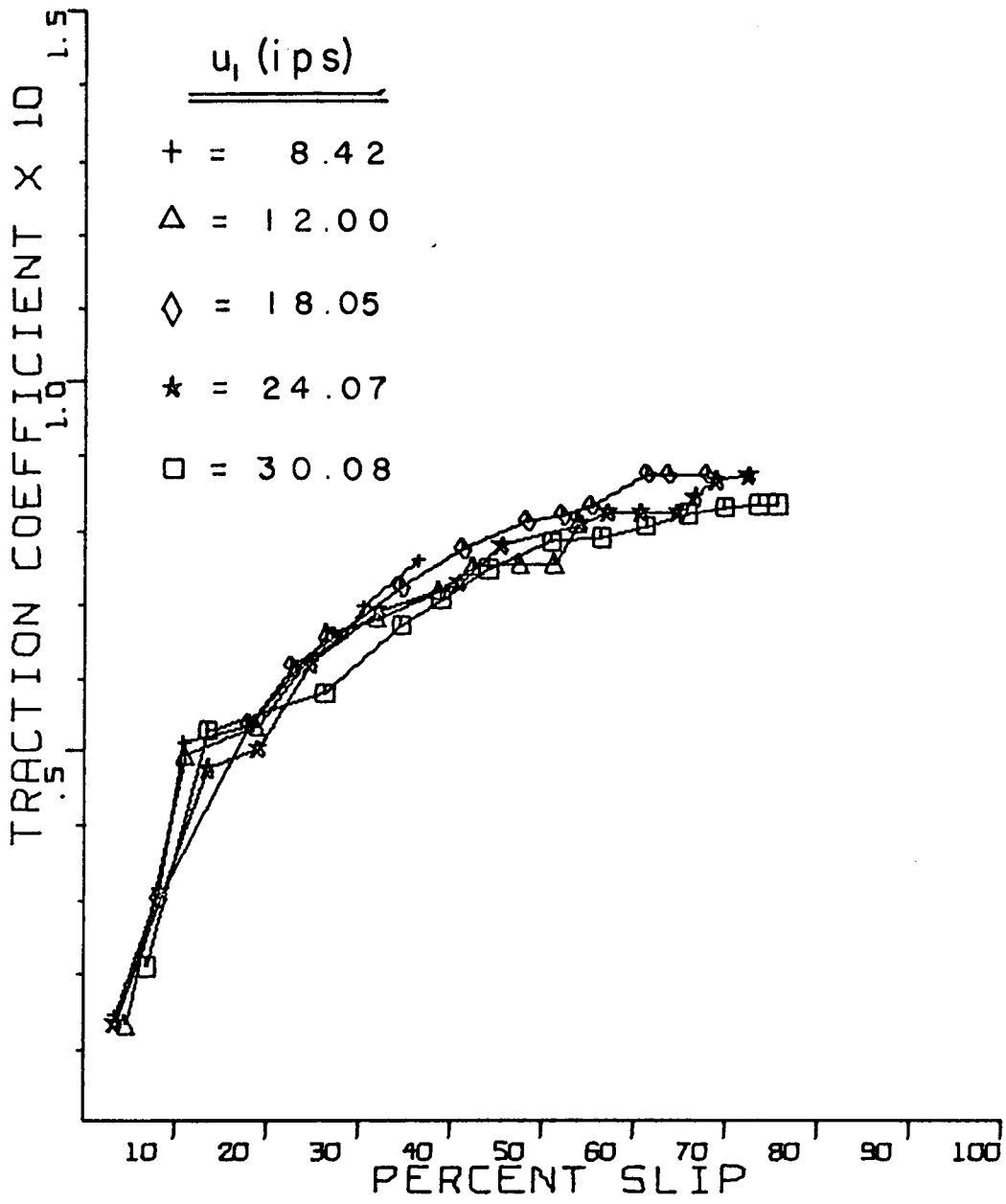

Figure 26. 40° Contact Angle and 450 KSI Maximum Contact Pressure Test Results

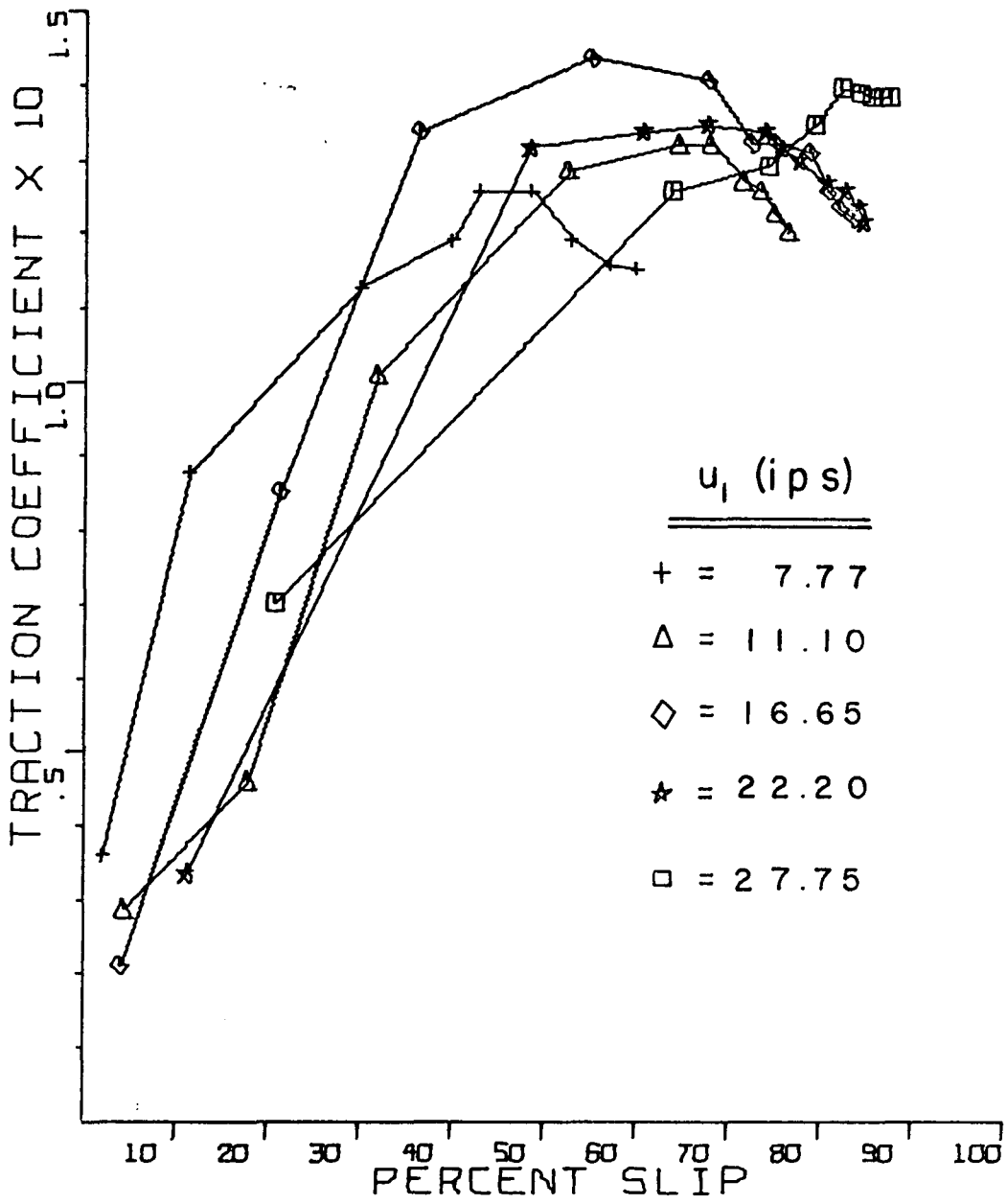

Figure 27. 45° Contact Angle and 300 KSI Maximum Contact Pressure Test Results

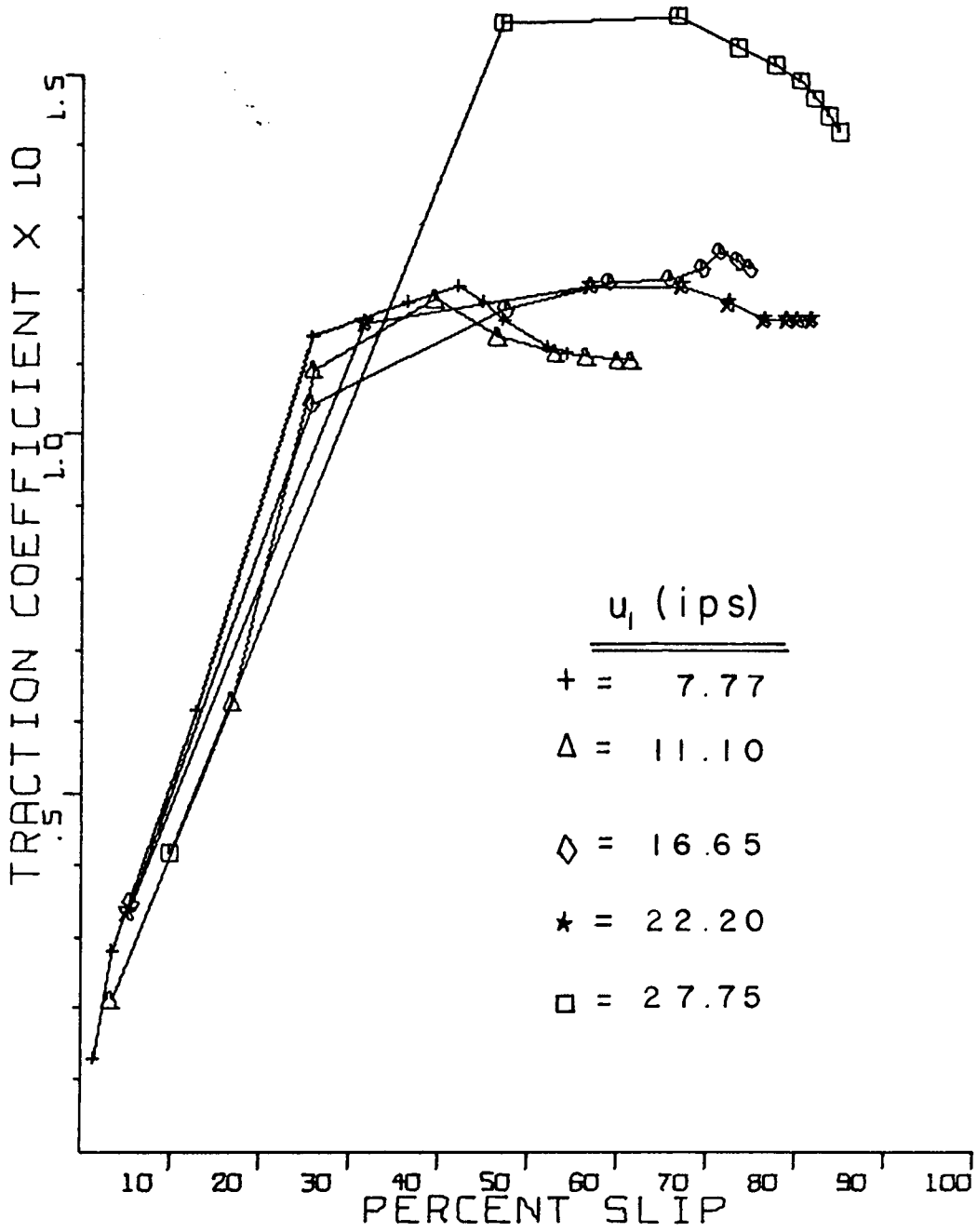

Figure 28. 45° Contact Angle and 333 KSI Maximum Contact Pressure Test Results

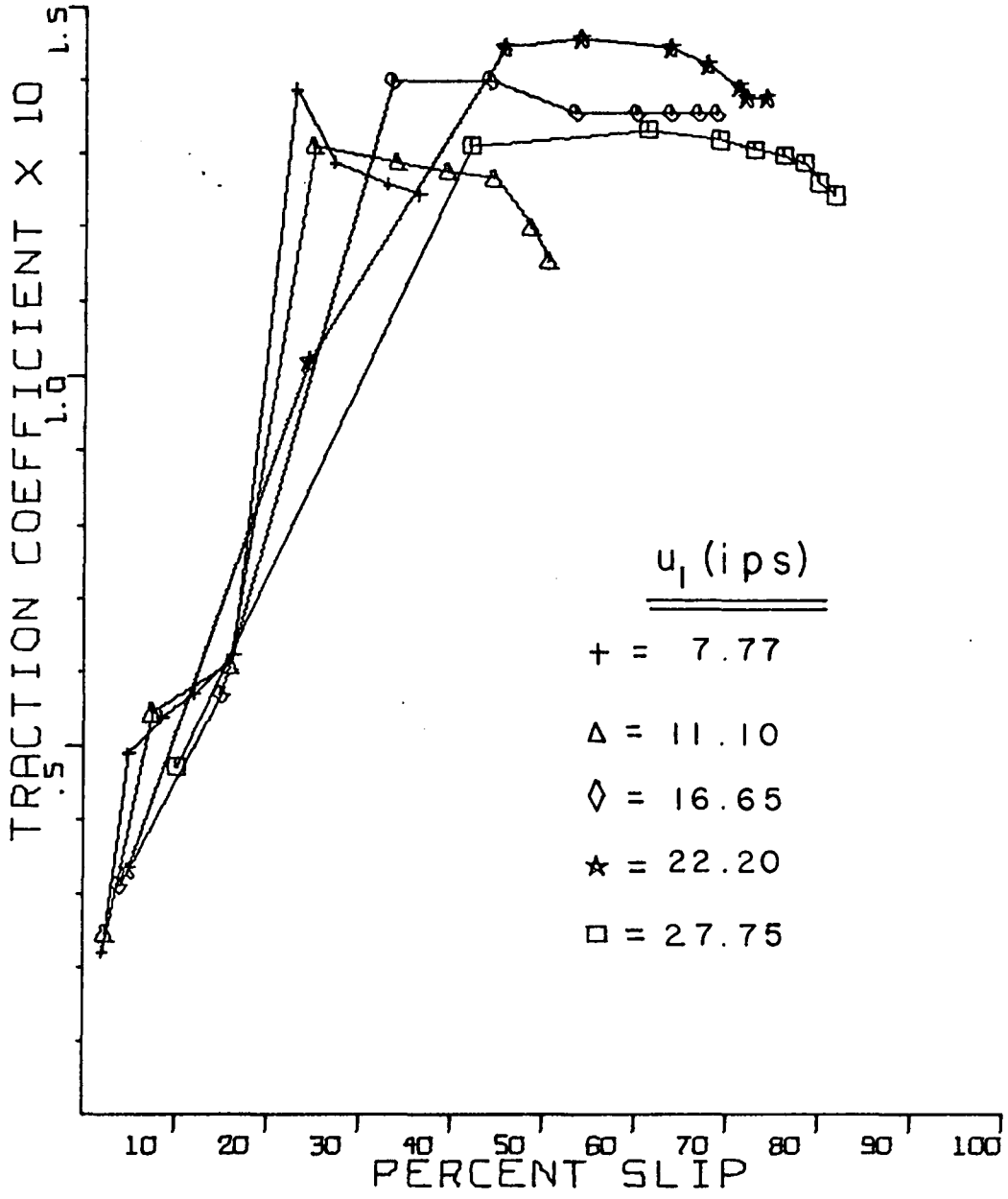

Figure 29. 45° Contact Angle and 350 KSI Maximum Contact Pressure Test Results

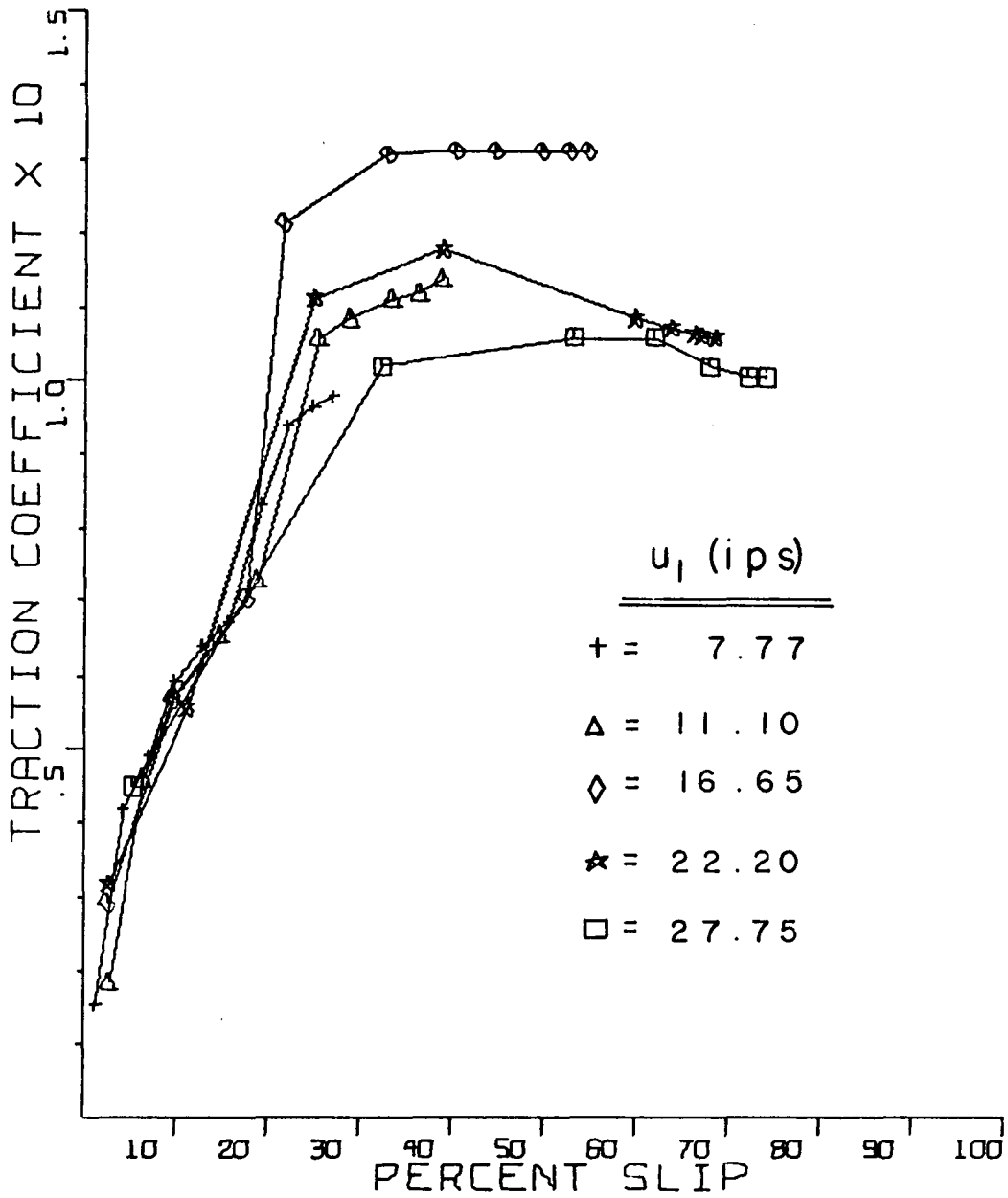

Figure 30. 45° Contact Angle and 400 KSI Maximum Contact Pressure Test Results

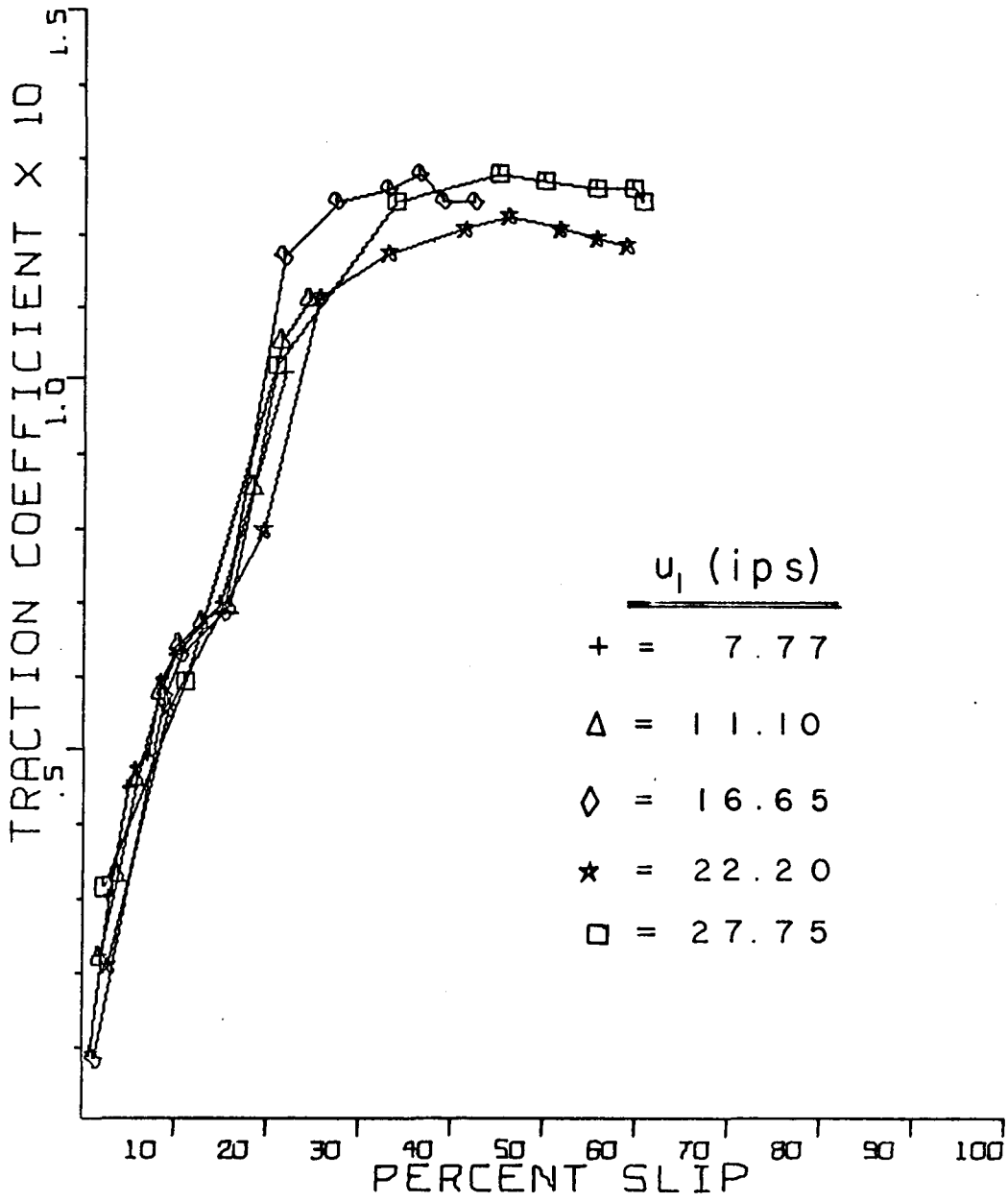

Figure 31. 45° Contact Angle and 450 KSI Maximum Contact Pressure Test Results

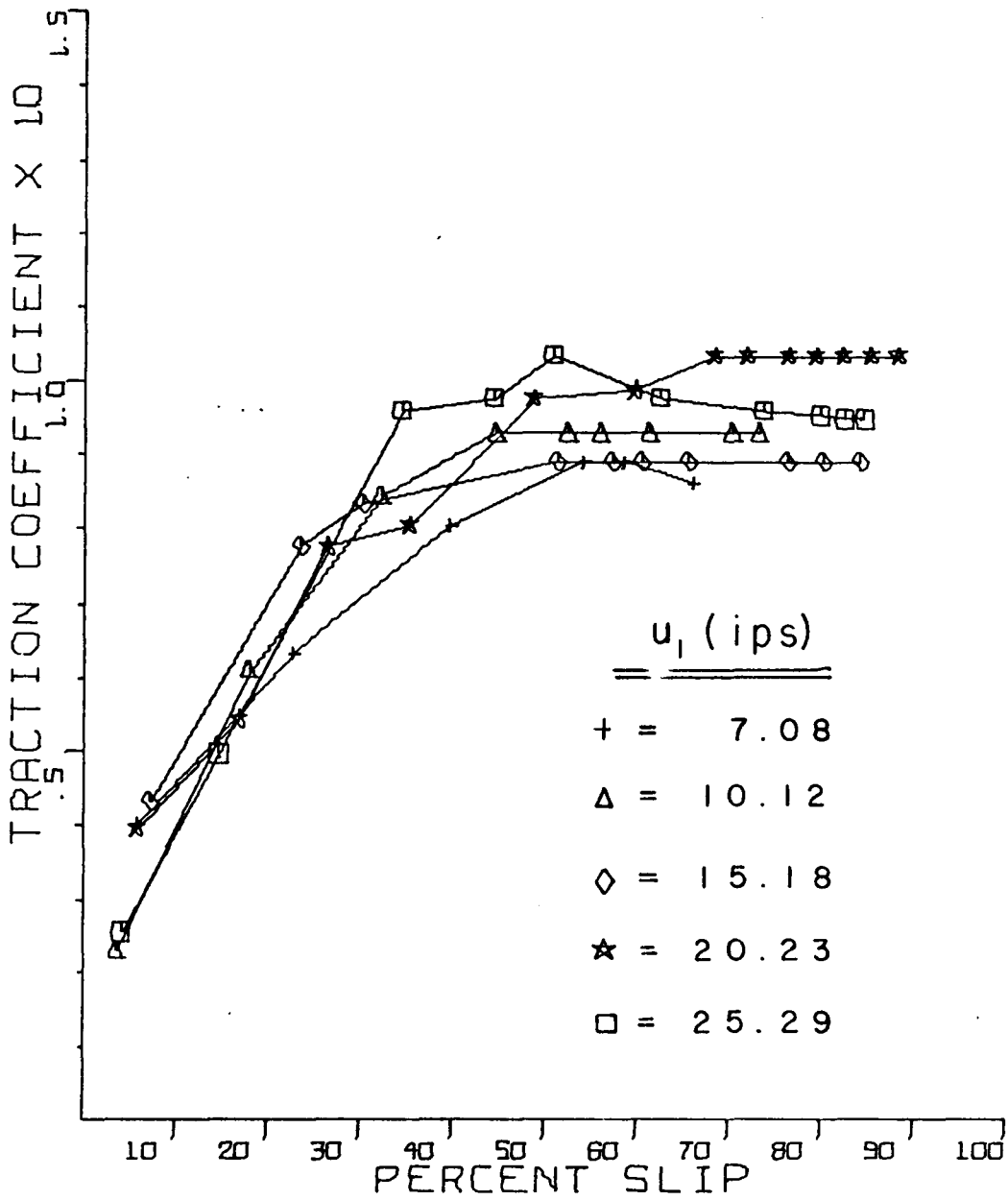

Figure 32. 50° Contact Angle and 300 KSI Maximum Contact Pressure Test Results

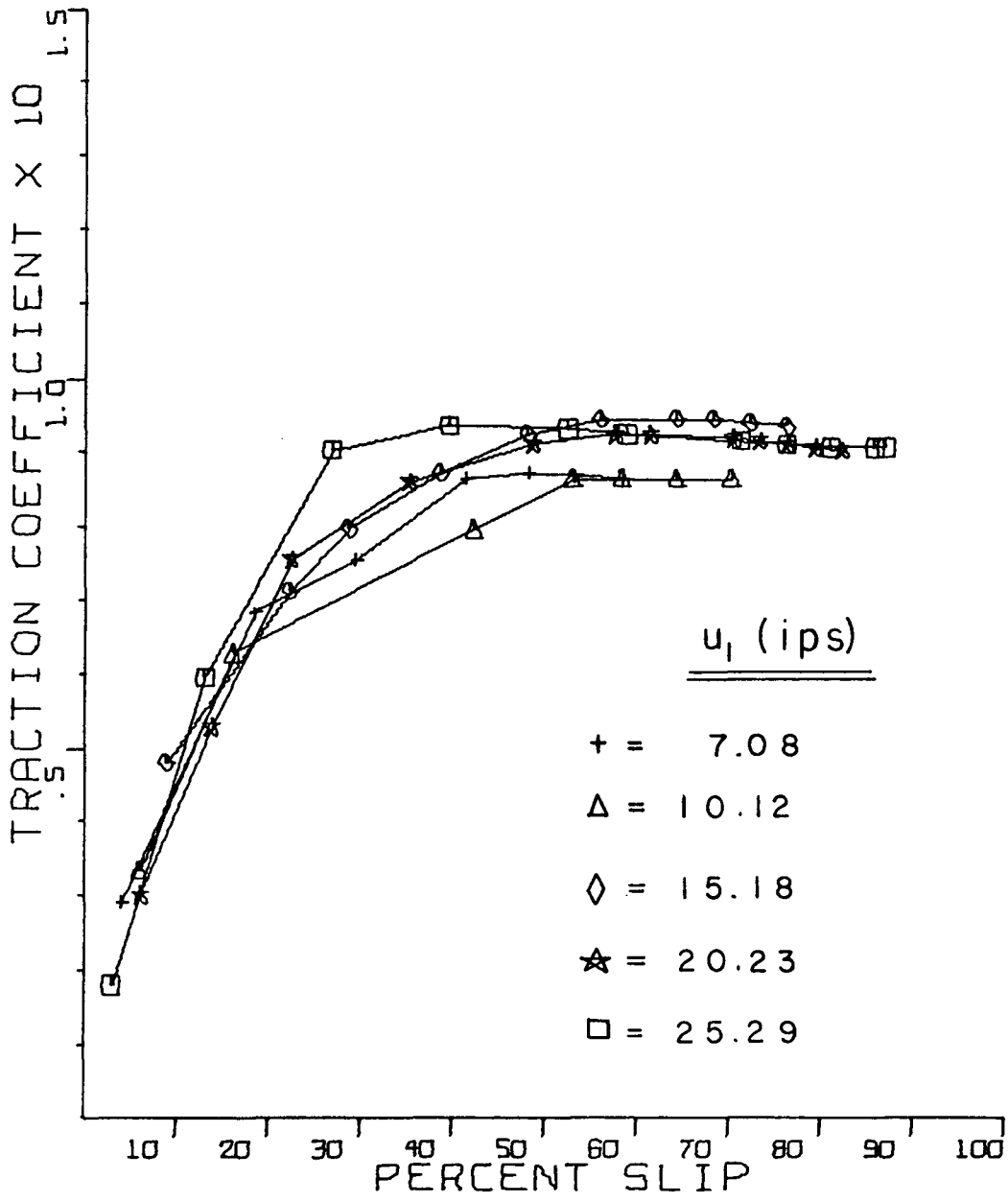

Figure 33. 50° Contact Angle and 333 KSI Maximum Contact Pressure Test Results

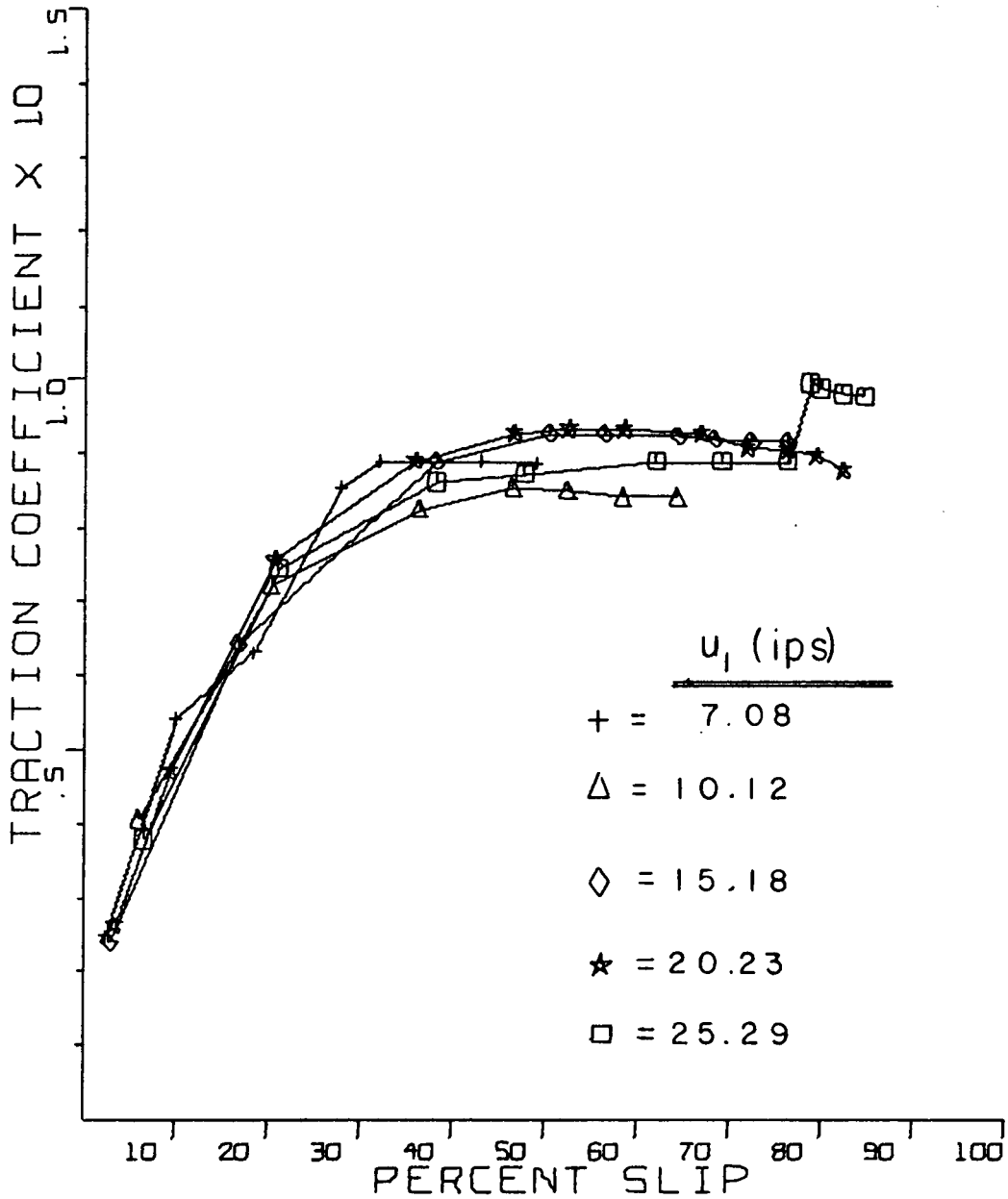

Figure 34. 50° Contact Angle and 350 KSI Maximum Contact Pressure Test Results

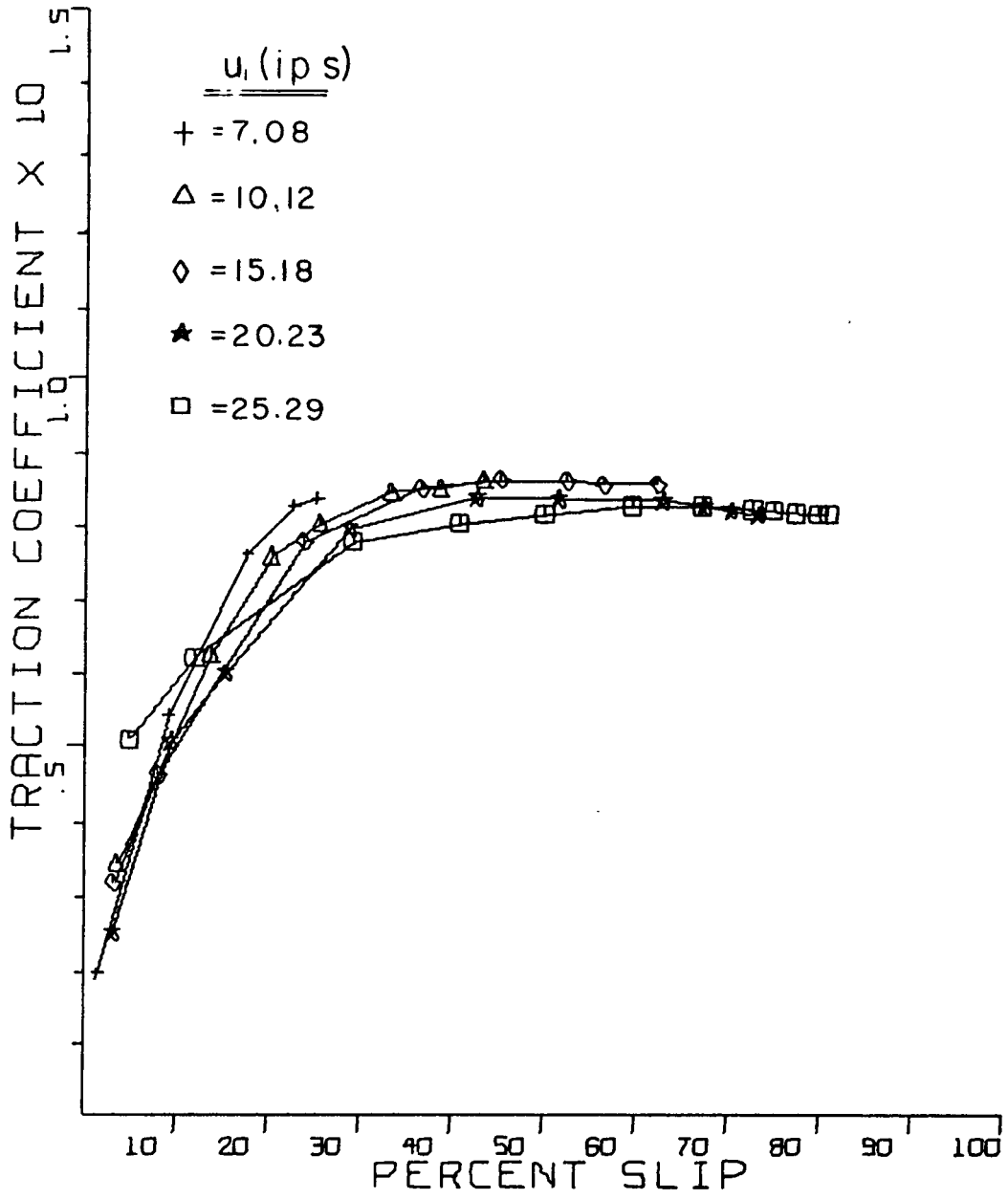

Figure 35. 50° Contact Angle and 400 KSI Maximum Contact Pressure Test Results

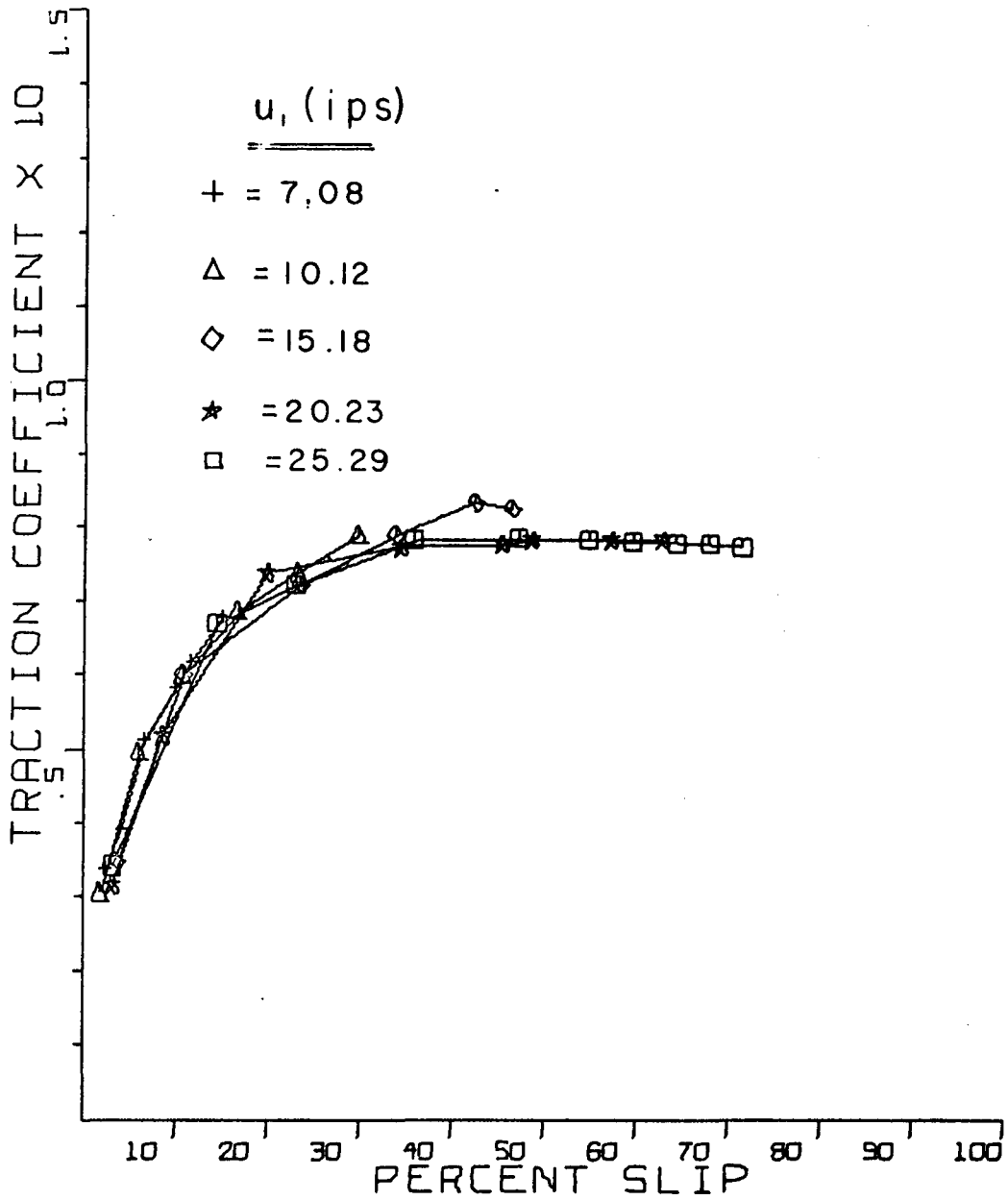

Figure 36. 50° Contact Angle and 450 KSI Maximum Contact Pressure Test Results

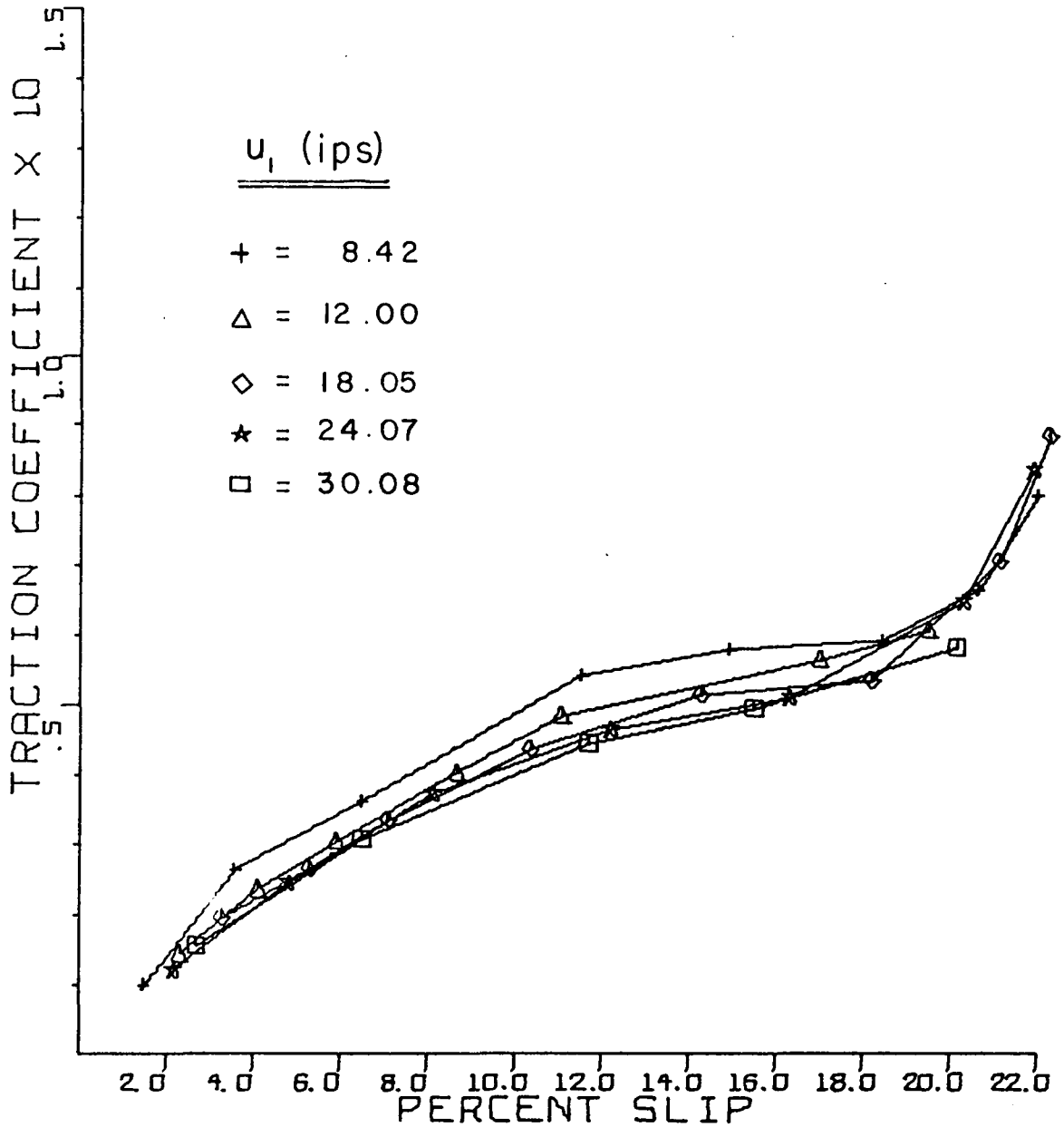

Figure 37. 40° Contact Angle and 300 KSI
Maximum Contact Pressure Test Results

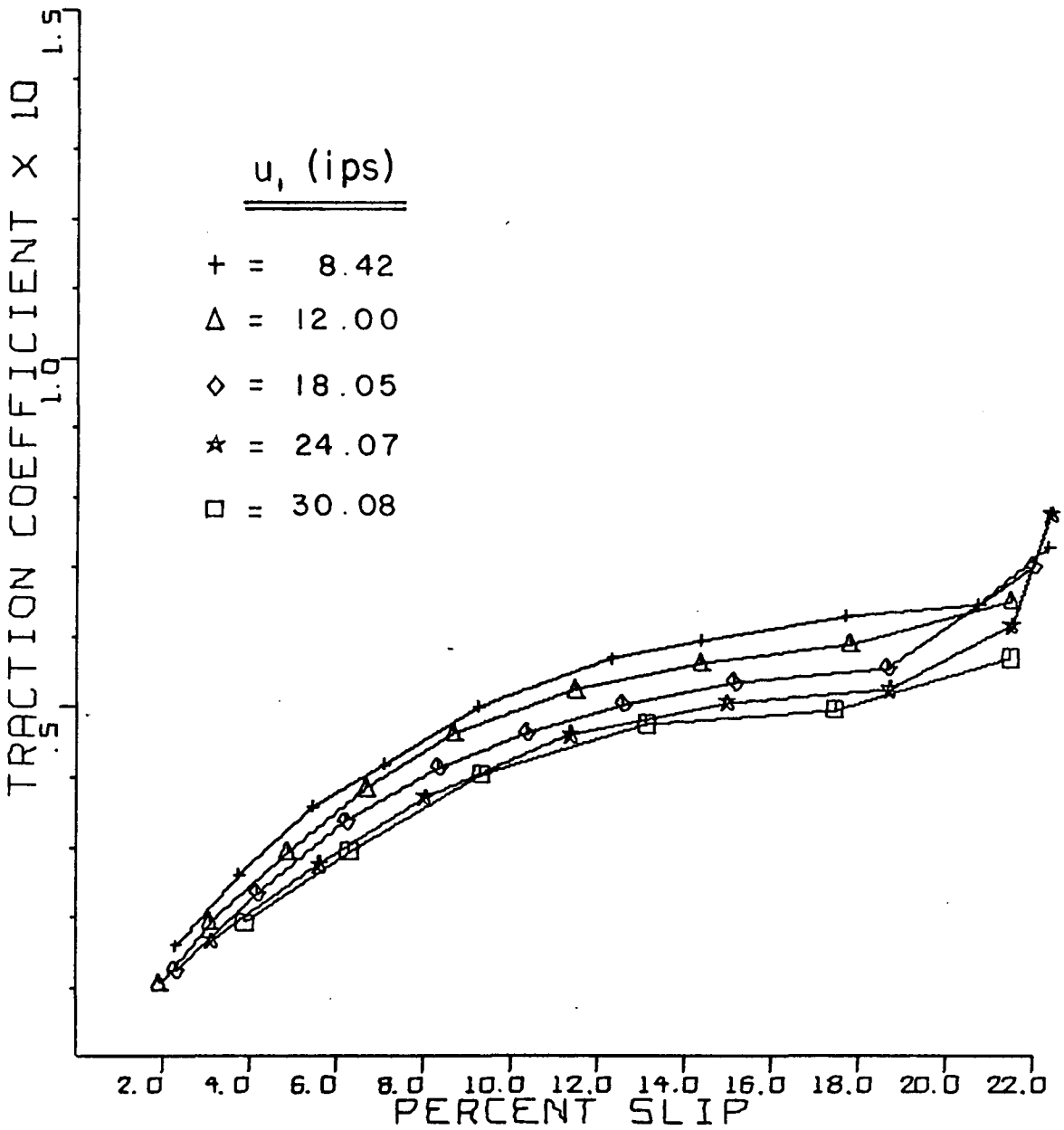

Figure 38. 40° Contact Angle and 333 KSI
Maximum Contact Pressure Test Results

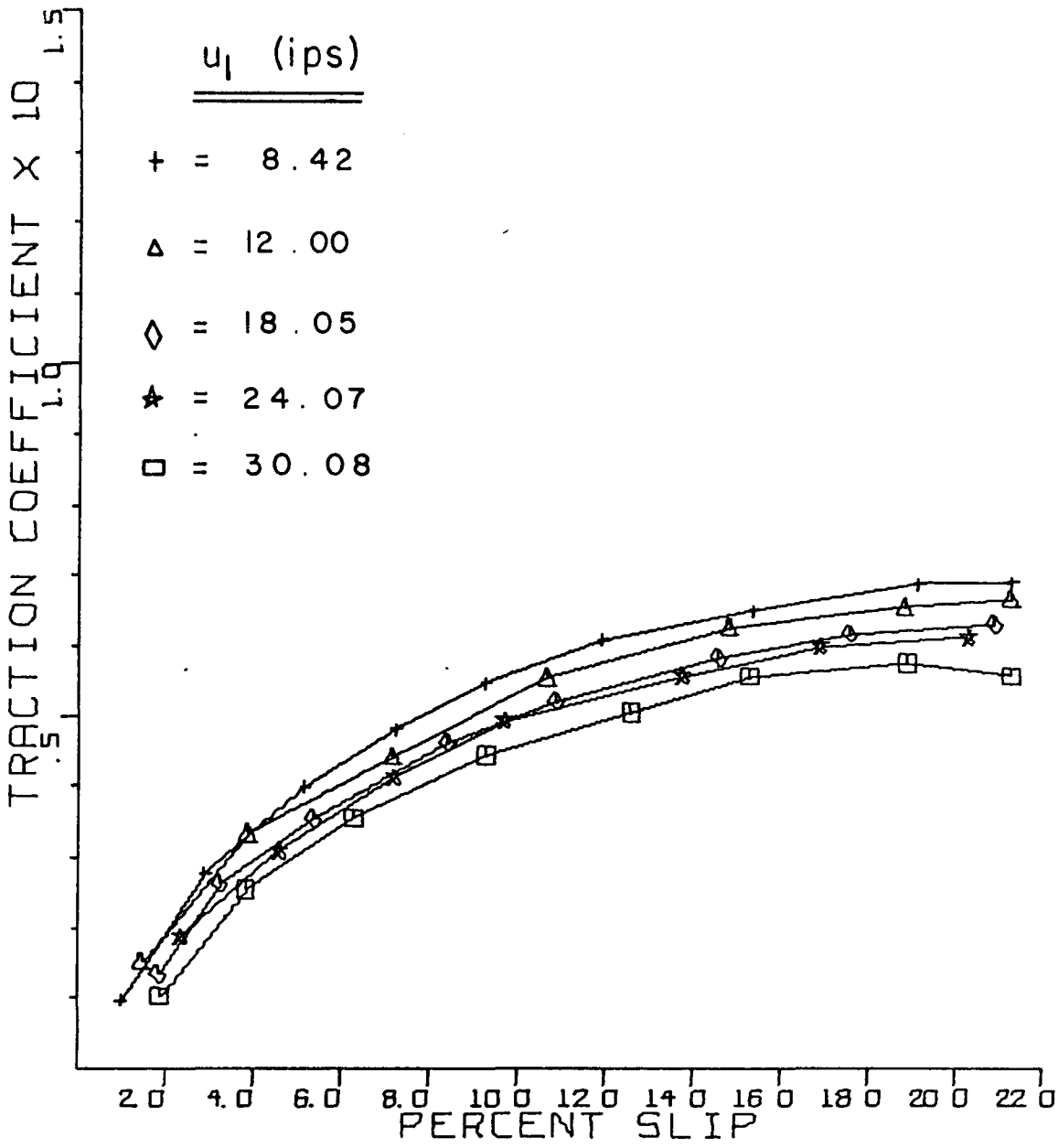

Figure 39. 40° Contact Angle and 350 KSI
Maximum Contact Pressure Test Results

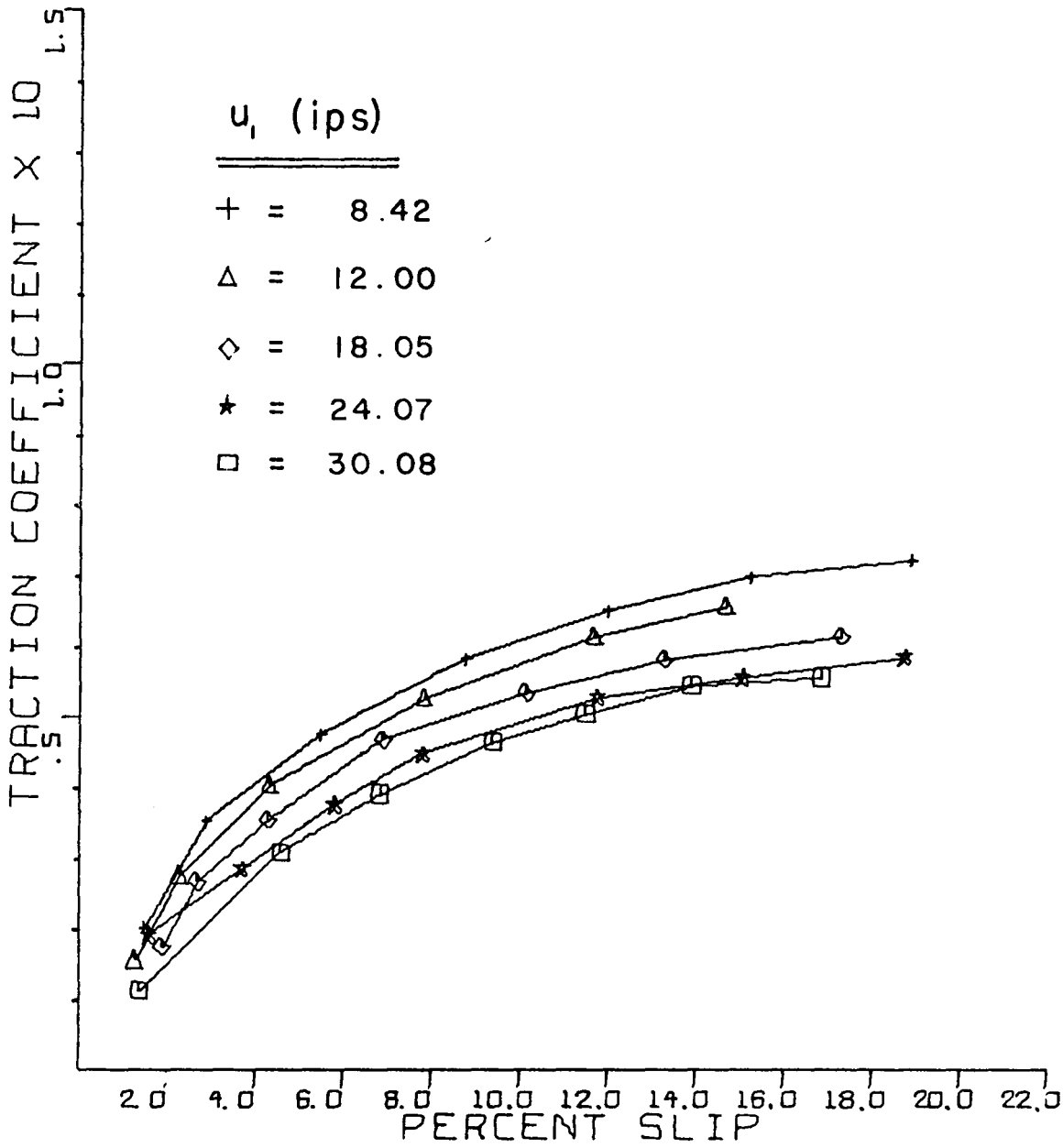

Figure 40. 40° Contact Angle and 400 KSI Maximum Contact Pressure Test Results

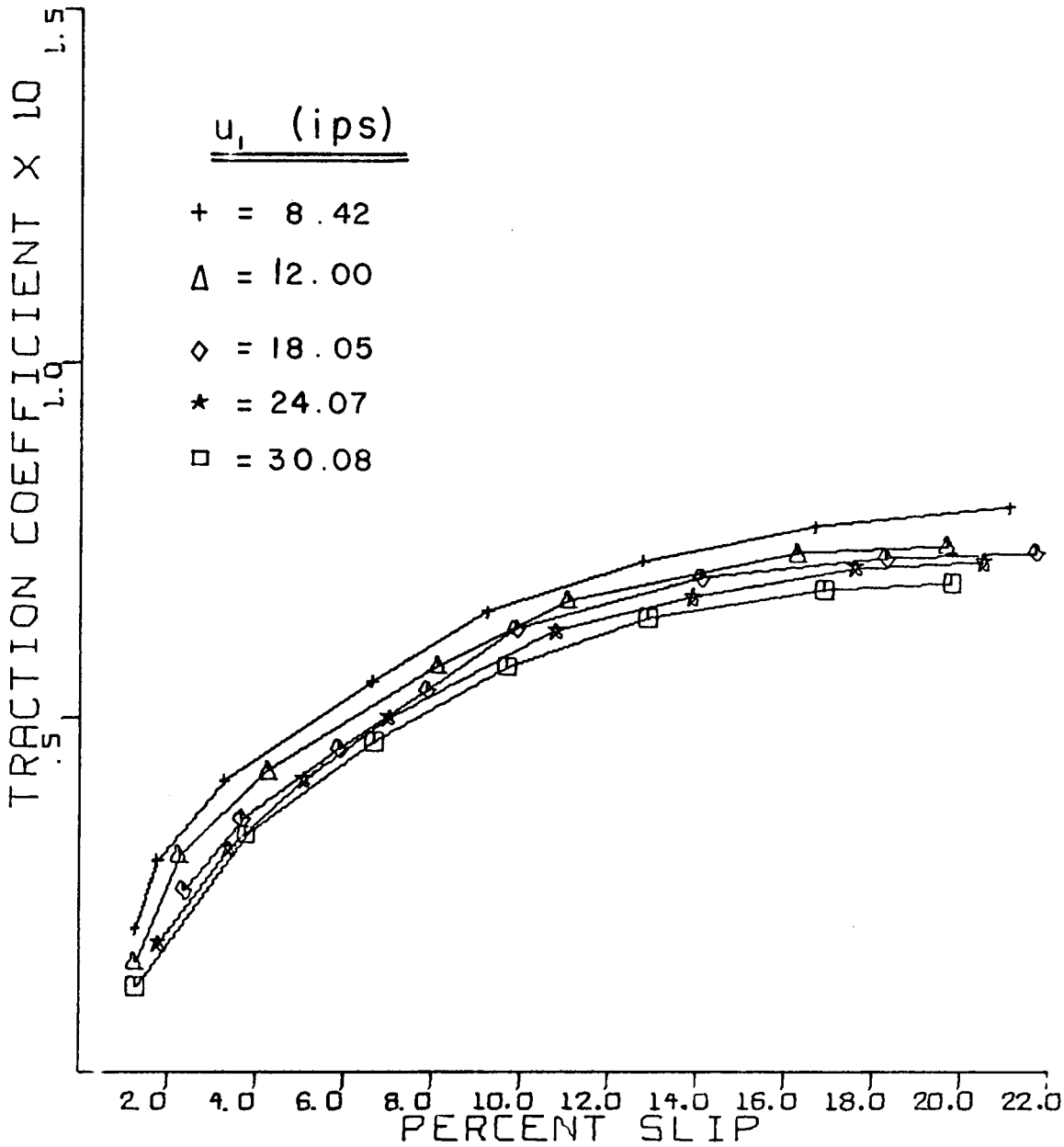

Figure 41. 40° Contact Angle and 450 KSI Maximum Contact Pressure Test Results

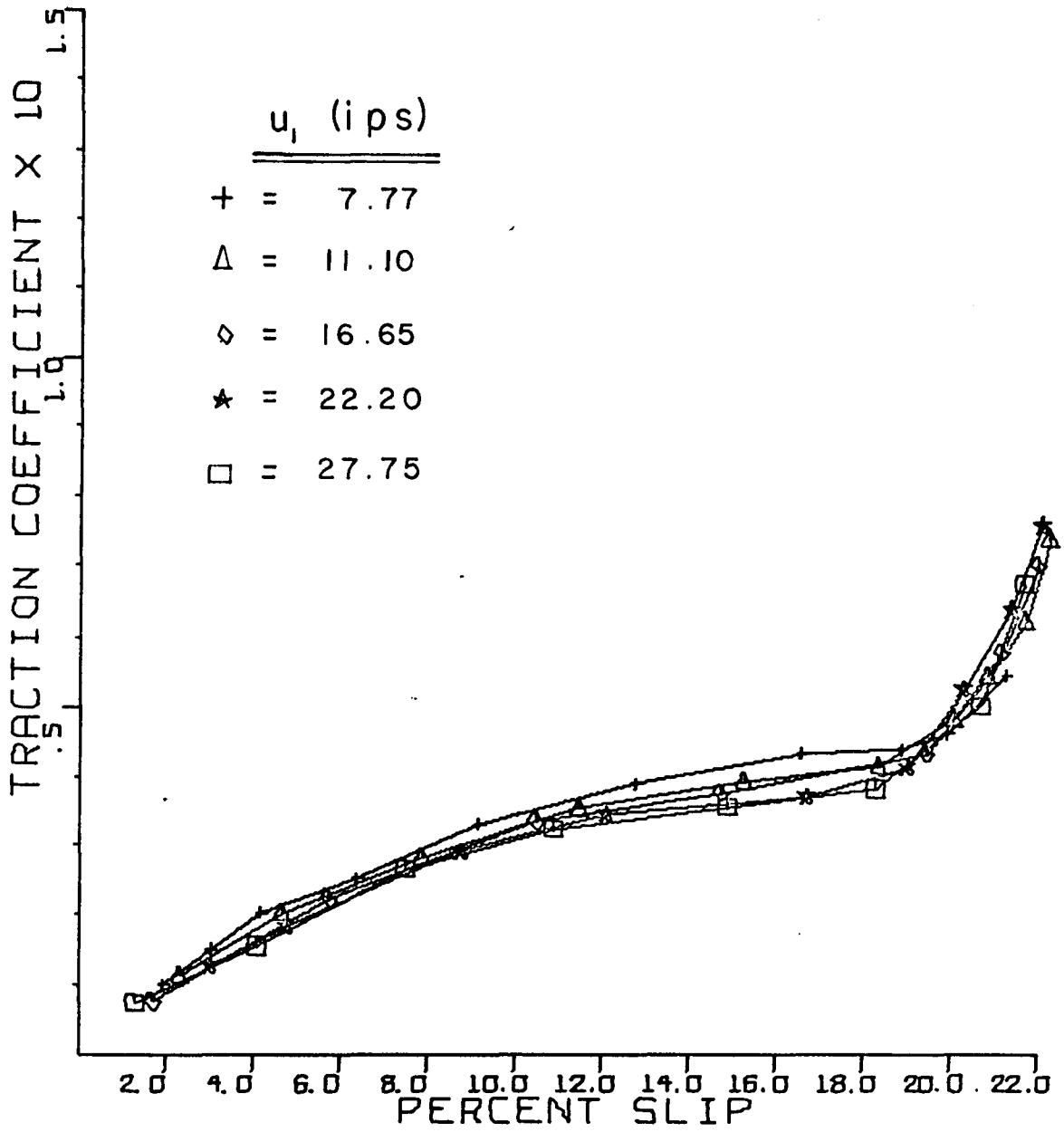

Figure 42. 45° Contact Angle and 300 KSI Maximum Contact Pressure Test Results

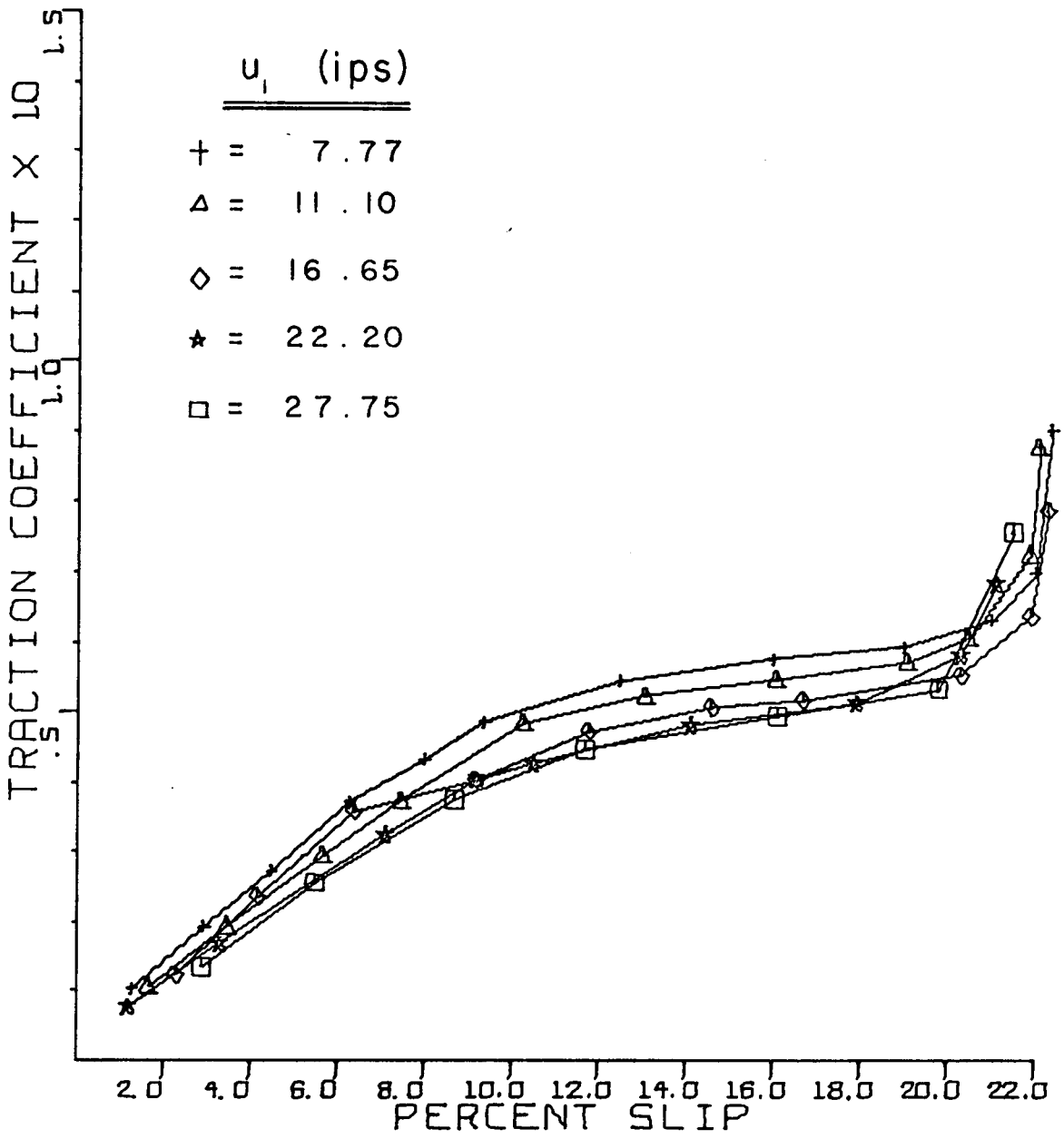

Figure 43. 45° Contact Angle and 333 KSI
Maximum Contact Pressure Test Results

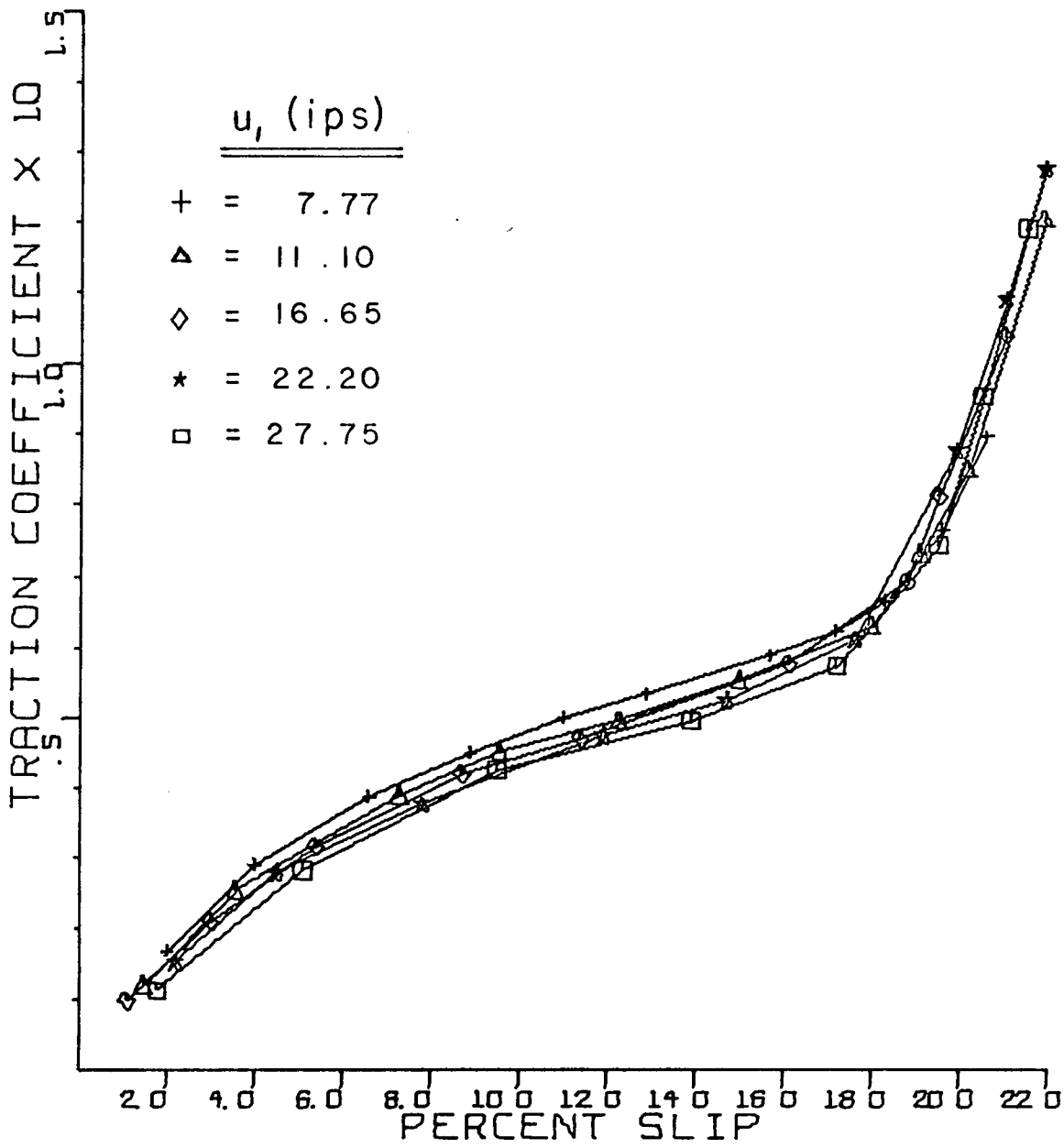

Figure 44. 45° Contact Angle and 350 KSI
Maximum Contact Pressure Test Results

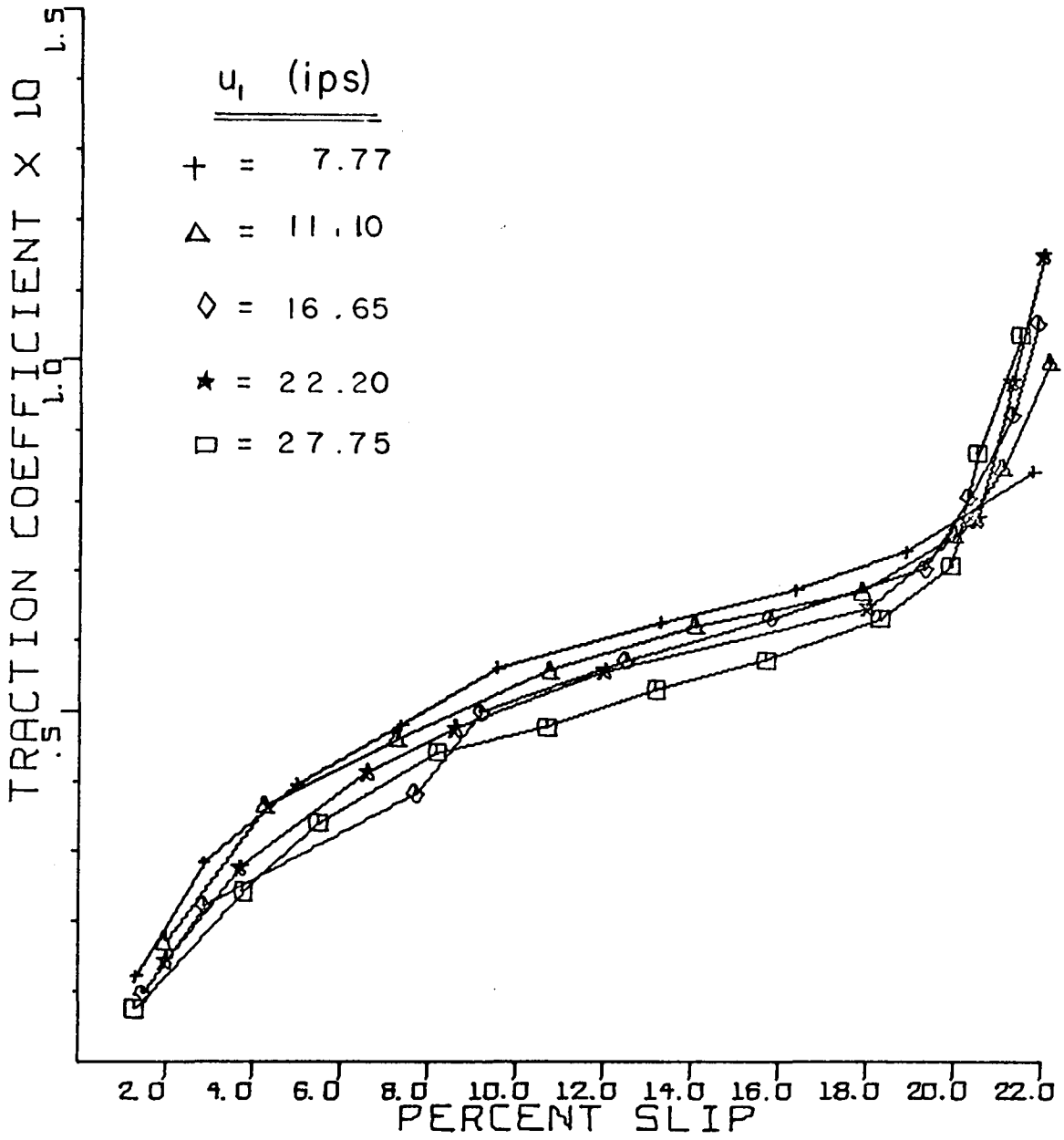

Figure 45. 45° Contact Angle and 400 KSI
Maximum Contact Pressure Test Results

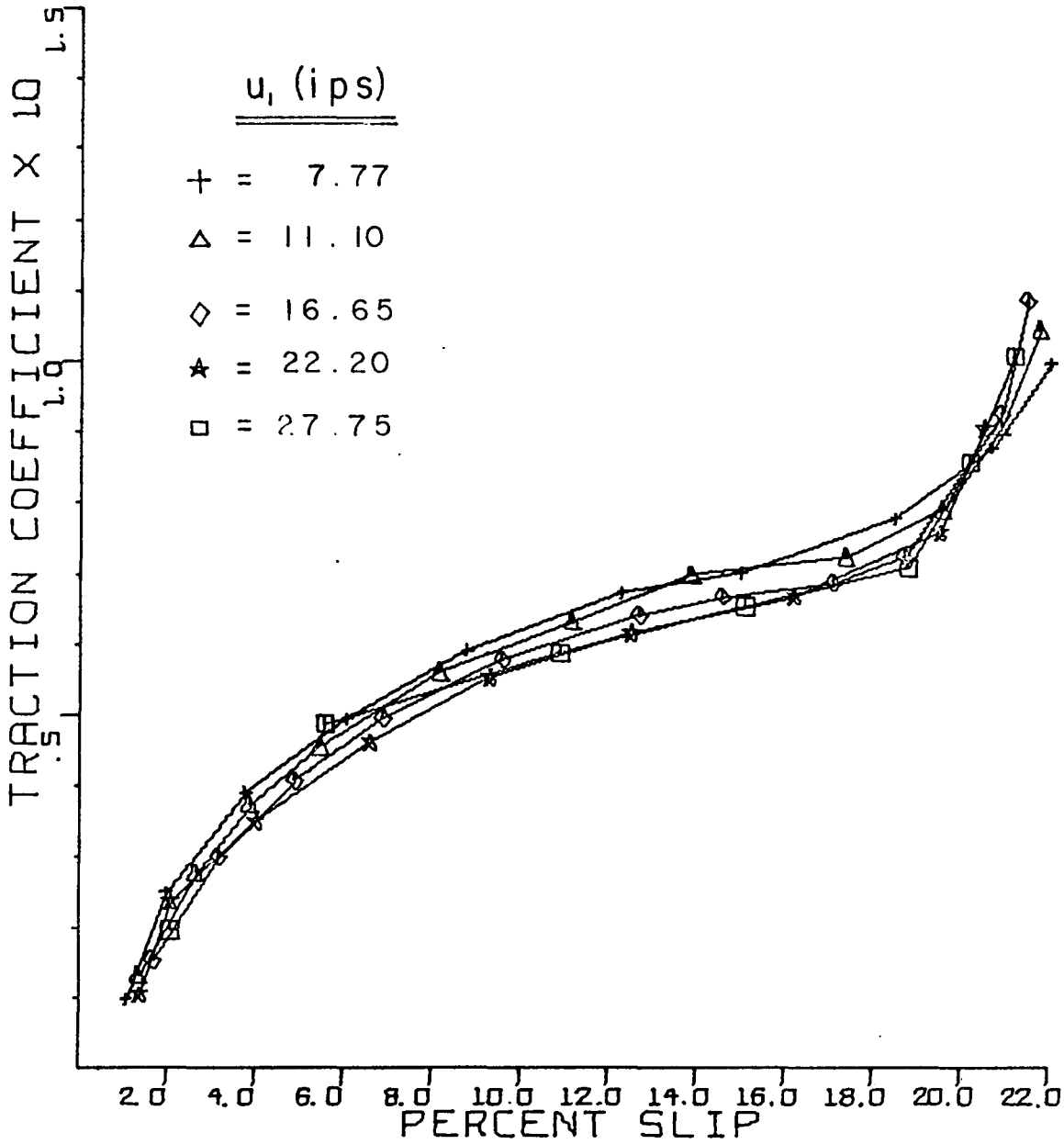

Figure 46. 45° Contact Angle and 450 KSI Maximum Contact Pressure Test Results

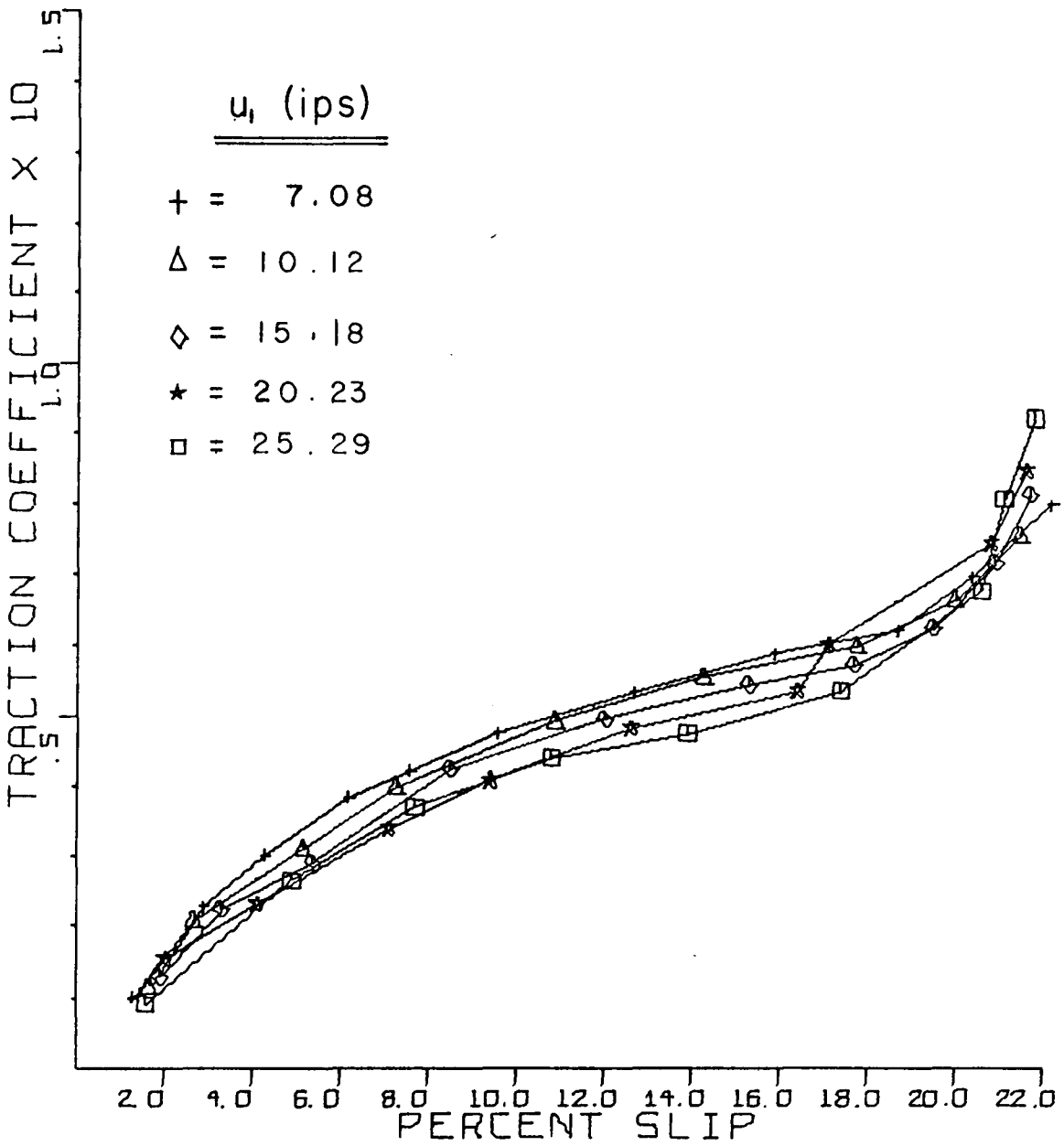

Figure 47. 50° Contact Angle and 300 KSI Maximum Contact Pressure Test Results

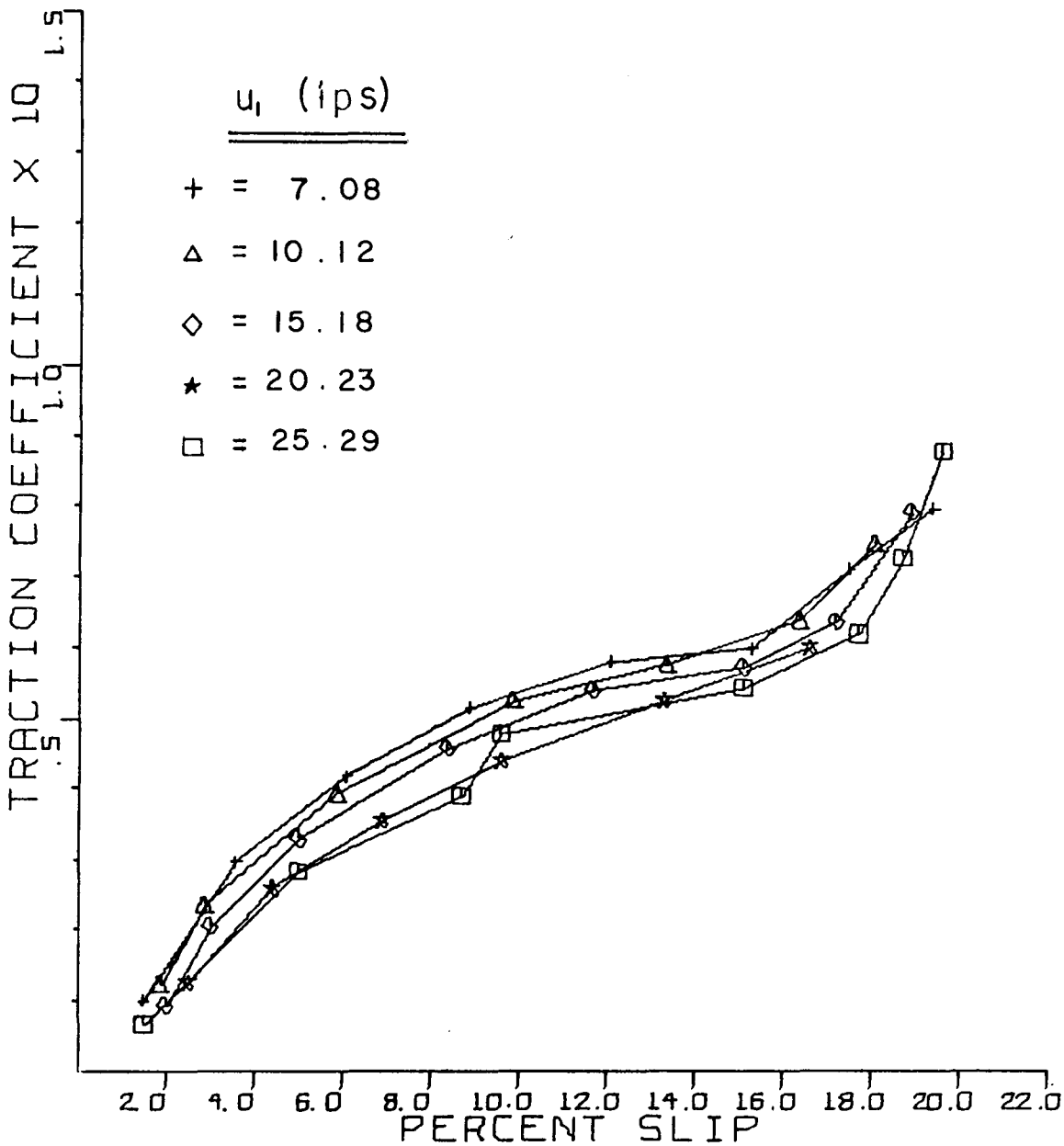

Figure 48. 50° Contact Angle and 333 KSI
Maximum Contact Pressure Test Results

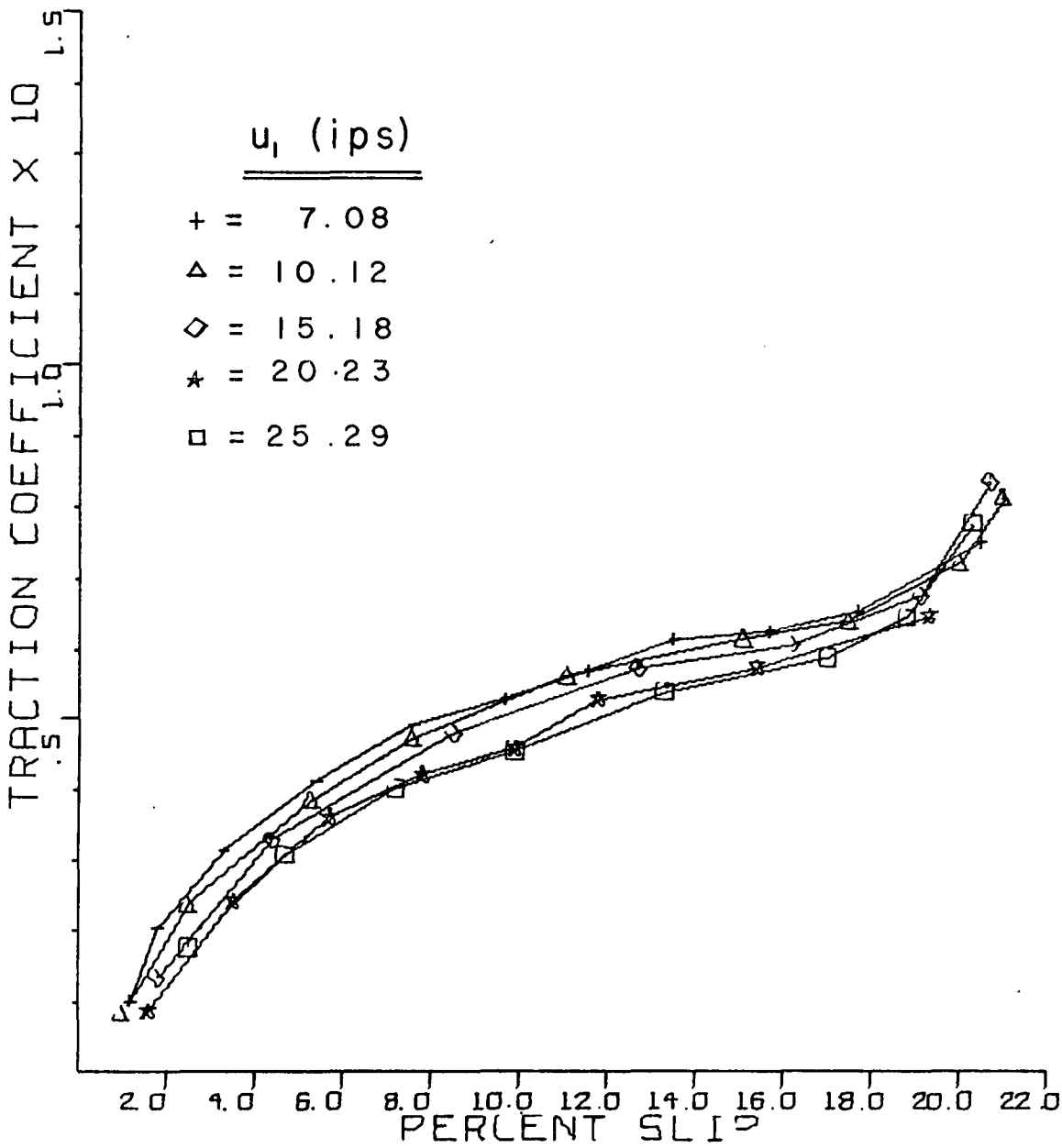

Figure 49. 50° Contact Angle and 350 KSI Maximum Contact Pressure Test Results

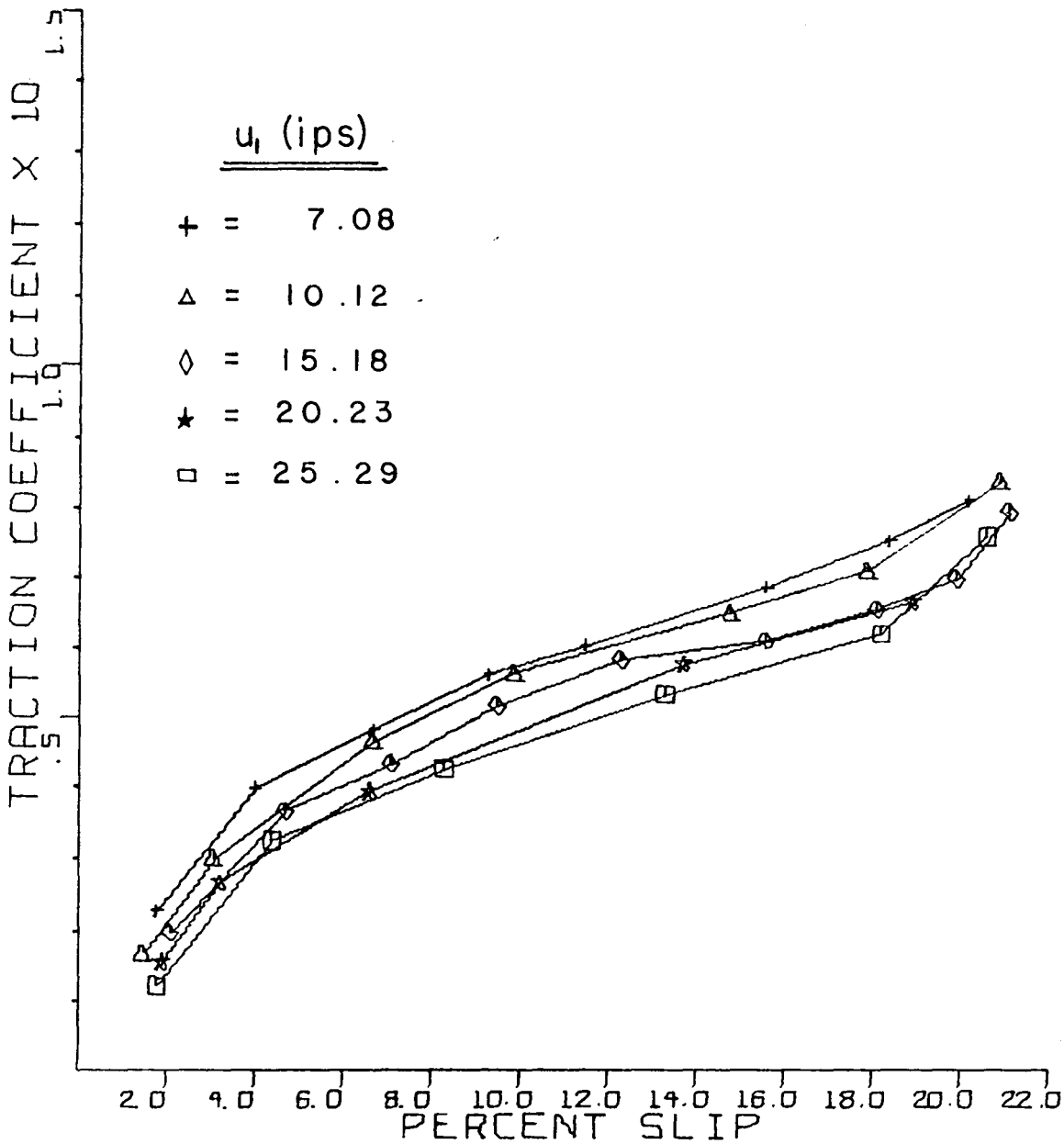

Figure 50. 50° Contact Angle and 400 KSI
Maximum Contact Pressure Test Results

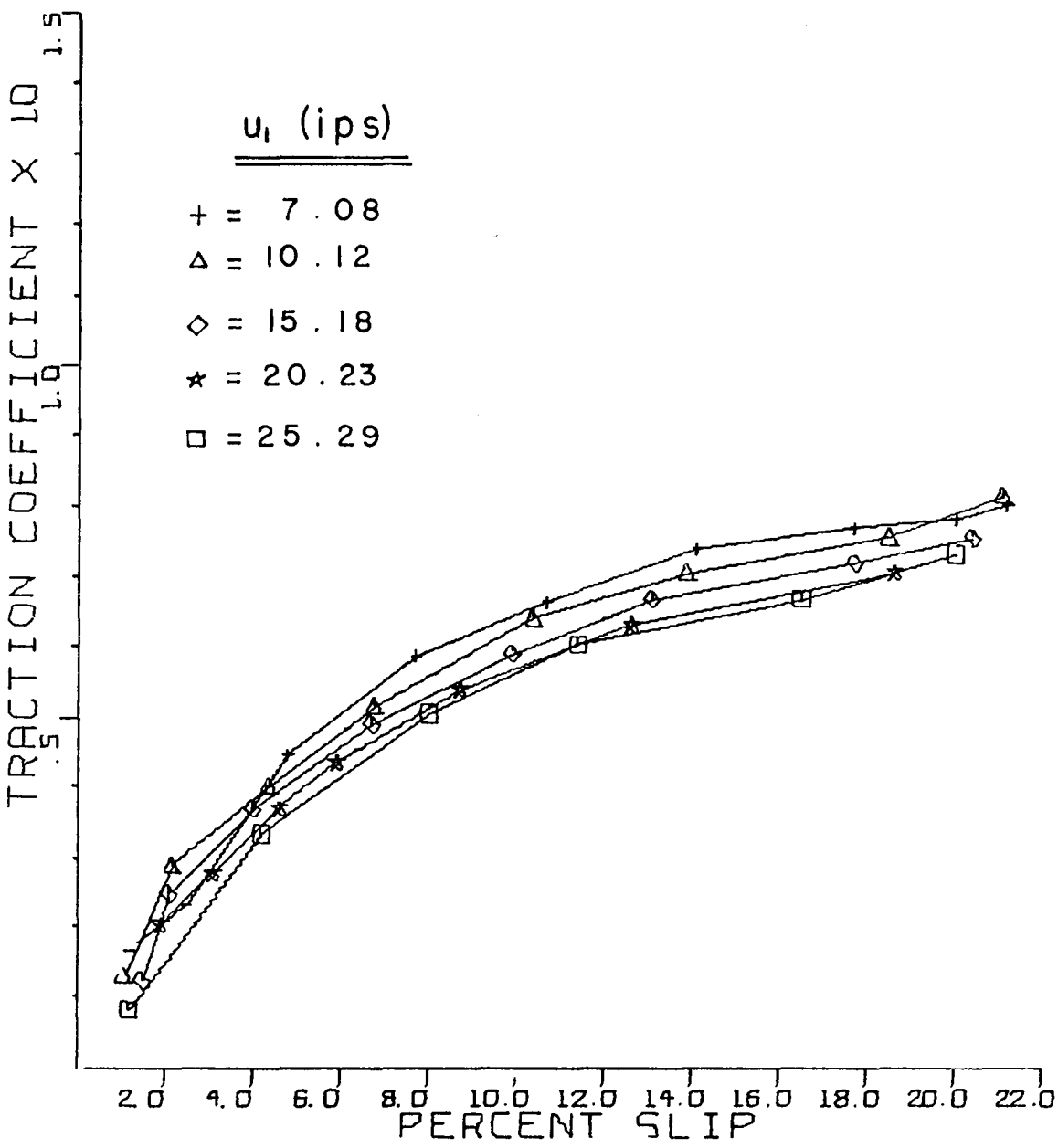

Figure 51. 50° Contact Angle and 450 KSI
Maximum Contact Pressure Test Results

TABLE IV

Surface Velocity (ips)

Contact Angle ψ	Driving ball angular velocity, w_1 (rad/sec)				
	44.3	62.8	94.25	125.7	157.1
40°	8.42	12	18.05	24.07	30.08
45°	7.77	11.1	16.65	22.2	27.75
50°	7.08	10.12	15.2	20.25	25.3

V. DISCUSSION OF RESULTS

The Figures 22 to 51 indicated that an inflection point in the curves occured in the 16-20 percent slip range and that the effects of rolling speed and contact angle on traction curves were different on each side of the inflection point. The results will be discussed in two parts, for slip values before the inflection point and for slip after the inflection point.

1. Slip From Zero to 20 Percent

At constant contact angle, rolling speed and percent slip, the coefficient of traction increases as the normal load increases as shown in Figures 52 through 54. All three graphs depict the coefficient of traction versus the percent slip, at the lowest velocity tested. For 40°, 45°, and 50° contact angles, the rolling velocities are 8.42, 7.77, and 7.08 inches per second, respectively. These results are typical of those observed at all higher rolling velocities tested.

The value of friction force in sliding can be found as

$$F_{o,h} = \int\int \tau_{o,h} dA$$

where

$\tau_{o,h}$ = viscous shear stress = $\eta(\frac{\partial u}{\partial z})_{o,h}$ (from Reference 1)

h = film thickness

$dA = \rho d\theta d\rho$

ρ = distance from center to any point in the contact area

θ = angular coordinate of contact area

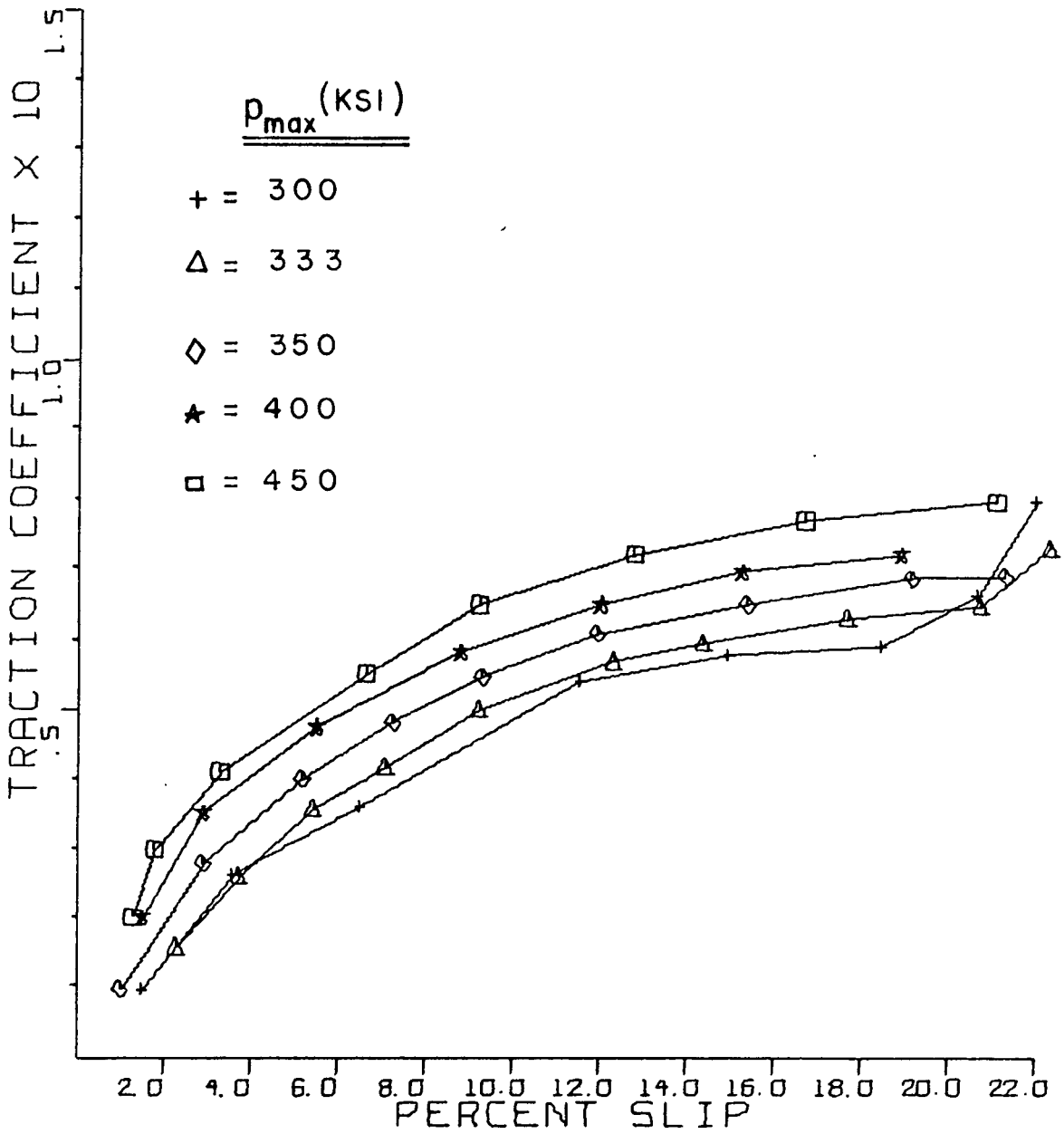

Figure 52. 40° Contact Angle and 8.42 in/sec Surface Velocity Test Results

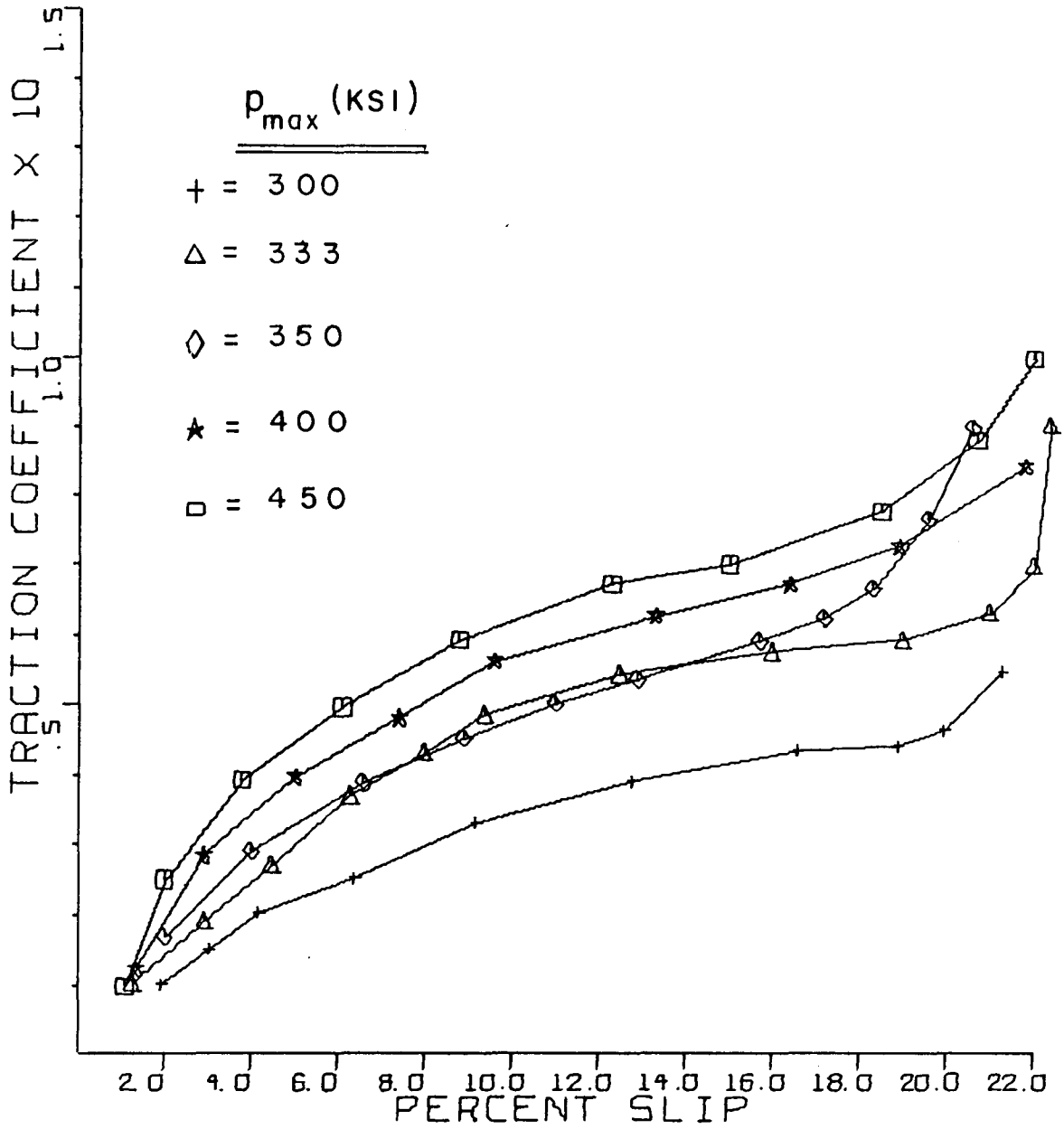

Figure 53. 45° Contact Angle and 7.77 in/sec Surface Velocity Test Results

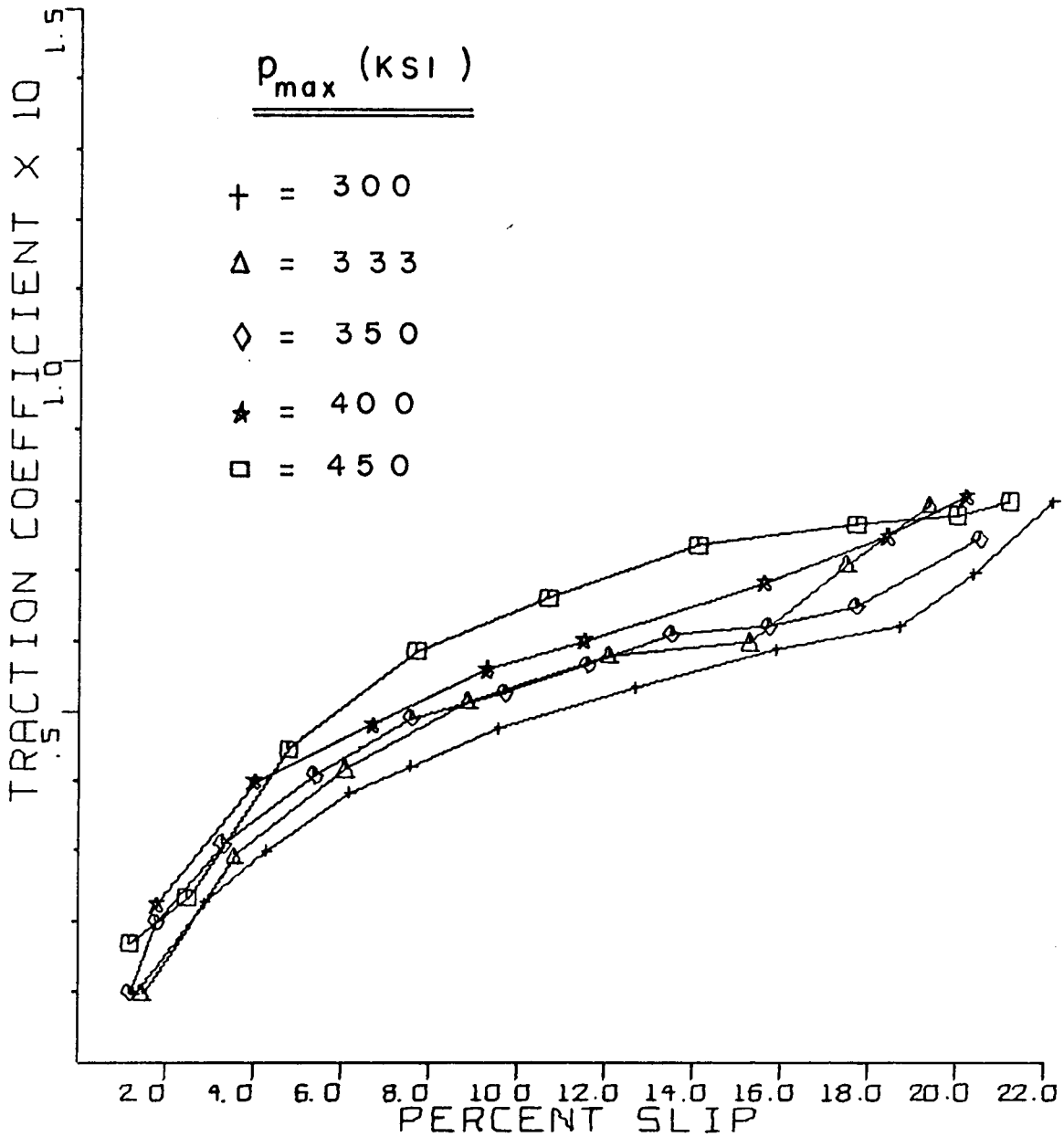

Figure 54. 50° Contact Angle and 7.08 in/sec Surface Velocity Test Results

The subscripts o,h are for the surfaces z = o, and z = h respectively (see Figure 60).

Hence

$$F_{o,h} = \int_0^2 \int_0^a \eta \left(\frac{\partial u}{\partial z}\right)_{o,h} \rho \, d\rho \, d\theta$$

Considering only the Petroff friction (20), then

$$\left(\frac{\partial u}{\partial z}\right)_{o,h} \simeq \frac{\Delta u}{h}$$

where

$$\Delta u = u_{1p} - u_{2p}$$

The simple exponential equation for pressure dependent viscosity is

$$\eta(p) = \eta_o \, e^{\alpha p}$$

where α = pressure viscosity coefficient (psi^{-1}). p is given as (1)

$$p = p_{max} \left(1 - \rho^2/a^2\right)^{1/2}$$

Substituting all these, the friction force becomes then

$$F = \int_0^2 \int_0^a \eta_o e^{\alpha p} \frac{\Delta u}{h} \rho \, d\rho \, d\theta$$

$$= \pi a^2 \eta_o \, e^{\overline{\alpha p}} \left(\overline{\frac{\Delta u}{h}}\right)$$

where $\left(\overline{\frac{\Delta u}{h}}\right)$ and $e^{\overline{\alpha p}}$ are the average values of the quantities $\frac{\Delta u}{h}$ and $e^{\alpha p}$ respectively for the contact area defined by

$$0 < \rho < a \quad \text{and} \quad 0 < \theta < 2\pi$$

For an applied normal load of W the coefficient of traction is given by

$$T.C. = \frac{F}{W} = \frac{\pi a^2 \eta_o \, e^{\overline{\alpha p}}}{W} \qquad \left(\frac{\overline{\Delta u}}{h} \right)$$

An expression for W is given as (1)

$$W = \frac{2}{3} p_{max} \pi a^2$$

then

$$T.C. = \frac{3}{2} \left(\frac{\overline{\Delta u}}{h} \right) \eta_o \frac{e^{\alpha p}}{p_{max}}$$

As the normal load increases, the increase in $e^{\overline{\alpha p}}$ will be greater than the increase in p_{max}. Therefore keeping the other variables fixed, the coefficient of traction will increase as the normal load increases.

The mid-point film thickness h_o for spheres in EHD lubrication is given by the following relation (1)

$$\frac{h_o^2}{6\eta_o u_1 a \alpha} \left(\frac{3 \times 11.43 W(1-\sigma^2)}{4\pi a E h_o} + 6.3 \right) = 1$$

where

u_1 = surface velocity of ball 1

σ = Poisson's ratio

E = Young's modulus.

The other variables are the same as defined before.

From Reference 1

$$a = \{(1 - \sigma^2) \frac{3WR}{2E}\}^{1/3}$$

For steel balls of 0.5 inch diameter,

$$\sigma = 0.3$$

$$E = 30 \times 10^6 \text{ psi}$$

$$R = \frac{R_1}{2} = 0.125 \text{ inch}$$

then

$$a = (1.78 \times 10^{-3}) W^{1/3}$$

After proper substitutions, h_o can be solved for using the quadratic formula

$$h_o = - (0.365 \times 10^{-5}) W^{2/3} + [(0.13 \times 10^{-10}) W^{4/3} + (1.69 \times 10^{-3}) u_1 \alpha \eta_o W^{1/3}]^{1/2}$$

Using Table III, η_o can be calculated at 100°F

$$\eta_o = \text{(Density) x (Kinematic Viscosity)}$$

$$= (0.886)\ (22.7 \times 10^{-2}) = 20.11 \times 10^{-2} \text{ poises}$$

$$= 29.16 \times 10^{-7} \frac{\text{lb-sec}}{\text{in}^2}$$

The pressure viscosity coefficient given by Table III is

$$\alpha = 2.19 \times 10^{-4} \text{ psi}^{-1}$$

Let the surface velocity be 30 inches per second (maximum surface velocity used during the tests).

Substituting all these into the equation of mid-point film thickness, then

$$h_o = - (0.365 \times 10^{-5}) W^{2/3} + [(0.13 \times 10^{-10}) W^{4/3} + (0.32 \times 10^{-10}) W^{1/3}]^{1/2}$$

The Hertzian equation for normal load is (1)

$$W = \frac{2}{3} p_{max} \pi a^2$$

but

$$a = 1.78 \times 10^{-3} W^{1/3}$$

Simultaneous solutions give values for normal loads for each assigned value of maximum Hertzian pressure.

Hence

$$W = 10.29 \text{ lb} \quad \text{at} \quad p_{max} = 300 \text{ KSI}$$

$$W = 31.25 \text{ lb} \quad \text{at} \quad p_{max} = 450 \text{ KSI}$$

Plugging these values of normal load into the equation of mid-point film thickness the following values of h_o can be found

$$h_o = 0.173 \times 10^{-5} \text{ inch} \quad \text{at } p_{max} = 300 \text{ KSI}$$

$$h_o = 0.100 \times 10^{-5} \text{ inch} \quad \text{at } p_{max} = 450 \text{ KSI}$$

Thus for a pressure range of 150 KSI the coefficient of traction will be increased by a factor of 1.73 due to the decrease of the film thickness.

At this point it is clear that according to EHD theory the coefficient of traction will increase as the normal load is increased.

The second phenomenon observed for the region ranging from 0 to 20 percent slip is the following: at constant load, rolling speed, and contact angle, the coefficient of traction increases as percent slip increases. However the slope of the curve decreases as the slip increases.

From the derived equation of coefficient of traction the increase in traction coefficient can be predicted as the sliding speed is increased. However the equation predicts a linear relation between slip and traction coefficient.

The decreasing slope observed in the traction curves as the percent slip is increased is similar to the stress-strain behavior exhibited by solid materials which do not have a defined yield point. It has been postulated that the lubricant in the contact zone may behave like a solid under the high pressures. As the slip increases (analogous to strain) the traction increases (analogous to stress). However the modulus of stress strain curve decreases with increasing strain.

The next phenomenon observed in the traction curves was the decrease of the traction coefficient as the rolling velocity was increased at constant contact angle, percent sliding, and load. There may be more than one factor that can affect this behavior.

The equation of traction coefficient is given as

$$T.C. = \frac{3}{2} \left(\frac{\overline{\Delta u}}{h} \right) \eta_o \frac{\overline{e^{\alpha p}}}{p_{max}}$$

Now T.C. has been experimentally determined and plotted as a function of $\frac{\Delta u}{u_1}$.

Writing the traction coefficient in terms of $\frac{\Delta u}{u_1}$ gives

$$T.C. = \frac{3}{2} \left(\frac{\overline{\Delta u}}{u_1} \right) \frac{u_1}{h} \eta_o \frac{\overline{e^{\alpha p}}}{p_{max}}$$

Observing Figure 3, the film thickness h, in the contact zone can be assumed to be equal to the mid-point film thickness h_o. But this latter is given as (1)

$$h_o = - (0.365 \times 10^{-5}) W^{2/3} + [(0.365 \times 10^{-5})^2 W^{4/3} + (0.01 \times 10^{-10}) u_1 w^{1/3}]^{1/2}$$

Let

$$a_1 = - (0.365 \times 10^{-5}) W^{2/3}$$

$$b_1 = (0.01 \times 10^{-10}) W^{1/3}$$

then

$$h_o = a_1 + (a_1^2 + b_1 u_1)^{1/2}$$

because of the constant terms

$$T.C. \quad \alpha \quad \frac{u_1}{h} = \frac{u_1}{a_1 + (a_1^2 + b_1 u_1)^{1/2}}$$

According to this equation, T.C. should increase as u_1 is increased. However experimental results do not agree with this prediction since the coefficient of traction decreases as the rolling velocity is increased for percent slip ranging from zero to 20.

Another factor which may affect the coefficient of traction is the inlet temperature.

The inlet temperature increases due to increasing shear rates caused by increasing rolling velocities. The inlet shear heating will then decrease the viscosity of the lubricant (21). Thus, observing the derived equation for T.C., it can be seen that, the coefficient of traction decreases as the viscosity is decreased.

It is also mentioned in Reference 21 that, for a rolling velocity of 30 inches per second, the film thickness predicted by the inlet shear heating theory would be 3.5 percent less than that predicted by isothermal theory. This percentage is the same order as the experimentally observed decrease in the traction coefficient for increasing rolling velocities.

Another factor which would affect the traction coefficient due to increased rolling velocities is oil starvation. It is shown by Wedeven (22) that, the increase in the centrifugal forces as the rolling velocity is increased pumps more lubricant into the contact zone. As the centrifugal forces acting on the lubricant exceed the cohesive forces after a certain value of rolling velocity, the lubricant starts to fly off the surface and oil starvation occurs which increases the coefficient of traction because of the decreased film thicknesses. It is noted that, oil starvation can occur without

having metallic contact (22).

From the traction curves ranging between zero to 20 percent sliding, it is clear that oil starvation has not occurred during the tests since the coefficient of traction decrease as the rolling velocity is increased.

Another phenomenon observed in the traction curves ranging between zero to 20 percent sliding is the following; at constant rolling velocity, percent sliding, and load, the traction coefficient was found to increase as the absolute value of the angular difference in the contact angle relative to 45°, $|\psi - 45°|$, was increased. This latter is called the effect of spin on traction coefficient. The author has found out that the effect of spin on traction was neglected by most of the workers in the field of EHD lubrication. Figures 55 through 59 indicate the effect of spin on traction. All five graphs depict the coefficient of traction versus the percent slip. In each figure, for 40°, 45°, and 50° contact angles, the rolling velocities are 8.42, 7.77, and 7.08 inches per second which correspond to the same angular velocity of the driving ball (see Table IV). The same configuration is repeated for five values of maximum Hertzian pressures, those being: 300 KSI, 333 KSI, 350 KSI, 400 KSI, and 450 KSI. Similar graphs were obtained for other values of rolling velocities but for the sake of simplicity they are not included in here.

This dependence of traction on spin will be discussed considering two factors; the centrifugal forces on lubricant particles

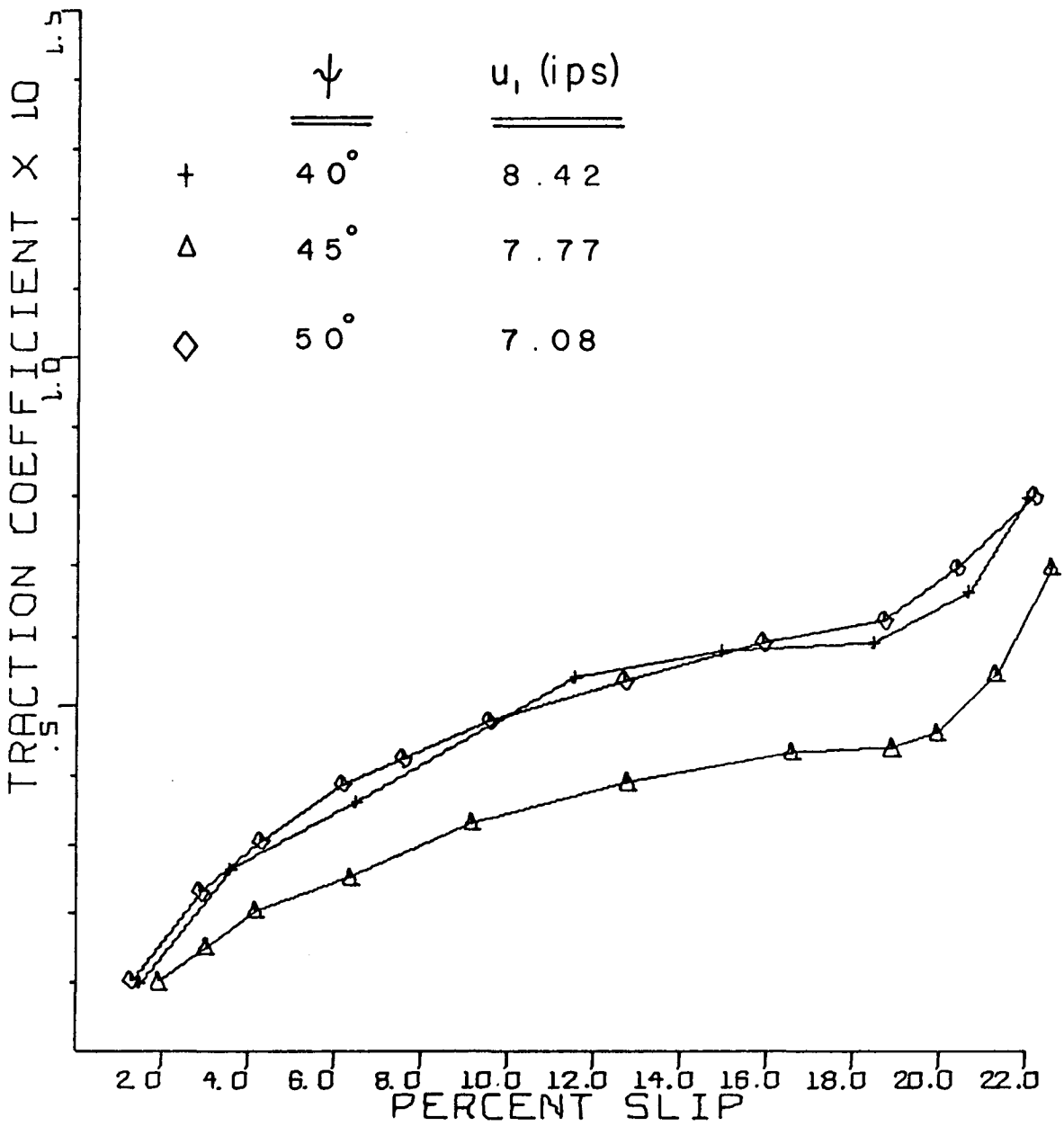

Figure 55. Effect of Spin on Traction Coefficient for 300 KSI Maximum Contact Pressure

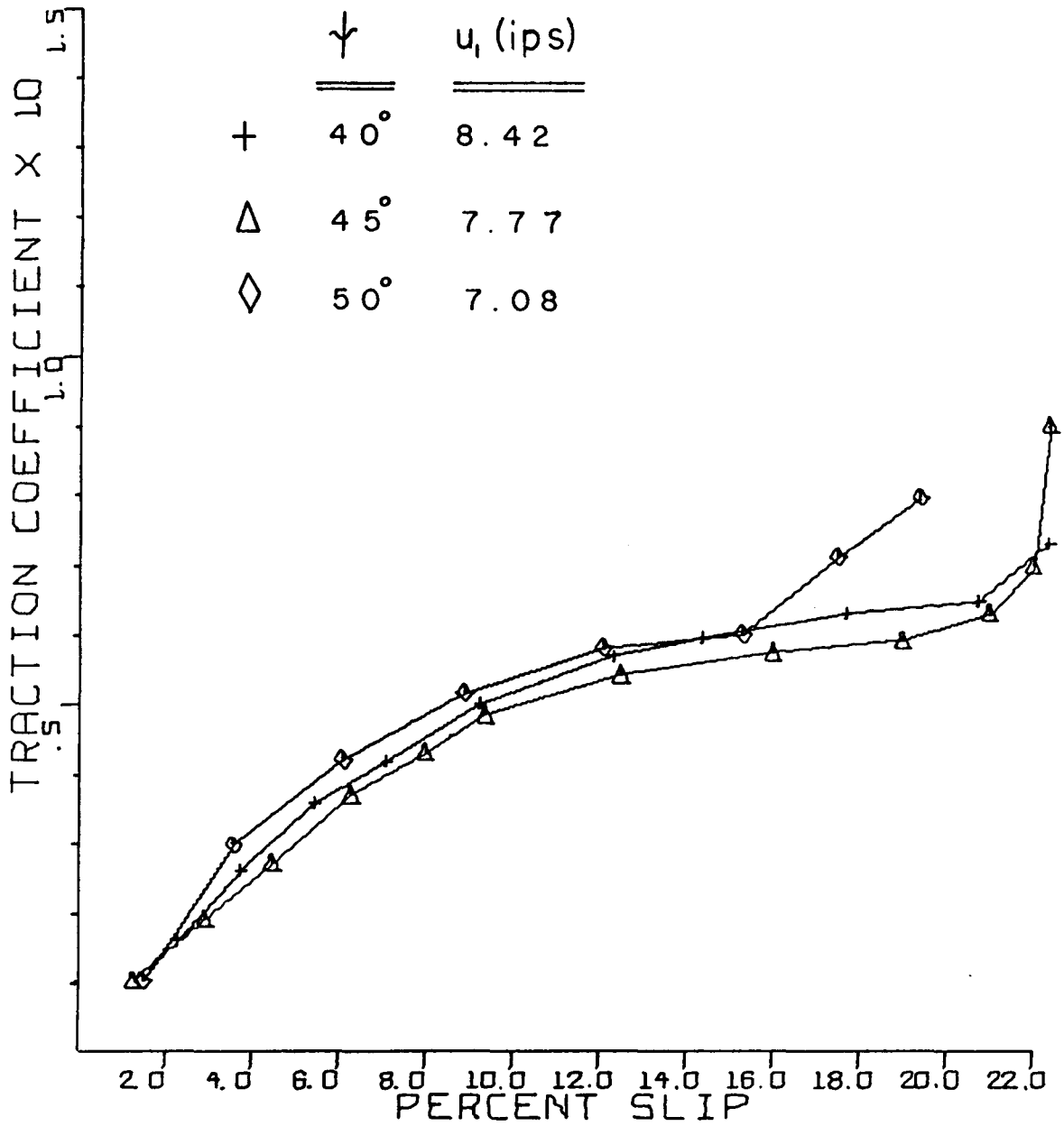

Figure 56. Effect of Spin on Traction Coefficient for 333 KSI Maximum Contact Pressure

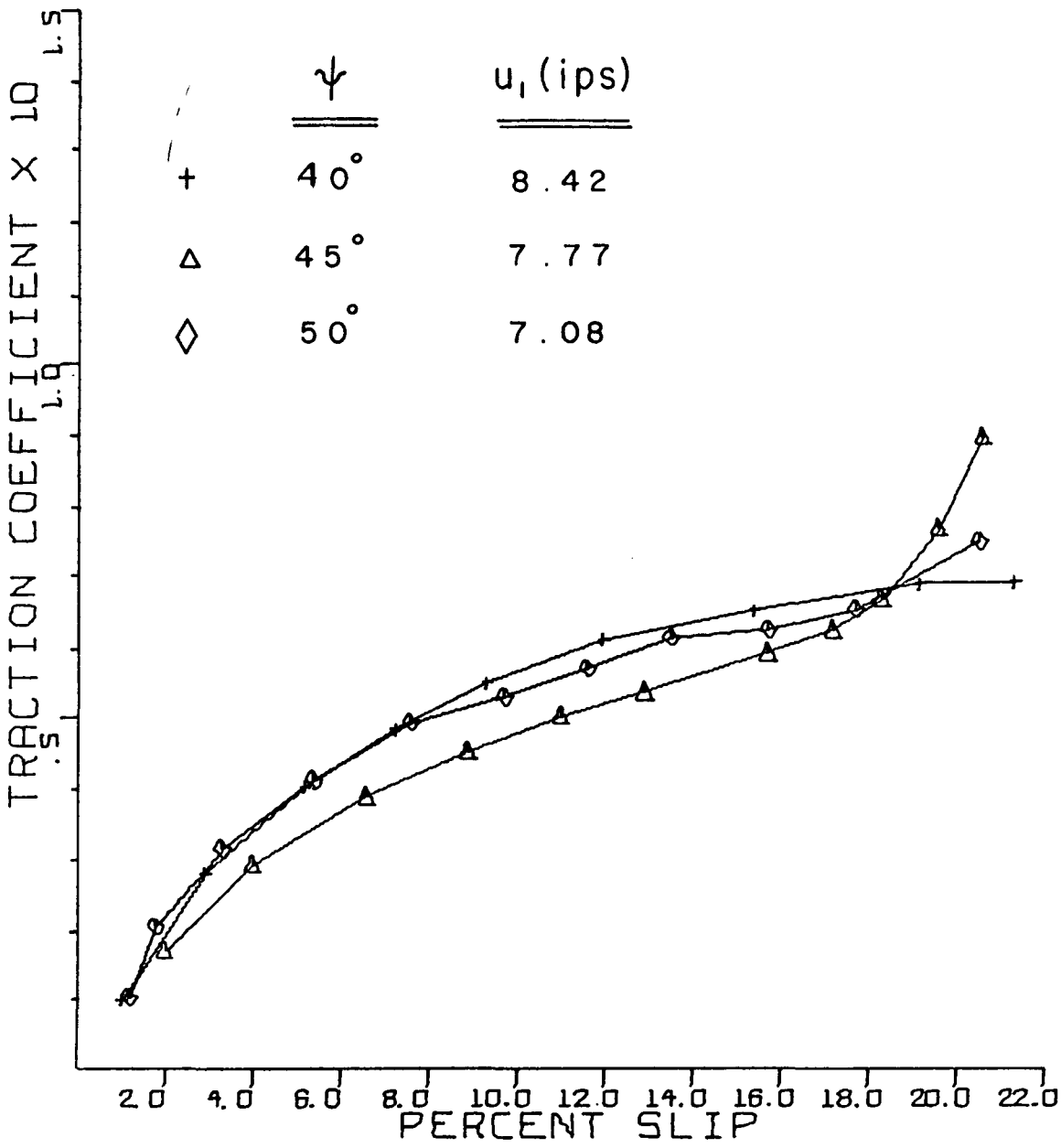

Figure 57. Effect of Spin on Traction Coefficient for 350 KSI Maximum Contact Pressure

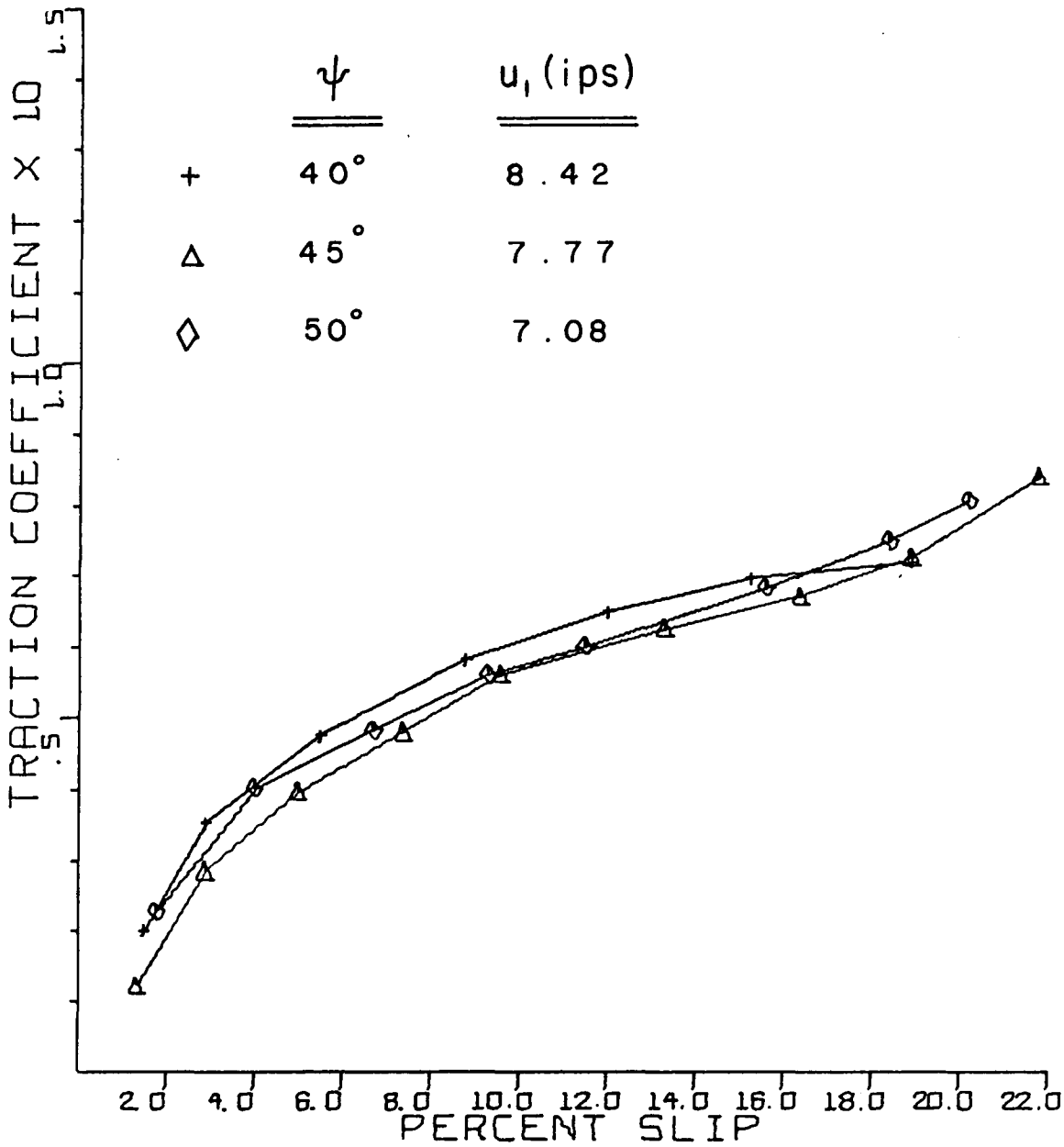

Figure 58. Effect of Spin on Traction Coefficient for 400 KSI Maximum Contact Pressure

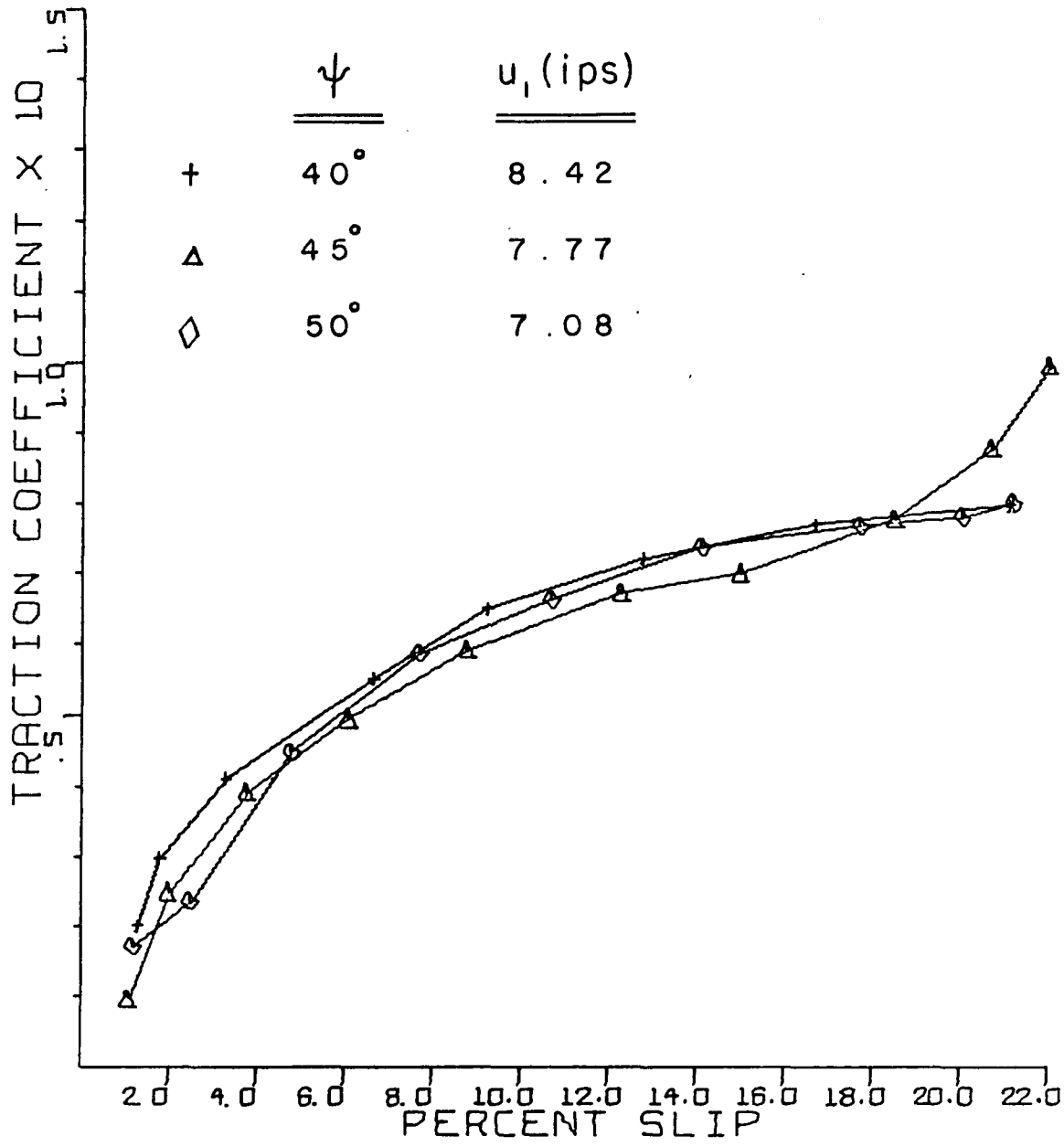

Figure 59. Effect of Spin on Traction Coefficient for 450 KSI Maximum Contact Pressure

due to spin, and the velocity field of the lubricant on the deformed surface of the driving ball relative to that of the driven ball.

The whirl produced in the lubricant film by the spin component of the velocity field gives rise to a centrifugal force which tries to push the lubricant particles out of the contact zone. The magnitude of this force f_c on any lubricant particle of mass m, which is between the deformed surfaces of the balls, will be

$$f_c = m \quad \omega_{spin}^2 \quad \rho$$

where ρ is the radial distance measured from the whirl origin c to the center of the lubricant particle.

It is obvious that this force will decrease the film thickness by pushing the lubricant film out of the contact zone. But in the previous discussion it was shown that any decrease in the film thickness produces a proportional amount of increase in the traction coefficient. Therefore, increasing amounts of spin result in increasing traction coefficient, which correlates with the experimental results.

The second factor that can shift the traction curves is the change in velocity field of the lubricant as spin is introduced into the system.

In Appendix C it was shown that the velocity field of the lubricant at the deformed boundary of the driving ball relative to

that of the driven ball was

$$\Delta\vec{u} = \Delta u_c \hat{i} + \vec{\omega}_{spin} \times \vec{\rho}$$

The traction coefficients were found by moment measurements about the axis of rotation of the driven ball. Since three driving balls were coupled to the driven ball, the contribution of the first term of the velocity field to the measured moment will be

$$M_1 = 3 \left(\bar{\eta} \frac{\Delta u_c}{h} \pi a^2\right) (R_1 \sin \psi)$$

where $\bar{\eta}$ = average viscosity for the interval $0 < \rho < a$

The direction and the sense of $\vec{M}_1$ will be the same as $\vec{\omega}_2$.

Since the second component of the velocity field is circular it will not produce any resultant tractive force on the contact plane, but it will generate a moment M_{spin} about the z axis which is normal to the contact area.

Due to circular shearing of the lubricant film a small area dA on the deformed surface of the driven ball will see a tractive force

$$d\vec{F}_{spin} = \eta \frac{\vec{\omega}_{spin} \times \vec{\rho}}{h} dA$$

Introducing cylindrical coordinates

$$dA = \rho d\theta \, d\rho$$

Then

$$d\vec{F}_{spin} = \eta \frac{\vec{\omega}_{spin} \times \vec{\rho}}{h} \quad (\rho \, d\theta \quad d\rho)$$

The moment $d\vec{M}_{spin}$ produced by this force about the z axis is

$$d\vec{M}_{spin} = \vec{\rho} \times d\vec{F}_{spin}$$

But $\vec{\rho} \times \vec{\omega}_{spin} \times \vec{\rho} = \rho^2 \vec{\omega}_{spin}$ since $\vec{\omega}_{spin} \perp \vec{\rho}$

Therefore

$$d\vec{M}_{spin} = \eta \frac{\vec{\omega}_{spin}}{h} \quad \rho^3 \, d\rho \, d\theta$$

The total moment due to spin, M_{spin} can be found by integrating these incremental moments over the deformed area. Thus

$$\vec{M}_{spin} = \int_0^2 \int_0^a \eta \frac{\vec{\omega}_{spin}}{h} \rho^3 \, d\rho \, d\theta$$

$$= \bar{\eta} \frac{\vec{\omega}_{spin}}{h} \left(\frac{\pi a^4}{2} \right)$$

As it can be seen the direction and the sense of $\vec{M}_{spin}$ is the same as $\vec{\omega}_{spin}$. Therefore only the component of $\vec{m}_{spin}$ along the axis of rotation of the driven ball will effect the moment measurements. Again considering the three driving balls, the effect of the second component of velocity field on moment measurement will be

$$M_2 = \pm 3 \, (\cos \psi) \, M_{spin}$$

$$= \pm \frac{3}{2} \pi a^4 \frac{\bar{\eta} \omega_{spin}}{h} \cos \psi$$

Here the plus or minus sign is introduced reminding that M_2 will either be added or subtracted from M_1. This fact was presented in Appendix C. It was shown that for contact angles less than 45° $\vec{\omega}_{spin}$ would be along the negative z axis and for contact angles greater than 45° it would be along the positive z axis.

The measured moment M about the axis of rotation of the driven ball from which the traction coefficient was found is the sum of M_1 and M_2. Thus

$$M = 3\,(\pi\, a^2\, \bar{\eta}\, \frac{\Delta u_c}{h})\,(R_1 \sin\psi) \pm \frac{3}{2}\,\pi\, a^4\, \bar{\eta}\, \frac{\omega_{spin}}{h} \cos\psi$$

with (+) if $\psi > 45°$

(−) if $\psi < 45°$

when $\psi = 45°$, $\omega_{spin} = 0$

and $M = M_1$

A rough idea of the order of magnitude of M_1 and M_2 can be obtained by examining the numerical values of the radii of deformed area as the maximum Hertzian pressure is changed.

From Appendix D

$$a = 3.54 \times 10^{-3} \text{ in} \quad \text{at } p_{max} = 300 \text{ KSI}$$

and

$$a = 5.32 \times 10^{-3} \text{ in} \quad \text{at } p_{max} = 450 \text{ KSI}$$

Hence, for moderate values of Δu_c

$$M_2 << M_1$$

The air turbine which was designed to eliminate the friction force in the output shaft bearing was calibrated in such a way that at zero shearing the measured torque was zero. Or,

$$M = 0 \quad \text{at} \quad \Delta u_c = 0$$

This condition says that in every measurement the effect of M_2 was automatically cancelled by the air turbine.

It is clear that in this experimental investigation the decrease of the film thickness due to centrifugal forces is the only factor which increases the traction coefficient as the quantity $| \psi - 45^\circ |$ is increased keeping the other variables fixed.

Although the second factor was cancelled in this work this factor must not be neglected especially in the type of applications where the percent sliding is small.

An interesting phenomenon is observed for the percent slip interval ranging between 16 to 20. Most of the traction curves are found to pass through an inflection point between 16 to 20 percent sliding. This inflection point can be seen in Figures 37 through 51. Thirty-one out of 225 traction curves are found to have an inflection point around 16 percent sliding. Eighty-five curves have an inflection point around 18 percent sliding. Sixty-three curves pass through an inflection point around 20 percent sliding. The remaining 40 curves have an inflection point between 20 to 25 percent sliding.

The traction curves in this zone were observed to intersect each other in such a way that the effects of spin, maximum pressure, and

rolling speed on the traction coefficient are reversed when the effects are compared on each side of the inflection point.

According to the theory of EHD lubrication these are unexpected behaviors for traction curves. Metallic contact was checked for each test and nothing was detected suggesting any amount of metallic contact. Therefore this phenomenon is left unexplained.

2. High Level Sliding

This interval ranges between 20 to 100 percent sliding. Metallic contact was detected for most of the traction curves before 90 percent sliding was reached.

In Appendix E the beginning of metallic contact for each set of test data is indicated by a star printed at the upper right corner of the data point.

Observations of recorded voltages suggested that the percentage of metallic contact was between 30 to 70 percent. Percent metallic contact was found by taking a time average which is the percent of the time that metallic contact occurs.

The high level sliding data can be summarized as follows:

(a) At constant contact angle, rolling speed and load, the coefficient of traction generally increases to a maximum as the percent sliding increases.

Using the derived equation for the coefficient of traction

$$T.C. = \frac{3}{2} \frac{\overline{\Delta u}}{h} \eta_o \frac{\overline{e^{\alpha p}}}{p_{max}}$$

and inserting u_1 into this equation as

$$T.C. = \frac{3}{2} \left(\frac{\overline{\Delta u}}{u_1} \right) \frac{u_1}{h} \eta_o \frac{\overline{e^{\alpha p}}}{p_{max}}$$

it is clear that the coefficient of traction increases as the percent slip increases.

Temperature effects can be thought to be the reason of the observed maximum of the traction curves as well. It is a well-known fact that, the viscosity decreases with temperature. Thus, including the effect of temperature, the simple exponential equation for pressure dependent viscosity can be written as [from Reference (24)]

$$\eta = \frac{\eta_o e^{\alpha p}}{1 + \delta(T-T_o)}$$

where

T_o = room temperature

T = temperature of the lubricant at the contact zone

δ = constant which should be determined experimentally

Substituting the temperature dependent viscosity into the equation of traction coefficient we get

$$T.C. = \frac{3}{2} \left(\frac{\overline{\Delta u}}{u_1} \right) \frac{u_1}{h} \eta_o \frac{e^{\alpha p}}{p_{max}} \frac{1}{(1+\delta(T-T_o)}$$

A decrease in the coefficient of traction can be predicted by this equation if the increase in the temperature dependent term is larger than the increase in the percent slip after a certain value of percent slip.

(b) At constant contact angle, load, and percent slip, the coefficient of traction does not show any typical pattern as the rolling velocity increases. Therefore the coefficient of traction does not depend on rolling velocity for high levels of slip.

(c) At constant contact angle, percent slip, and rolling velocity, the coefficient of traction decreases as the load increases for most of the curves. This behavior was observed only in the field of hydrodynamic lubrication.

(d) At constant load, rolling velocity, and sliding speed the coefficient of traction decreases as the absolute value of the angular difference, $| \psi - 45 |$ increases.

This behavior was not expected for EHD lubrication because of the arguments given at the beginning of this chapter while analyzing the low level sliding data ranging from 0 to 20 percent slip.

VI. CONCLUSIONS AND RECOMMENDATIONS

The value of the contact angle between two spheres, one driving and one driven, under EHD lubricated conditions is found to have an effect upon the traction curve. For driving axes which are perpendicular, the coefficient of traction is increased as the absolute value of the angular difference $| \psi - 45^\circ |$ is increased in the low level percentages of slip which range between 0 to 20. For percent slip values ranging from 20 to 100 the coefficient of traction is decreased as the absolute angular difference is increased for contact pressures from 300 to 450 KSI.

An inflection point is discovered for the percent slip interval ranging between 0 to 20. The coefficient of traction increases with pressure before the inflection point and decreases for most of the curves as the pressure is increased after the inflection point. The coefficient of traction decreases as the rolling velocity is increased before the inflection point and it does not show any typical pattern of dependency on rolling velocity after the inflection point.

It is recommended that further research be undertaken to investigate the percentage of metallic contact in the region of high level percentages of slip ranging between 20 to 100 percent. The frequency response of the voltage recorder used during the tests was 50 cycles per second. The minimum division was 2 mm corresponding to 20 m Volt. Since maximum voltage change due to metallic contact was 15 m Volt it will be recommended for the future investigator to use a better voltage recorder so that percent metallic contacts can be determined

accurately. Studies concerning the film thicknesses and the temperature in the contact region would provide a proper foundation for completing the theoretical analysis especially for the phenomena that are left undetermined.

It is also recommended that further testing be undertaken for different lubricants for which the base stock is known and where direct comparison can be made between oils with the same base viscosities and varying pressure viscosity coefficients, and with the same pressure viscosity coefficients and varying viscosities. This study would show if the effects seen in this work could be reproduced and studied as a function of viscosity and pressure viscosity coefficient. A statistical data analysis will also be recommended to determine the significance of the results.

REFERENCES

1. Cameron, A., The Principles of Lubrication, John Wiley and Sons, Inc., New York, 1966.

2. Hewko, L. O., "Roller Traction Drive Unit for Extremely Quiet Power Transmission," American Institute of Aeronautics, Paper No. 67-429, July 17, 1967.

3. Carson, R. W., "Better Traction Drives are Here", Machine Design, April 18, 1974.

4. Green, R. L., and F. L. Longenfeld, Machine Design, May 2, 1974.

5. Hann, J. F., "Experimental Investigation of the Effect of Spin on Traction in Elastohydrodynamically Lubricated Contacts," M.S. Thesis, VPI&SU, Blacksburg, Virginia, 1972.

6. Crook, A. W., The Lubrication of Rollers, IV: Measurement of Friction and Effective Viscosity," "Philosophical Trans. of the Royal Society, Series A., Vol. 255, pp. 371-382, July, 1971.

7. Tallian, T. E., "EHD Hertzian Contact, Part 2", Mech. Eng'g., Vol. 93, No. 12, pp. 17-22, December 1971.

8. Smith, F. W., "Lubricant Behaviour in Concentrated Contact-- Some Rheological Problems," ASLE Trans., 3, pp. 18-25, 1960.

9. Gentle, C. R. and A. Cameron, "Mechanics and Thermodynamics in Lubrication," NASA SP-318, 1973.

10. Townsend, D. P., C. W. Allen, and E. V. Zaretsky, JOLT, Trans. of ASME, Paper No. 73-Lub-39.

11. Miller, R. S., "On the Mechanical Behavior of Entrained Materials in Concentrated Contacts", ASLE Trans., Preprint No. 74 LC-2A-2.

12. Trachman, E. G., and H. S. Cheng, "Rheological Effects on Friction in EHD Lubrication", NASA CR 2206, March, 1973.

13. Plint, M. A., "Traction in EHD Contacts", Proceedings of the Institute of Mech. Engineers, 182, Part 1, No. 14, pp. 300-306, 1968.

14. Johnson, K. L., and A. D. Roberts, "Observations of Viscoelastic Behavior of an EHD Lubricant Film", Proc. of Royal Soc. of London, A. 337, pp. 217-242, 1974.

15. Rounds, F. G., "Effects of Lubricant Composition on Friction as Measured with Thrust Ball Bearings," Journal of Chem. and Eng'g. Data, Vol. 5, No. 4, pp. 499-507, October, 1960.

16. Zaretsky, E. V., "Antiwear and E. P. Additive Effects During Roller and Spinning Contact with Synthesized Hydrocarbon Oil", NASA TM X-52931, N 71-14786, January, 1971.

17. Cullwick, E. G., "The Fundamentals of Electromagnetism", Third Edition, Cambridge Univ. Press, 1966.

18. Drysdale, C. W., A. C. Jolley and G. F. Tagy, Electrical Measuring Instruments, Second Edition, John Wiley and Sons, N. Y., 1952.

19. Furey, M. J., "Metallic Contact and Friction Between Sliding Surfaces," ASLE Trans., 4, pp. 1-11, 1961.

20. Petroff, N. P., The Engineer, 113, pp. 224-225, 294-295, 351-352, March, 1912.

21. Greenwood, J. A., and J. J. Kanzlarich, "Inlet Shear Heating in EHD Lubrication", JOLT, Trans. of ASME, October, 1973.

22. Wedeven, L. D., "Traction and Film Thickness Measurements Under Starved EHD Conditions", JOLT, Trans. of ASME, April, 1975.

23. Operating and Servicing Manual for Model 5304A Electronic Counter, Hewlett-Packard and Company, 1972.

24. Kannel, J. W. and J. A. Walowit, "Simplified Analysis for Tractions Between Rolling-Sliding EHD Contacts", JOLT, Trans. of ASME, 93, Series F, No. 1, pp. 39-46, January 1971.

APPENDIX A

LIST OF EQUIPMENT

1. Electronic Measuring Unit, Model 5300 A, Hewlett-Packard Company.
2. Electronic Timer/Counter, Model 5304 A, Hewlett-Packard Company.
3. Oscilloscope, Type 561 A, Ser. No. B081193, Tektronix, Inc.
4. Vari-Speed Electric Moto Drive, 213 to 1279 rpm, one horsepower, Reeves Pulley Company.
5. Electronic Voltage Recorder, Model Mark II, Brush Corporation.
6. Voltmeter, Simpson 260, Series 6P, Simpson Electric Company.
7. Powerstat Variable Transformer, Type S649, 230 V, 60 ∿, 9A, Superior Electronic Company.
8. Thrust Bearings, Part Number NTA 411, The Torrington Company.
9. Thrust Washers, Part Number TRB 411, The Torrington Company.
10. Flexible Shafting, Model LB 25, Core No. 8924 MH, Stove Manufacturing Company.
11. Stainless Steel Balls, .5 inch diameter, PIC Design Corporation.
12. Photoconductive Cell, Type CL 504 L, Clarix Corporation.
13. Lamp, Type GE 46, General Electric Company.
14. Platform Balance, Ohaus, 0 to 200 gram, Fisher Scientific Company.
15. Radial Ball Bearing, Model R-12, no shield type, New Departure-Hyatt Bearings Division of General Motors Corporation.
16. Traction Fluid, Santotrac 40, Monsanto Company.
17. Probe Ring, 0 to 60 pounds, Ann Arbour Instrument Works Corporation.
18. Microscope, 1 x 10^3 magnification, The Gartner Scientific Corporation.

APPENDIX B

UNCERTAINTY IN SPEED MEASUREMENT

At a rotational speed of 1500 rpm, a total of 250 revolutions will elapse during a counter sampling period of 10 seconds. Since there are two holes in each disc there will be two counts per revolution. This will result in 500 counts for the sampling period. The accuracy of the frequency measurement is determined at low frequencies by the $\pm$ 1 count ambiguity in measurement (23). Therefore, the $\pm$ 1 count will result in a maximum uncertainty of 0.2% at 1500 rpm. At lower speeds, the uncertainty will be proportionately higher. The percent uncertainties in counter measurement for certain rotational speeds are given in Table V.

TABLE V

Percent Uncertainty in Speed Measurement

RPM	% Uncertainty
60	5.000
90	3.330
120	2.500
150	2.000
180	1.670
240	1.125
300	1.000
600	0.500
1200	0.250

APPENDIX C

KINEMATICS OF ROLLING SPHERES IN CONTACT

Before giving the kinematic description of the system that was used, it is worthwhile to give some basic ideas about the elastic deformation and pressure within the contact zone.

If two dry surfaces are loaded together there is an elastic flattening. The pressures so generated are semi-elliptical. This means that if the radius of "point" contact with balls is "a," then if ρ is the distance measured from the center of the contact, the pressure p at any point ρ is

$$p = p_{max}(1-\rho^2/a^2)^{\frac{1}{2}}$$

This elastic formulation of two contacting surfaces was first given by Hertz (1).

For steel balls, under a normal load of W, the following equations are given (1).

$$W = \frac{2\Pi}{3} p_{max} a^2$$

$$a = 3.56 \times 10^{-3}(RW)^{\frac{1}{3}}$$

$$p_{max} = 3.75 \times 10^{4}(W/R^2)^{\frac{1}{3}}$$

where

$R = \frac{R_1}{2}$ = reduced radius (for balls of equal radii)

R_1 = radius of the ball in contact

The spin velocity generated by two rotating balls having an angle of contact, ψ, and under a normal load, N, will be derived next. Following

that, a general three dimensional kinematic view of the system will be given, where sliding velocity as well as spin velocity will be considered.

In Figure 60a two rotating balls in contact, with an angle of contact ψ are shown, where the axis of rotation of the driving ball is perpendicular to that of the driven ball. The projection of the elastically deformed circular contact zone is shown by the straight segment AB. This projected area with the origin C, and a radius of "a," is magnified in Figure 60b.

A right-handed cartesian coordinate system is chosen such that the z axis is along the normal of the contact area. The x axis has the same direction and sense as does the rolling velocity u. Point C being the origin of the system, the y axis goes from C to A.

If the relative velocity of two balls at point C (where the maximum Hertzian pressure occurs) is zero, then

$$u_{C1} = u_{C2}$$

or in terms of the angular velocities of the rotating balls,

$$\omega_1 R_1 \cos\psi = \omega_2 R_1 \sin\psi$$

Therefore,

$$\frac{\omega_2}{\omega_1} = \text{ctn}\psi$$

The velocities of the driving and the driven balls at point B are:

$$u_{b1} = w_1(R_1\cos\psi + a\ \sin\psi)$$

and

$$u_{b2} = w_2(R_1\sin\psi + a\ \cos\psi)$$

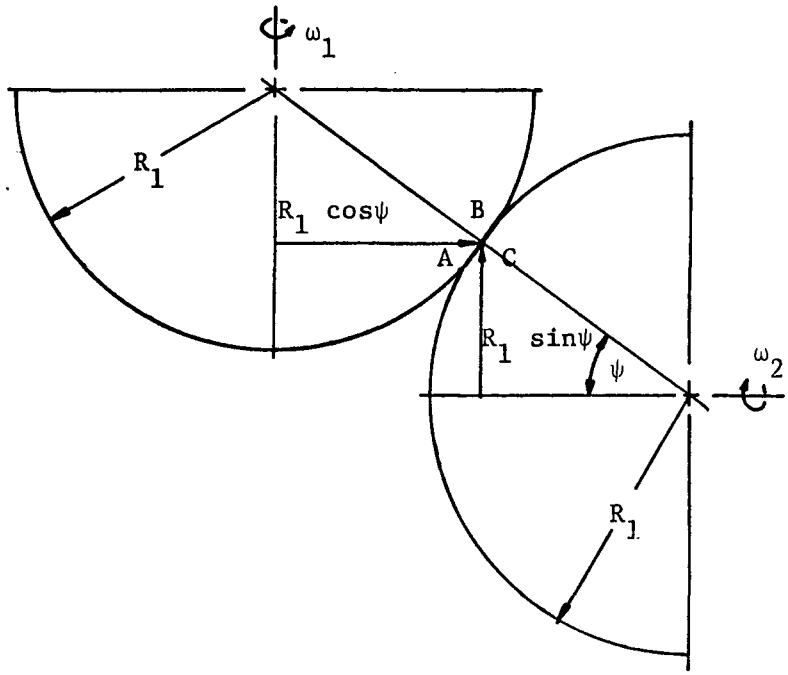

a)

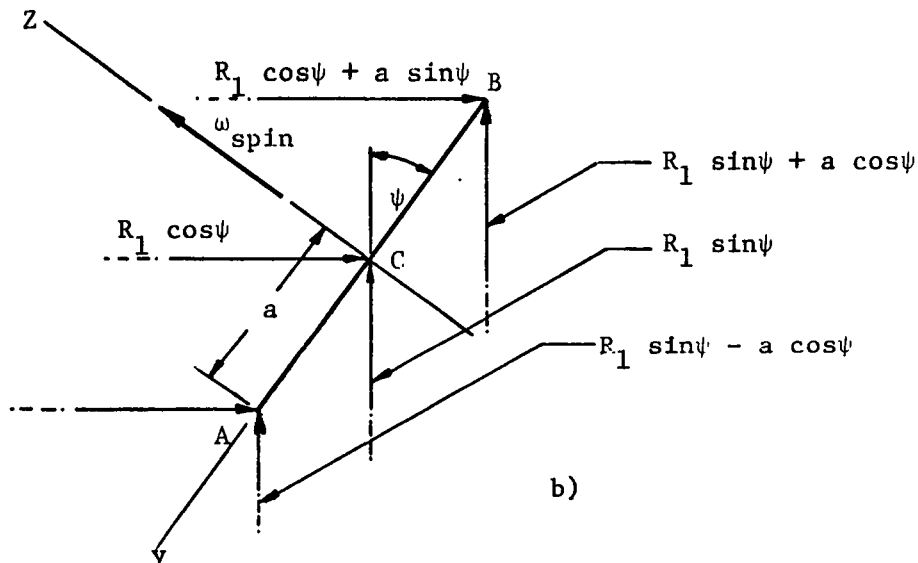

b)

Figure 60. a) Spheres in Contact
b) Projection of Contact Area, Magnified

respectively. The angular velocity created by the difference of these last two velocities is called "spin," and will be referred to as $_{spin}$.

$$\omega_{spin} = \frac{u_{b1} - u_{b2}}{a}$$

$$= \frac{w_1(R_1\cos\psi + a\sin\psi) - \omega_2(R_1\sin\psi + a\cos\psi)}{a}$$

Substituting $\omega_2 = \omega_1 \text{ctn}\psi$ we get,

$$\omega_{spin} = \omega_1(\sin\psi - \cos\psi \text{ ctn}\psi)$$

or using vector notation

$$\vec{\omega}_{spin} = \omega_i(\sin\psi - \cos\psi \text{ ctn}\psi)\ \hat{k}$$

where $\hat{k}$ is the unit vector along the z axis.

Examining the term in the parentheses it can be seen that the sense of ω_{spin} is the same as the positive z axis for contact angles ψ greater than 45°; its sense is along the negative z axis for contact angles less than 45°, and ω_{spin} goes to zero as ψ approaches 45°. In Table VI the values for ω_{spin} are tabulated for five angular velocities of the driving ball ω_1 at which the tests were run and for some contact angles ψ.

If the surfaces are lubricated there is a gross slip at the interface. For this case the driving and the driven balls move relative to each other at the center of the contact area. The velocity of the lubricant film on the surface of the driving ball relative to the driven ball can be formulated as

$$\vec{\Delta u} = \Delta u_i\ \hat{i} + \vec{\omega}_{spin} \times \vec{\rho}$$

TABLE VI

Values of ω_{spin} (rad/min)

w_1 (rad/min)	Contact Angle ψ			
	40°	45°	50°	55°
2658	- 717.8*	0	602	1108.8
3770	-1018.2	0	854	1572.8
5655	-1527.2	0	1281	2359.2
7540	-2036.3	0	1708	3145.6
9425	-2545.4	0	2135	3932

* The minus sign in 40° contact angle column indicates that the vector $\vec{\omega}_{spin}$ is in the direction of -z axis, (see Figure 60b).

where $\vec{\rho} = x\,\hat{i} + y\,\hat{j}$; and $0 < |\vec{\rho}| < a$

$$\Delta u_C = u_{C1} - u_{C2} = u_{P1} - u_{P2}$$

"P" refers to any point on the elastically deformed contact area.

Since $\vec{\omega}_{spin}$ is along the z axis, $\vec{\Delta u}$ has only two components and lies on the plane of contact. Hence

$$\vec{\Delta u} = \Delta u_x\,\hat{i} + \Delta u_y\,\hat{j} .$$

APPENDIX D

CALCULATION OF THE RADII OF THE ELASTICALLY DEFORMED SURFACES

In Reference 1 the following relations are given for elastically deformed surfaces of steel balls:

$$a = (3.56 \times 10^{-3})(RW)^{\frac{1}{3}}$$

$$W = \frac{2\Pi}{3} p_{max} a^2$$

where

a = radius of the deformed zone

W = applied normal load

R = reduced radius of contacting balls

For 0.5 inch diameter steel balls in contact

$$R = 0.125 \text{ inch}$$

Therefore

$$a = (12.81 \times 10^{-9}) p_{max}$$

Using the latter equation, for the range of maximum Hertzian pressure between 300 KSI and 450 KSI, the radius of contact will range between 3.84×10^{-3} inch and 5.76×10^{-3} inch.

APPENDIX E

TRACTION AND SLIP DATA

(a) Data for percent slip between zero to 100.

ψ	p_{max} (KSI)	u_1 (psi)	% Slip	T.C.	% Slip	T.C.
40°	300	8.42	8.87	.0451	58.03	.0862
			25.66	.0721	70.02	.0869
			43.05	.0827	71.82*	.0910
40°	300	12.00	8.50	.0412	71.04*	.1103
			30.75	.0896	75.24	.1075
			50.90	.0999	79.44	.1055
			63.07*	.1137	81.95	.1055
40°	300	18.05	6.27	.0352	77.62	.1069
			24.46	.0827	81.25	.1069
			36.20	.0999	84.33	.1069
			47.40	.1069	87.13	.1069
			68.94	.1069		
40°	300	24.07	15.65	.0507	59.92	.1020
			28.24	.0758	68.52	.0999
			38.31	.0827	78.18	.0965
			53.63	.0951	84.47	.0951
40°	300	24.07	15.65	.0507	59.92	.1020
			28.24	.0758	68.52	.0999
			38.31	.0827	78.18	.0965
			53.63	.0951	84.47	.0951
40°	300	30.08	21.00	.0592	64.75	.0999
			26.81	.0896	70.29	.0979
			40.41	.1020	77.34	.0965
			58.00	.1089		
40°	333	8.42	11.87	.0454	65.23*	.0857
			26.86	.0630	67.03*	.0989
			43.05	.0792	70.62	.0857
			58.63	.0807	73.02	.0832

* Metallic contact is detected for the data point.

APPENDIX E - TRACTION AND SLIP DATA - continued

ψ	p_{max} (KSI)	u_1 (psi)	% Slip	T.C.	% Slip	T.C.
40°	350	30.08	9.69	.0369	71.46	.0824
			17.07	.0477	75.32	.0833
			30.34	.0673	79.02	.0833
			45.28	.0759	84.89	.0824
			57.03	.0781	87.07	.0824
			58.70	.0803	87.91*	.0868
40°	400	8.42	12.47	.0445	43.64	.0712
			19.66	.0567	50.24	.0706
			26.26	.0625	56.83	.0698
			35.25	.0675	60.43	.0695
40°	400	12.00	18.58	.0523	62.23	.0741
			34.11	.0596	68.52	.0733
			47.54	.0660	72.30	.0727
			54.68	.0750		
40°	400	18.05	5.71	.0233	63.91	.0756
			22.78	.0581	68.66	.0741
			38.45	.0669	72.02	.0727
			52.44	.0698	76.22	.0727
			59.43	.0712	79.02	.0727
40°	400	24.07	6.00	.0267	66.43	.0744
			18.79	.0523	70.20	.0756
			27.40	.0654	75.03	.0829
			40.20	.0712	79.02	.0814
			49.22	.0721	83.21	.0800
			58.03	.0727		
40°	400	30.08	4.32	.0262	51.32	.0741
			16.07	.0471	61.39	.0800
			22.45	.0581	68.11	.0814
			34.53	.0689	71.13*	.0930
			40.41	.0712	76.33*	.0988
40°	450	8.42	3.48	.0143	23.26	.0614
			8.27	.0313	28.06	.0655
			11.00	.0512	30.46*	.0696
			17.87	.0533	34.65*	.0758

*Metallic contact is detected for the data point.

APPENDIX E - TRACTION AND SLIP DATA - continued

ψ	p_{max} (KSI)	u_1 (psi)	% Slip	T.C.	% Slip	T.C.
40°	333	12.00	16.49	.0641	74.82	.0807
			30.75	.0782	78.18	.0802
			58.03	.0857	80.28	.0802
			67.69	.0832		
40°	333	18.05	11.87	.0479	72.02	.0857
			21.10	.0555	79.02	.0807
			45.72	.0756	84.89	.0857
			60.83	.0883		
40°	333	24.07	8.93	.0529	73.98	.0984
			19.00	.0605	80.49	.0958
			32.22	.0731	85.73	.0933
			53.84	.0958	88.46	.0923
			60.97	.0984	90.14	.0908
40°	333	30.08	7.67	.0252	61.39	.0656
			16.07	.0353	66.43*	.0676
			22.28	.0479	70.62*	.0731
			42.93	.0580	76.83*	.0756
			53.00	.0671	80.86*	.0746
40°	350	8.42	7.70	.0422	60.43	.0694
			20.90	.0477	67.02*	.0716
			31.65	.0586	72.42*	.0738
			45.44	.0690		
40°	350	12.00	8.09	.0398	64.75	.0707
			28.66	.0629	72.72	.0707
			43.34	.0777	76.50*	.0868
			54.68	.0777		
40°	350	18.05	11.03	.0512	74.54	.0829
			29.22	.0638	78.46	.0824
			37.61	.0738	83.21	.0820
			53.28	.0855	86.01	.0816
			67.27	.0868		
40°	350	24.07	4.95	.0302	53.21	.0868
			16.70	.0594	66.00	.0837
			26.56	.0629	71.67	.0833
			33.48	.0738	78.81*	.0868
			47.96	.0816		

* Metallic contact is detected for the data point.

APPENDIX E - TRACTION AND SLIP DATA - continued

ψ	p_{max} (KSI)	u_1 (psi)	% Slip	T.C.	% Slip	T.C.
40°	450	12.00	4.74	.0131	38.73	.0717
			11.50	.0494	42.51	.0750
			19.00	.0533	47.54	.0754
			26.56	.0660	51.32*	.0754
			32.01	.0680	53.84*	.0809
40°	450	18.05	8.23	.0301	48.24	.0811
			18.02	.0538	52.16	.0819
			22.78	.0614	55.24	.0832
			27.26	.0655	61.39	.0875
			34.53	.0721	63.63	.0875
			41.25	.0774	67.83	.0875
40°	450	24.07	3.48	.0133	54.05	.0807
			13.50	.0476	56.98	.0823
			19.00	.0502	60.55	.0823
			24.67	.0619	64.54*	.0844
			32.01	.0690	66.43*	.0866
			40.83	.0727	68.73*	.0873
			45.44	.0778	72.30*	.0888
40°	450	30.08	7.00	.0209	56.35	.0789
			13.60	.0527	61.22	.0805
			76.31	.0578	65.76	.0821
			34.53	.0670	69.78	.0830
			38.90	.0705	73.48	.0834
			44.10	.0746	75.49	.0834
			50.98	.0783		
45°	300	7.77	2.14	.0361	48.57	.1260
			11.43	.0879	52.85	.1193
			30.00	.1130	57.14	.1160
			40.00	.1193	60.00	.1155
			42.86	.1260		
45°	300	11.1	4.50	.0289	68.00	.1324
			18.00	.0461	71.50	.1274
			32.00	.1011	73.50	.1260
			52.50	.1287	75.00	.1230
			64.50	.1324	76.50	.1205

* Metallic contact is detected for the data point.

APPENDIX E - TRACTION AND SLIP DATA - continued

ψ	p_{max} (KSI)	u_1 (psi)	% Slip	T.C.	% Slip	T.C.
45°	300	16.65	4.10	.0212	75.00	.1324
			21.33	.0852	78.67	.1312
			36.33	.1340	80.67	.1260
			55.00	.1438	82.00	.1260
			67.67	.1410	82.33	.1224
			72.33	.1324		
45°	300	22.20	11.25	.0336	77.50	.1300
			48.25	.1318	80.50	.1270
			60.50	.1340	82.50	.1260
			67.50	.1350	84.00	.1237
			73.75	.1340	84.50	.1218
			72.50	.1318		
45°	300	27.75	20.80	.0702	84.20	.1393
			63.80	.1260	85.40	.1387
			74.20	.1293	86.60	.1387
			79.20	.1350	87.40	.1387
			82.20	.1400		
45°	333	7.77	1.43	.0132	42.14	.1207
			3.57	.0282	45.00	.1184
			12.86	.0616	47.14	.1160
			25.71	.1136	52.14	.1122
			36.43	.1184	54.30	.1113
45°	333	11.10	3.50	.0213	53.00	.1113
			17.00	.0629	56.50	.1108
			26.00	.1090	60.00	.1103
			39.50	.1189	61.50	.1103
			46.50	.1136		
45°	333	16.65	5.67	.0349	69.33	.1231
			25.67	.1042	71.33	.1255
			47.33	.1174	73.33	.1241
			59.00	.1212	74.67	.1231
			65.67	.1217		
45°	333	22.20	5.25	.0335	76.25	.1160
			31.50	.1155	78.75	.1160
			56.75	.1207	80.00	.1160
			67.00	.1207	81.50	.1160
			72.25	.1184		

* Metallic contact is detected for the data point.

APPENDIX E - TRACTION AND SLIP DATA - continued

ψ	p_{max} (KSI)	u_1 (psi)	% Slip	T.C.	% Slip	T.C.
45°	333	27.75	10.00	.0417	80.40	.1492
			47.00	.1572	82.00	.1468
			66.60	.1582	83.60	.1444
			73.40	.1539	84.80	.1421
			77.60	.1515		
45°	350	7.77	2.10	.0222	22.90	.1390
			5.00	.0491	27.10	.1290
			8.60	.0539	32.90	.1259
			12.10	.0572	36.40	.1246
			16.40	.0624		
45°	350	11.10	2.50	.0247	39.50	.1277
			7.50	.0546	44.50	.1268
			16.00	.0611	48.50	.1201
			25.00	.1312	50.50	.1157
			34.00	.1290		
45°	350	16.65	4.00	.0312	60.00	.1357
			15.00	.0570	63.67	.1357
			33.33	.1400	66.67	.1357
			44.00	.1401	68.67	.1357
			53.33	.1357		
45°	350	22.20	4.75	.0332	67.50	.1424
			24.25	.1021	71.00	.1393
			45.50	.1446	71.25	.1379
			53.75	.1459	74.00	.1379
			63.50	.1446		
45°	350	27.75	10.20	.0472	76.00	.1300
			42.00	.1312	78.20	.1290
			61.20	.1335	79.80	.1264
			69.00	.1321	81.60	.1246
			72.80	.1308		
45°	400	7.77	1.40	.0153	15.70	.0672
			4.30	.0418	19.30	.0832
			7.10	.0491	22.10	.0938
			10.00	.0592	25.00	.0965
			12.90	.0639	27.10	.0978

APPENDIX E - TRACTION AND SLIP DATA - continued

ψ	P_{max} (KSI)	u_1 (psi)	% Slip	T.C.	% Slip	T.C.
45°	400	11.10	3.00	.0185	25.50	.1057
			6.50	.0461	29.00	.1084
			10.00	.0575	33.50	.1110
			15.00	.0655	36.50	.1118
			19.00	.0730	39.00	.1137
45°	400	16.65	2.67	.0291	40.33	.1308
			9.67	.0566	44.67	.1308
			17.67	.0704	49.67	.1308
			21.67	.1211	52.67	.1308
			33.00	.1301	54.67	.1308
45°	400	22.20	2.75	.0307	63.75	.1070
			11.25	.0556	66.25	.1062
			25.00	.1110	67.00	.1060
			39.00	.1176	68.50	.1057
			59.75	.1084		
45°	400	27.75	5.40	.0449	68.00	.1018
			32.40	.1018	72.20	.1004
			53.20	.1057	74.20	.1004
			62.00	.1057		
45°	450	7.77	1.00	.0092	7.10	.0492
			2.10	.0221	8.60	.0596
			2.90	.0302	10.00	.0429
			5.00	.0450	15.00	.0700
			5.70	.0476	22.00	.1010
45°	450	11.10	2.00	.0221	13.00	.0675
			4.00	.0332	16.00	.0695
			6.00	.0462	18.50	.0856
			8.50	.0581	21.50	.1054
			10.50	.0645	24.50	.1110
45°	450	22.20	2.75	.0207	41.25	.1203
			9.25	.0556	46.00	.1220
			19.50	.0795	51.50	.1203
			25.50	.1110	55.50	.1190
			33.00	.1170	58.75	.1180

APPENDIX E - TRACTION AND SLIP DATA - continued

ψ	p_{max} (KSI)	u_1 (psi)	% Slip	T.C.	% Slip	T.C.
45°	450	27.75	2.40	.0314	50.00	.1267
			11.20	.0592	55.60	.1257
			21.00	.1018	59.60	.1257
			33.80	.1240	60.60	.1240
			45.00	.1277		
50°	300	7.08	5.82	.0402	54.19	.0891
			22.79	.0632	58.43	.0891
			39.76	.0805	66.06	.0862
50°	300	10.12	3.75	.0230	56.05	.0931
			18.04	.0610	61.40	.0931
			32.30	.0845	70.31	.0931
			44.77	.0931	73.27	.0931
			52.49	.0931		
50	300	15.18	7.35	.0431	60.41	.0891
			23.58	.0776	65.55	.0891
			30.31	.0834	76.24	.0891
			51.30	.0891	80.20	.0891
			57.24	.0891	84.16	.0891
50°	300	20.23	5.86	.0395	71.79	.1035
			16.85	.0544	76.24	.1035
			26.36	.0776	79.21	.1035
			35.26	.0805	82.18	.1035
			48.63	.0377	85.15	.1035
			59.61	.0989	88.12	.1035
			68.23	.1035		
50°	300	25.29	4.26	.0254	62.47	.0977
			14.72	.0496	73.63	.0960
			34.43	.0960	79.81	.0954
			44.41	.0977	82.42	.0949
			50.83	.1035	84.56	.0949
50°	333	7.08	4.13	.0295	48.25	.0875
			18.55	.0686	53.34	.0871
			29.58	.0757	58.43*	.0867
			41.46	.0867		

* Metallic contact is detected for the data point.

APPENDIX E - TRACTION AND SLIP DATA - continued

ψ	p_{max} (KSI)	u_1 (psi)	% Slip	T.C.	% Slip	T.C.
50°	333	10.12	6.16	.0337	58.43	.0867
			16.26	.0631	64.37	.0867
			42.39	.0799	70.30	.0867
			53.08	.0867		
50°	333	15.18	8.93	.0482	56.05	.0947
			22.40	.0715	64.37	.0947
			28.73	.0799	68.33	.0947
			38.63	.0875	72.28	.0942
			48.13	.0926	76.24	.0938
50°	333	20.23	6.16	.0304	61.40	.0926
			13.88	.0531	70.31	.0921
			22.50	.0757	73.27	.0917
			35.26	.0862	76.24	.0913
			48.63	.0913	79.21	.0909
			57.54	.0926	82.18	.0905
50°	333	25.29	3.07	.0181	71.26	.0917
			13.05	.0598	76.24	.0913
			26.83	.0905	81.00	.0909
			39.66	.0938	85.75	.0909
			52.43	.0934	86.93	.0909
			58.90	.0926		
50°	350	7.08	2.43	.0251	32.13	.0890
			10.06	.0545	43.16	.0890
			18.55	.0633	49.09	.0887
			27.88	.0854		
50°	350	10.12	6.16	.0409	52.49	.0850
			20.42	.0723	58.43	.0847
			36.45	.0825	64.37	.0847
			46.55	.0854		
50°	350	15.18	3.00	.0242	64.37	.0923
			16.85	.0645	68.33	.0920
			28.23	.0890	72.28	.0916
			50.51	.0927	76.24	.0916
			56.45	.0927		

APPENDIX E - TRACTION AND SLIP DATA - continued

ψ	p_{max} (KSI)	u_1 (psi)	% Slip	T.C.	% Slip	T.C.
50°	350	20.23	3.49	.0265	58.42	.0934
			9.43	.0473	66.74	.0927
			20.71	.0756	71.79	.0909
			35.86	.0890	76.24	.0905
			46.55	.0927	79.21	.0898
			52.49	.0934	82.18	.0878
50°	350	25.29	6.64	.0381	76.24	.0890
			21.13	.0745	78.62*	.0996
			28.23	.0861	79.81*	.0989
			47.74	.0872	82.18*	.0981
			61.99	.0850	84.56*	.0978
			69.12	.0890		
50°	400	7.08	1.58	.0193	22.78	.0824
			9.22	.0542	25.34	.0834
			17.70	.0758		
50°	400	10.12	3.79	.0342	33.48	.0843
			13.88	.0623	38.83	.0848
			20.42	.0756	45.58	.0860
			25.76	.0800		
50°	400	15.18	3.39	.0315	45.36	.0860
			8.14	.0461	52.49	.0858
			23.98	.0775	56.45	.0853
			36.65	.0848	62.39	.0853
50°	400	20.23	3.19	.0247	51.60	.0834
			3.43	.0506	62.88	.0831
			15.37	.0597	67.34	.0824
			28.73	.0792	70.30	.0817
			42.69	.0836	73.27	.0812
50°	400	25.29	4.98	.0508	67.22	.0824
			12.10	.0618	72.68	.0819
			29.21	.0775	75.05	.0817
			40.85	.0800	77.43	.0814
			50.11	.0812	79.81	.0821
			59.61	.0824	81.00	.0812

* Metallic contact is detected for the data point.

APPENDIX E - TRACTION AND SLIP DATA - continued

ψ	p_{max} (KSI)	u_1 (psi)	% Slip	T.C.	% Slip	T.C.
50°	450	7.08	2.43	.0342	10.06	.0584
			4.13	.0395	11.76	.0619
			6.67	.0515	15.16	.0679
50°	450	10.12	2.00	.0309	16.85	.0687
			6.16	.0498	23.39	.0739
			10.91	.0601	29.92	.0790
50°	450	15.18	3.79	.0350	33.88	.0790
			10.91	.0601	42.59	.0833
			23.58	.0722	46.55	.0825
50°	450	20.23	3.15	.0319	45.36	.0777
			8.54	.0519	48.63	.0782
			19.82	.0739	57.24	.0783
			34.37	.0773	62.88	.0782
50°	450	25.29	3.31	.0344	54.86	.0783
			14.48	.0670	59.61	.0780
			23.03	.0722	64.37	.0778
			35.86	.0782	67.93	.0777
			47.26	.0785	71.49	.0773

(b) Data for percent slip between zero to 22.

ψ	p_{max} (KSI)	u_1 (psi)	% Slip	T.C.	% Slip	T.C.
40°	300	8.42	1.50	.0100	14.95	.0580
			3.60	.0265	18.45	.0592
			6.50	.0362	20.65	.0665
			11.55	.0542	22.00	.0800
40°	300	12.00	2.35	.0144	11.10	.0485
			4.15	.0236	17.05	.0565
			5.96	.0305	19.55	.0607
			8.72	.0403		

APPENDIX E - TRACTION AND SLIP DATA - continued

ψ	p_{max} (KSI)	u_1 (psi)	% Slip	T.C.	% Slip	T.C.
40°	300	18.05	1.95	.0105	14.30	.0515
			3.30	.0195	18.22	.0535
			5.32	.0265	21.15	.0705
			7.12	.0335	22.30	.0855
			10.37	.0437		
40°	300	24.07	2.18	.0121	16.32	.0510
			4.82	.0245	20.31	.0647
			8.12	.0372	21.92	.0835
			12.20	.0465		
40°	300	30.08	2.72	.0050	15.50	.0158
			6.50	.0098	20.17	.0186
			11.70	.0142		
40°	333	8.42	2.30	.0161	12.33	.0571
			3.75	.0262	14.40	.0597
			5.45	.0360	17.70	.0632
			7.10	.0420	20.75	.0650
			9.25	.0502	22.35	.0732
40°	333	12.00	1.95	.0107	11.52	.0526
			3.12	.0195	14.40	.0565
			4.90	.0295	17.82	.0592
			6.70	.0386	21.51	.0655
			8.72	.0465		
40°	333	18.05	2.31	.0125	12.60	.0505
			4.20	.0235	15.15	.0536
			6.22	.0338	18.67	.0557
			8.35	.0415	22.00	.0705
			10.37	.0465		
40°	333	24.07	3.12	.0167	14.96	.0507
			5.60	.0276	18.70	.0526
			8.00	.0372	21.50	.0618
			11.35	.0461	22.40	.0778
40°	333	30.08	3.90	.0193	13.12	.0476
			6.30	.0295	17.45	.0457
			9.32	.0405	21.47	.0571

APPENDIX E - TRACTION AND SLIP DATA - continued

ψ	p_{max} (KSI)	u_1 (psi)	% Slip	T.C.	% Slip	T.C.
40°	350	8.42	1.00	.0100	11.95	.0610
			2.92	.0280	15.38	.0651
			5.18	.0402	19.15	.0688
			7.25	.0483	21.32	.0691
			9.30	.0548		
40°	350	12.00	1.50	.0155	14.85	.0627
			3.90	.0336	18.85	.0656
			7.20	.0445	21.30	.0667
			10.70	.0556		
40°	350	18.05	1.85	.0136	10.9	.0522
			3.25	.0265	14.6	.0584
			5.37	.0356	17.6	.0617
			8.42	.0465	20.5	.0631
40°	350	24.07	2.38	.0190	13.75	.0557
			4.60	.0311	16.90	.0600
			7.20	.0415	20.30	.0613
			9.70	.0495		
40°	350	30.08	1.90	.0105	12.60	.0506
			3.85	.0256	15.30	.0557
			6.30	.0358	18.90	.0576
			9.30	.0446	21.30	.0588
40°	400	8.42	1.50	.0202	12.00	.0651
			2.90	.0353	15.25	.0692
			5.50	.0476	18.90	.0722
			8.80	.0582		
40°	400	12.00	1.30	.0156	7.85	.0527
			2.30	.0276	11.70	.0615
			4.35	.0405	14.70	.0657
40°	400	18.05	1.90	.0175	10.15	.0534
			2.70	.0266	13.30	.0582
			4.30	.0355	17.30	.0615
			6.90	.0468		
40°	400	24.07	1.60	.0191	11.75	.0527
			3.70	.0285	15.05	.0556
			5.80	.0376	18.73	.0585
			7.80	.0448		

APPENDIX E - TRACTION AND SLIP DATA - continued

ψ	p_{max} (KSI)	u_1 (psi)	% Slip	T.C.	% Slip	T.C.
40°	400	30.08	1.40	.0112	11.50	.0505
			4.60	.0308	13.90	.0545
			6.85	.0391	16.85	.0556
			9.40	.0465		
40°	450	8.42	1.30	.0203	9.25	.0651
			1.80	.0300	12.80	.0722
			3.30	.0412	16.70	.0771
			6.65	.0552	21.10	.0798
40°	450	12.00	1.30	.0157	11.10	.0667
			2.30	.0307	16.30	.0734
			4.30	.0426	19.70	.0745
			8.15	.0575		
40°	450	18.05	2.40	.0256	9.90	.0625
			3.70	.0357	14.10	.0698
			5.90	.0456	18.30	.0726
			7.90	.0540	21.70	.0735
40°	450	24.07	1.80	.0182	10.80	.0623
			3.40	.0315	13.90	.0671
			5.10	.0412	17.60	.0712
			7.00	.0500	20.50	.0721
40°	450	30.08	1.30	.0121	12.90	.0641
			3.80	.0335	16.90	.0687
			6.70	.0466	19.80	.0691
			9.70	.0572		
45°	300	7.77	1.95	.0101	16.60	.0435
			3.05	.0152	18.90	.0441
			4.20	.0205	19.95	.0463
			6.40	.0253	21.30	.0547
			9.20	.0332	22.60	.0700
			12.80	.0391		
45°	300	11.10	2.35	.0115	18.40	.0417
			4.70	.0205	20.10	.0486
			7.90	.0285	20.9	.0547
			11.50	.0356	21.75	.0626
			15.30	.0395	22.30	.0744

APPENDIX E - TRACTION AND SLIP DATA - continued

ψ	p_{max} (KSI)	u_1 (psi)	% Slip	T.C.	% Slip	T.C.
45°	300	16.65	1.70	.0076	19.45	.0435
			5.75	.0224	21.20	.0580
			10.50	.0336	22.00	.0705
			14.75	.0377		
45°	300	22.20	3.00	.0127	19.00	.0415
			4.75	.0185	20.30	.0527
			8.75	.0193	21.40	.0642
			12.10	.0347	22.10	.0761
			16.70	.0372		
45°	300	27.75	1.30	.0075	14.90	.0357
			4.10	.0156	18.30	.0384
			7.50	.0267	20.70	.0503
			10.90	.0325	21.70	.0678
45°	333	7.77	1.30	.0103	12.50	.0544
			2.95	.0192	16.00	.0576
			4.50	.0272	19.00	.0593
			6.30	.0371	21.00	.0632
			8.00	.0432	22.00	.0700
			9.40	.0486	22.40	.0902
45°	333	11.10	1.70	.0107	16.10	.0547
			3.50	.0194	19.10	.0572
			5.70	.0295	20.50	.0607
			7.50	.0373	21.90	.0726
			10.30	.0485	22.10	.0878
			13.1	.0523		
45°	333	16.65	2.30	.0123	14.60	.0506
			4.20	.0235	16.70	.0517
			6.40	.0357	20.30	.0553
			9.20	.0402	21.90	.0636
			11.80	.0472	22.30	.0787
45°	333	22.20	1.20	.0077	14.10	.0481
			3.30	.0168	17.90	.0512
			7.10	.0324	20.30	.0581
			9.20	.0402	21.10	.0682
			10.50	.0426		

APPENDIX E - TRACTION AND SLIP DATA - continued

ψ	p_{max} (KSI)	u_1 (psi)	% Slip	T.C.	% Slip	T.C.
45°	333	27.75	2.90	.0134	16.10	.0494
			5.50	.0255	19.80	.0532
			8.70	.0374	21.50	.0756
			11.70	.0446		
45°	350	7.17	2.00	.0170	15.70	.0591
			4.00	.0292	17.20	.0624
			6.60	.0389	18.30	.0667
			8.90	.0452	19.60	.0767
			11.00	.0502	20.60	.0898
			12.90	.0536		
45°	350	11.10	1.50	.0121	15.00	.0556
			3.60	.0256	18.00	.0632
			7.30	.0391	19.10	.0734
			9.60	.0453	20.20	.0853
			12.30	.0458	21.90	.1207
45°	350	16.65	1.10	.0098	16.10	.0578
			3.00	.0211	18.80	.0693
			5.40	.0317	19.50	.0814
			8.70	.0421	21.00	.1042
			11.40	.0471		
45°	350	22.20	2.20	.0153	17.60	.0612
			4.50	.0281	19.90	.0878
			7.80	.0378	21.00	.1092
			11.90	.0476	21.90	.1278
			14.70	.0526		
45°	350	27.75	1.80	.0113	17.20	.0575
			5.10	.0284	19.50	.0745
			9.50	.0427	20.50	.0955
			13.90	.0497	21.50	.1194
45°	400	7.77	1.35	.0123	13.30	.0627
			2.90	.0286	16.40	.0673
			5.00	.0397	18.90	.0728
			7.40	.0481	21.80	.0842
			9.60	.0562		

APPENDIX E - TRACTION AND SLIP DATA - continued

ψ	p_{max} (KSI)	u_1 (psi)	% Slip	T.C.	% Slip	T.C.
45°	400	11.10	2.00	0.0174	17.90	0.0671
			4.30	0.0367	20.00	0.0752
			7.30	0.0462	21.10	0.0848
			10.80	0.0558	22.20	0.0998
			14.10	0.0622		
45°	400	16.65	1.50	0.0098	15.80	0.0632
			2.90	0.0225	19.30	0.0703
			5.70	0.0384	20.30	0.0805
			9.20	0.0498	21.30	0.0922
			12.50	0.0572	21.90	0.1052
45°	400	22.20	2.00	0.0146	18.00	0.0647
			3.70	0.0278	20.50	0.0773
			6.60	0.0414	21.30	0.0967
			8.60	0.0476	22.00	0.1148
			12.00	0.0557		
45°	400	27.75	1.30	0.0076	15.70	0.0573
			3.80	0.0244	18.30	0.0632
			5.50	0.0342	19.90	0.0707
			8.20	0.0442	20.50	0.0867
			10.70	0.0478	21.50	0.1035
			13.20	0.0531		
45°	450	7.77	1.10	0.0098	12.30	0.0673
			2.00	0.0251	15.00	0.0701
			3.80	0.0392	18.50	0.0778
			6.10	0.0496	20.70	0.0880
			8.80	0.0592	22.00	0.0998
45°	450	11.10	1.40	0.0132	13.90	0.0698
			2.70	0.0278	17.40	0.0724
			3.90	0.0375	19.60	0.0791
			5.50	0.0456	20.90	0.0908
			8.20	0.0561	21.80	0.1046
			11.20	0.0632		
45°	450	16.65	1.70	0.0154	14.60	0.0667
			3.20	0.0300	17.10	0.0687
			4.90	0.0408	18.70	0.0724
			6.90	0.0496	20.90	0.0926
			9.60	0.0578	21.50	0.1087
			12.70	0.0641		

APPENDIX E - TRACTION AND SLIP DATA - continued

ψ	p_{max} (KSI)	u_1 (psi)	% Slip	T.C.	% Slip	T.C.
45°	450	22.20	1.40	0.0105	12.50	0.0616
			2.10	0.0237	16.20	0.0667
			4.00	0.0351	19.50	0.0758
			6.60	0.0462	20.50	0.0906
			9.30	0.0554		
45°	450	27.75	2.10	0.0196	15.10	0.0654
			4.10	0.0315	18.80	0.0708
			7.60	0.0487	20.20	0.0857
			10.90	0.0588	21.20	0.1008
50°	300	7.08	1.30	.0102	12.70	.0536
			2.90	.0231	15.90	.0591
			4.30	.0305	18.70	.0623
			6.20	.0387	20.40	.0698
			7.60	.0424	22.20	.0801
			9.60	.0478		
50°	300	10.12	1.70	.0118	14.30	.0558
			2.70	.0212	17.80	.0602
			5.20	.0315	20.00	.0667
			7.30	.0402	21.50	.0759
			10.90	.0496		
50°	300	15.18	1.90	.0131	15.30	.0546
			3.30	.0227	17.70	.0575
			5.40	.0293	19.50	.0627
			8.50	.0427	20.90	.0718
			12.00	.0498	21.70	.0815
50°	300	20.23	2.00	.0157	16.40	.0537
			4.10	.0235	19.10	.0603
			7.10	.0342	20.80	.0745
			9.40	.0411	21.60	.0848
			12.60	.0485		
50°	300	25.29	1.60	.0092	17.40	.0538
			4.90	.0268	20.60	.0678
			7.70	.0373	21.10	.0808
			10.80	.0442	21.80	.0927
			13.90	.0477		

APPENDIX E - TRACTION AND SLIP DATA - continued

ψ	p_{max} (KSI)	u_1 (psi)	% Slip	T.C.	% Slip	T.C.
50°	333	7.08	1.5	.0102	12.10	.0582
			3.60	.0298	15.30	.0601
			6.10	.0421	17.50	.0712
			8.90	.0517	19.40	.0797
50°	333	10.12	1.90	.0125	13.40	.0578
			2.90	.0238	16.40	.0641
			5.90	.0396	18.10	.0748
			9.90	.0527		
50°	333	15.18	2.00	.0095	11.70	.0542
			3.00	.0207	15.10	.0574
			5.00	.0331	17.20	.0638
			8.40	.0460	18.9	.0792
50°	333	20.23	2.50	.0127	9.60	.0442
			4.40	.0261	13.30	.0527
			6.90	.0357	16.60	.0602
50°	333	25.29	1.50	.0067	15.10	.0545
			5.00	.0285	17.70	.0621
			8.70	.0392	18.70	.0727
			9.60	.0482	19.60	.0878
50°	350	7.08	1.20	.0102	11.60	.0568
			1.80	.0203	13.50	.0612
			3.30	.0314	15.70	.0623
			5.40	.0411	17.70	.0653
			7.60	.0492	20.50	.0748
			9.70	.0528		
50°	350	10.12	1.00	.0085	15.10	.0614
			2.50	.0238	17.50	.0638
			5.30	.0385	20.00	.0721
			7.60	.0472	21.00	.0812
			11.10	.0561		
50°	350	15.18	1.80	.0134	16.20	.0605
			4.40	.0328	19.10	.0673
			8.50	.0479	20.70	.0834
			12.70	.0571		

APPENDIX E - TRACTION AND SLIP DATA - continued

ψ	p_{max} (KSI)	u_1 (psi)	% Slip	T.C.	% Slip	T.C.
50°	350	20.23	1.60	.0088	9.90	.0485
			3.50	.0242	11.80	.0527
			5.70	.0361	15.40	.0572
			7.80	.0421	19.30	.0645
50°	350	25.29	2.50	.0176	13.30	.0537
			4.70	.0307	17.00	.0586
			7.20	.0401	18.80	.0643
			9.90	.0454	20.30	.0775
50°	400	7.08	1.80	.0228	11.50	.0602
			4.00	.0402	15.60	.0685
			6.70	.0483	18.40	.0751
			9.30	.0561	20.20	.0808
50°	400	10.12	1.50	.0168	14.80	.0648
			3.10	.0302	17.90	.0708
			6.70	.0467	20.90	.0835
			9.90	.0563		
50°	400	15.18	2.10	.0197	15.60	.0608
			4.70	.0368	18.10	.0653
			7.10	.0435	19.90	.0696
			9.50	.0516	21.10	.0791
			12.30	.0581		
50°	400	20.23	1.90	.0156	13.70	.0575
			3.20	.0267	18.90	.0663
			6.60	.0396		
50°	400	25.29	1.80	.0121	13.30	.0532
			4.40	.0326	18.20	.0618
			8.30	.0427	20.60	.0756
50°	450	7.08	1.20	.0172	14.10	.0738
			2.50	.0237	17.70	.0768
			4.80	.0448	20.00	.0781
			7.70	.0587	21.20	.0801
			10.70	.0663		

APPENDIX E - TRACTION AND SLIP DATA - continued

ψ	p_{max} (KSI)	u_1 (psi)	% Slip	T.C.	% Slip	T.C.
50°	450	10.12	1.10	.0135	10.40	.0641
			2.20	.0293	13.90	.0705
			4.40	.0405	18.50	.0756
			6.80	.0517	21.10	.0815
50°	450	15.18	1.50	.0126	9.90	.0590
			2.10	.0251	13.10	.0667
			4.00	.0372	17.20	.0718
			6.70	.0491	20.40	.0754
50°	450	20.23	1.90	.0208	8.70	.0540
			3.10	.0281	12.60	.0631
			4.60	.0373	18.60	.0705
			5.90	.0438		
50°	450	25.29	1.20	.0085	11.40	.0603
			4.20	.0336	16.50	.0677
			8.00	.0506	20.00	.0731

APPENDIX F

EDDY CURRENT BRAKE

The design procedure of the eddy-current brake is presented below (from Reference 18).

$$T = (\phi^2 b^2 \times \omega) \div (1000\ Ak\gamma) \qquad [1]$$

where

T = braking torque (dyne-cm) due to a disc passing through poles of a magnet of strength ϕ (magnetic lines of force) at a rotational speed ω (radians per second)

A = pole area of magnet (cm^2)

b = radius of disc (cm)

x = thickness of disc (cm)

γ = resistivity (micro-ohm cm)

k = factor which is a function of the distance the magnetic poles were from the center of the disc

Rearranging the above equation, the following is obtained:

$$\phi^2 = (1000\ Ak\gamma T) \div (b^2 \times \omega) \qquad [2]$$

The strength of an electromagnet can be determined by use of the Hopkin's formula (18).

$$\phi = (.4\Pi N) \div (\Sigma[\ell \div (A\mu)]) \qquad [3]$$

where

N = number of ampere-turns of magnetic coil

ℓ = length of each segment in magnetic path (cm)

A = area of each segment in magnetic path (cm^2)

μ = magnetic permeability of each segment in magnetic path

Squaring the above

$$\phi^2 = (.4\pi N)^2 \div (\Sigma[\ell \div (A\mu)])^2 \qquad [4]$$

Equating equations [2] and [4] and rearranging,

$$T = [(.4\pi Nb)^2 x\omega] \div [1000\ Ak\gamma(\Sigma\ell \div (A\mu))^2] \qquad [5]$$

The required torque (10 in-lb at 1200 rpm) was produced by using an aluminum disc (0.145 inch thick and 4 inch diameter) and a magnet iron ring for the core of electromagnet of 7.1 in^2 in cross section. The air gap was set at 0.18 inch.

The eddy-current brake is shown in Figure 18.

APPENDIX G

CALCULATION OF COEFFICIENT OF TRACTION

The coefficient of traction is defined as

$$T.C. = \frac{F}{W}$$

where

F = tractive force

W = normal load.

The procedure of calculating the coefficient of traction for a test run is presented below. Test conditions were

$$\psi = 40°;\ p_{max} = 300 \text{ psi};\ u_1 = 842 \text{ ips}$$

Test results were

$$u_2 = 7.673 \text{ ips};\ F_b = 6.54 \text{ gm} = 0.014 \text{ lb}$$

where

F_b = force exerted by the lever arm on the platform balance

As described in Section 3 of Chapter III the lever arm was attached to the eddy-current brake to measure the moment produced by the brake on the output shaft. Therefore from the measured values

$$\text{Percent Slip} = \frac{\Delta u}{u_1} \times 100 = \frac{u_1 - u_2}{u_1} \times 100$$

$$= \frac{8.42 - 7.673}{8.42} \times 100 = 8.87$$

Each driving ball will produce a moment, m_1, about the axis of rotation of the driven ball of magnitude (see Figure 60),

$$M_1 = F\ R_1 \sin\psi$$

where

R_1 = radius of the driven ball = 0.25 inch

The total moment will be equal then to

$$M = 3M_1 = \frac{3}{4} F \sin\psi$$

The torque due to viscous traction is balanced by the torque of eddy-current brake.

As is stated in Section 1 of Chapter III, the bearing friction losses are compensated by an air turbine. Also, before readings were done some time was allowed so that the angular acceleration of the output shaft would fade down. Thus, it is clear that there was not anything that could effect the measurements.

The torque generated by the eddy-current brake is

$$M = L \times F_b$$

where

L = moment arm = 12 inch

Equating the torques

$$F = 16 \frac{F_b}{\sin\psi}$$

From the geometry of the loading system the following relation between the normal load W, and the platform load P was derived.

$$W = \frac{1.05 + 0.64\ P}{\cos\psi}$$

Substituting the relations for F_T and W into the equation of coefficient of traction,

$$T.C. = \frac{16 \times F_b \times \text{ctn}\psi}{1.05 + 0.64\ P},$$

from the test conditions $\psi = 40°$.

To get the required maximum Hertzian pressure of 300 KSI, a platform load of 7.9 lb was used during the test (see Table II). Substituting all of these values into the equation of traction coefficient

$$T.C. = \frac{16 \times 0.014 \times 1.192}{1.05 + 0.64 \times 7.9} = 0.0451$$

This procedure shows how the first pair of data in Appendix E were calculated.

APPENDIX H

CALCULATION OF DEFLECTION IN DRIVING UNITS

Considering Figure 60 the compressive force F_c on each driving unit (ball, collet, and shaft) can be written as

$$F_c = 2W \sin\psi$$

but from the geometry W is given as

$$W = \frac{0.64\ P + 1.05}{\cos\psi}$$

Let the contact angle be 45° and the platform load be 20 lb which corresponds nearly for a maximum Hertzian pressure of 400 KSI. Then

$$F_c = 2(0.64 \times 20 + 1.05) = 27.7 \text{ lb}$$

Assume the equivalent length and the diameter of the driving unit to be 5 inch and 3/8 inch, respectively. The change in length, $\Delta\ell$, of the driving unit is

$$\Delta\ell = \frac{F_c}{E}\frac{\ell}{A}$$

where

ℓ = length of driving unit = 5 inch

E = Young's modulus = 30×10^6 psi

A = crossectional area of driving unit

$= \frac{\Pi}{4} \times (\frac{3}{8})^2 = 0.11 \text{ in}^2$

then

$$\Delta \ell = \frac{(27.7)(5)}{(30 \times 10^{6})(0.11)} = 4.2 \times 10^{-5} \text{ inch}$$

The change in length of the driving units will increase the dowel space bounded by three balls.

The indentation marks of the set screws holding each driving unit are observed using a microscope. The yield of the indentation in the tangential direction is found to be $2 - 3 \times 10^{-3}$ inches. Therefore, the change in length of the driving unit is approximated to be 2.5×10^{-3} inches. To compensate for the increase in dowel spaces the dowel diameters were decreased 5×10^{-3} inches.

APPENDIX I

UNCERTAINTIES IN CALCULATED PRESSURES

A probe ring is used to check the calculated maximum Hertzian pressures corresponding to each platform load.

The probe ring was placed between the two driven balls to measure the horizontal force W_h applied to each carriage supporting the output shafts. From the geometry of the test rig

$$W_h = 3W \cos\psi$$

where

ψ = angle of contact

W = normal load

The latter is given as (1)

$$W = \frac{2\Pi}{3} p_{max} a^2$$

From Appendix D

$$a = (12.81 \times 10^{-9}) p_{max}$$

For a contact angle of 45° W_h can be written as

$$W_h = \frac{\Pi}{\sqrt{2}} (12.81 \times 10^{-9})^2 p_{max}^3$$

As it can be predicted from the last equation, the percent uncertainty in p_{max} is the cube root of what it was in W_h, where

$$\% \text{ Uncertainty in } W_h = \frac{(W_h)\text{calc} - (W_h)\text{meas}}{(W_h)\text{calc}} \times 100$$

For some values of maximum Hertzian pressure, measured and calculated values of W_h are listed in Table VII. The calculated percent uncertainties are also listed for each case.

TABLE VII

Percent Uncertainty in Calculated Pressure

P_{max} (KSI)	Horizontal Force W_H		
	Calculated	Measured	% Uncertainty in P_{max}
200	5.02	1.2	+ 27.57
250	9.80	4.5	+ 23.24
300	16.94	12.4	+ 2.99
333	22.36	20.4	+ 0.89
350	26.90	27.3	- 0.39
400	40.16	39.2	+ 0.49
450	57.18	56.2	+ 0.41

The vita has been removed from the scanned document

EXPERIMENTAL INVESTIGATION OF THE EFFECT OF SPIN ON TRACTION IN ELASTOHYDRODYNAMICALLY LUBRICATED CONTACTS

by

Arsavir T. Andonian

(ABSTRACT)

Tests were conducted to determine the effect of spin on traction using elastohydrodynamically lubricated spheres, three driving and two driven, at maximum Hertzian contact pressures of 300 KSI, 333 KSI, 400 KSI, and 450 KSI. The angle between the axis of the driven ball and the normal to the plane of contact was varied from 40° to 50° and data were taken to determine the relation between coefficient of traction and percent slip for various rolling velocities ranging from 7.08 in/sec to 30.08 in/sec. For the percentages of slip ranging from 0 to 20 the coefficient of traction was found to increase as the angle between the axis of the driven ball and the normal to the plane of contact deviated from 45°. The cause of this increase was possibly due to the spin component of velocity across the contact area. However, this effect was reversed in the 20 to 100 percent slip range. The coefficient of traction increased as the maximum Hertzian pressure was increased for percent slips ranging between 0 to 20. The effect of maximum Hertzian pressure on coefficient of traction was reversed for percent slip values ranging between 20 to 100. An inflection point was incurred in the 16 to 20 percent range. The coefficient of traction increased with the rolling

velocity after the inflection point. The traction curves also went to a maximum and then decreased as the percent slip was increased.